U. S. ARMY
TRANSPORTATION RESEARCH COMMAND
FORT EUSTIS, VIRGINIA

TRECOM TECHNICAL REPORT 63-63

WIND-TUNNEL INVESTIGATION OF SINGLE AND TANDEM LOW-ASPECT-RATIO WINGS IN GROUND EFFECT

Task 1D021701A04803
(Formerly Task 9R99-01-005-03)
Contract DA 44-177-AMC-882(T)

March 1964

prepared by:

LOCKHEED-CALIFORNIA COMPANY
A Division of Lockheed Aircraft Corporation
Burbank, California

DISCLAIMER NOTICE

When Government drawings, specifications, or other data are used for any purpose other than in connection with a definitely related Government procurement operation, the United States Government thereby incurs no responsibility nor any obligation whatsoever; and the fact that the Government may have formulated, furnished, or in any way supplied the said drawings, specifications, or other data is not to be regarded by implication or otherwise as in any manner licensing the holder or any other person or corporation, or conveying any rights or permission, to manufacture, use, or sell any patented invention that may in any way be related thereto.

* * *

DDC AVAILABILITY NOTICE

Qualified requesters may obtain copies of this report from

Defense Documentation Center
Cameron Station
Alexandria, Virginia 22314

* * *

This report has been released to the Office of Technical Services, U. S. Department of Commerce, Washington 25, D. C., for sale to the general public.

* * *

The findings and recommendations contained in this report are those of the contractor and do not necessarily reflect the views of the U. S. Army Mobility Command, the U. S. Army Materiel Command, or the Department of the Army.

HEADQUARTERS
U S ARMY TRANSPORTATION RESEARCH COMMAND
FORT EUSTIS, VIRGINIA

This series of experimental investigations was undertaken to define further the basic aerodynamics of wings operating in ground effect. The results indicate that the ground effect phenomenon markedly affects the relative influence of configuration variables such as aspect ratio, thickness, taper, and end plates. The results also indicate that other variables such as sweep, camber, and position of maximum thickness should be investigated to determine their effect.

The correlation between theory and the present experimental results is not satisfactory in the region where high maximum lift/drag ratios are attained. If this region is found to be of practical use, it will be necessary to refine the simple theory to account for the effects of the above variables and the powerful effect of end-plate configuration.

WILLIAM D. HINSHAW
Project Engineer

WILLIAM E. SICKLES
Group Leader
Ground Effect Research Group

APPROVED.

FOR THE COMMANDER:

LARRY M. HEWIN
Technical Director

iv

Task 1D021701A04803
(Formerly Task 9R99-01-005-03)
Contract DA 44-177-AMC-882(T)
TRECOM Technical Report 63-63
March 1964

WIND-TUNNEL INVESTIGATION OF SINGLE AND TANDEM LOW-ASPECT-RATIO WINGS IN GROUND EFFECT

LOCKHEED REPORT 16906

Prepared by
LOCKHEED-CALIFORNIA COMPANY
A Division of Lockheed Aircraft Corporation
Burbank, California

for
U. S. ARMY TRANSPORTATION RESEARCH COMMAND
Fort Eustis, Virginia

PREFACE

This report is an analysis of the results obtained in a comprehensive wind-tunnel test program of wings operating in ground effect. A series of low-aspect-ratio wing models, with a variety of different end-plate configurations, was tested to determine the effects of various parameters. The investigation included (1) single wings, by the use of the image technique, and (2) certain tandem wing arrangements, tested over a ground board.

The study was conducted by the Marine Vehicles Division, ASW and Ocean Systems Organization, Lockheed-California Company, under contract DA 44-177-AMC-382(T) to the U.S. Army Transportation Research Command. Mr. William D. Hinshaw was the Project Engineer for USATRECOM, while Mr. John R. Brown was Project Manager for Lockheed.

The analysis was conducted by Mr. William P. Stevens, as Project Engineer, assisted by Mr. Samuel G. Hansen. The wind-tunnel testing was supervised by Mr. Carl M. Onspaugh.

This report analyzes the data obtained in the Lockheed low-speed wind tunnel during the period from 6 February to 26 March, 1963. The basic wind-tunnel test data may be obtained from the Lockheed Fluid Dynamics Laboratory Report L-53. Wind Tunnel Investigation of Single and Tandem Low Aspect Ratio Wings in Ground Effect (U), dated May 1963, which is available on loan by request to Technical Library, U.S.A. TRECOM, Fort Eustis, Va.

CONTENTS

ILLUSTRATIONS

ILLUSTRATIONS

ILLUSTRATIONS

ILLUSTRATIONS

ILLUSTRATIONS

SYMBOLS

b	wing span, ft
c	wing-mean aerodynamic chord, ft
d	end-plate depth, ft (measured from wing-tip chord and wing-trailing-edge intersection)
g	planform gap between tandem wings, ft
h	minimum structural clearance height from the plane of symmetry, or ground plane, ft
h_o	ground-clearance height at a specified fore and aft station, ft (usually the quarter chord)
K	constant value of τ
q	dynamic pressure, psf
V	true airspeed, knots
S	total wing planform area, ft^2 (includes both tandem wings)
W	airplane gross weight, lb
AR	aspect ratio
C_t/C_r	taper ratio
d/c	end-plate-depth ratio
g/c	tandem-wing-gap ratio
t/c	airfoil-thickness ratio
h/b	height parameter based on wing span
$h/\sqrt{S}$	minimum structural clearance height parameter based on wing area
L/D	lift-to-drag ratio
$(L/D)_{max}$	maximum lift-to-drag ratio

R.N.	Reynolds Number
C_f	skin-friction coefficient
C_l	rolling-moment coefficient
C_m	pitching-moment coefficient
C_n	yawing-moment coefficient
C_D	drag coefficient
$C_{D_{min}}$	minimum drag coefficient
C_L	lift coefficient
C_Y	side-force coefficient
α	angle of attack, deg (referenced to wing bottom in "image" test; referenced to fuselage bottom in "ground plane" tests)
δ_F	trailing-edge flap deflection, deg
δ_N	nose-droop angle, deg
τ	end-plate, bottom-edge tilt angle, deg (referenced to wing bottom)
θ	bank angle, deg
ψ	yaw angle, deg

Other symbols used in the text are explained where they occur. Force and moment coefficients and flow-orientation angles are of standard NASA definition and sign.

Abbreviations

C.D.P.	common-data pivot
I.G.E.	in ground effect
O.G.E.	out of ground effect

SUMMARY

A wind-tunnel investigation has been made to determine the effects of various end-plate and camber changes on the aerodynamic characteristics in ground effect of five low-aspect-ratio wings differing in aspect ratio, thickness ratio, and taper ratio. A single-wing investigation was made at a Reynolds Number of 2.55×10^6 by the use of the image technique, and a limited investigation of tandem wings was conducted at a Reynolds Number of 1.30×10^6 by the use of a ground board.

The single-wing models included rectangular 11.7% thick Clark Y models at aspect ratios of 1, 2, and 4; a rectangular 6% thick Clark Y at aspect ratio 2; and a 11.7% thick Clark Y with 0.6 taper ratio and aspect ratio 2. The tandem-wing investigation included six different aspect-ratio combinations of forward and aft wings with end plate, camber, and incidence made optimum from the single-wing investigation. The influence of ground effect is noted for lift, drag and pitching moment, and one of the wings was tested in roll and yaw with six-component data noted.

Comparison of lift/drag ratio on the basis of the minimum structural clearance height parameter, $h/\sqrt{S}$, shows that the addition of end plates improves L/D at aspect ratio 1 but reduces L/D at aspect ratio 4. However, based on clearance of the wing trailing edge structure, a considerable improvement of L/D is noted for all configurations with end plates. The L/D falls off with increased depth of flat end plate at a given value of $h/\sqrt{S}$. Benefits are obtained by employing airfoil contour and a wedge bottom to the end plate, particularly at low aspect ratio. A large loss of L/D occurs when the lower edge of the end plate is not parallel to the surface.

Camber influences were investigated by means of leading-edge and trailing-edge flaps. It is shown that small, positive trailing-edge camber, $+5^\circ$, improves L/D, whereas small reverse camber, -5°, reduces L/D. At lift coefficient values over 0.9 it is noted that $+15^\circ$ flap deflection shows better L/D than $+5^\circ$. Nose droop on the aspect-ratio-2 wing had little influence on the data except near the stall.

In comparing in and out of ground effect $(L/D)_{max}$ ratios for various aspect-ratio wings, it is noted that with end plates off, $h_o/\sqrt{S}$ appears to show as good a correlation as h_o/b which is employed in Wieselsberger's theory. With end plates on and zero flap deflection, a correlation of all wings is noted down to $h/\sqrt{S}$ of .04, where $(L/D)_{max}$ is about twice the out of ground effect value. Correlation deteriorates at lower values of $h/\sqrt{S}$, and it is postulated that no universal correlating parameter should be expected over the full range of ground clearance height due to the presence of a combination of lifting line and chordal influences. A large increase of $(L/D)_{max}$ is noted for the 6% thick wing as compared with the 12% thick wing and, with zero flap deflection, L/D is greater at all lift coefficients below 0.8.

A "common-data pivot" concept has been evolved. This allows excellent correlation between three-component data taken from tests of end plate configurations having their bottom edges maintained parallel to the ground and those with their bottom edges fixed parallel to the lower wing surface. An empirical approach to estimating rolling moment due to bank angle is also proposed.

Although the tandem-wing tests were only exploratory in nature, they showed smooth trends. Pitch runs showed static stability and very small out-of-trim pitching moment at the weighted quarter chord c.g. The fact that static stability is present in spite of body instability and downwash effects substantiates the basic idea behind the tandem configuration where advantage is taken of the plunge stability of the tandem surfaces.

In general, the tapered wing, as compared with the straight wing, shows slightly greater L/D with end plates off, and slightly lower L/D with end plates on.

INTRODUCTION

The phenomenon of aerodynamic wings operating in close proximity to the ground is a subject that has interested investigators since the early days of aviation. The first practical theory in this field was developed by Wieselsberger (reference 1). Serebrisky (reference 2) is another early investigator who attempted to show correlation between theory and wind-tunnel tests. Other notable contributors since that time have been LeSueur, Pistolesi, Tonnies and Raymond, to mention a few. Precise correlation between experiment and theory has yet to be realized. It appears, however, that the simple theory of Wieselsberger is as adequate for correlation purposes as the most refined theories developed to date.

Until recently, all investigations of the aerodynamic characteristics of wings in ground effect were related primarily to the take-off and landing phases for conventional aircraft. Recently, however, interest has been directed toward improvements in the lift-drag ratio of air-cushion vehicles (GEM's) and the generation of efficient surface transport systems. Considerable interest was aroused with the publishing of NASA TN D-926 (reference 3) and NASA TN D-970 (reference 4), where it seemed that a substantial improvement in L/D was possible by the use of end plates on wings operating in ground proximity. Also, the use of end plates allows greater clearance heights between prime structure and the ground.

In NASA TN D-926, the effect of aspect ratio was investigated by the utilization of the "image" technique. All wings had a thickness ratio of 21% and a few runs were made at one ground height with end plates on an aspect-ratio-1 wing. The advantages of a thinner wing section (comparing data of reference 2) and end plates were indicated in reference 3. In NASA TN D-970, a more extensive test of the aspect-ratio-1 wing was conducted over water in a towing tank. Both 11%- and 21%-thick sections were tested with end plates flush with the trailing edge and the bottom edges parallel to the water surface.

Although references 3 and 4 provided valuable clues toward the task of optimizing wings in ground effect, sufficient information for a systematic design study was not available. Accordingly, the Lockheed-California Company undertook several programs to extend the state of the art in this area.

The first program (reference 5) consisted of an aerodynamic investigation of a rectangular wing model of aspect ratio 2, with various end-plate configurations, tested in the Lockheed low-speed wind tunnel, by the utilization of the ground-board technique. Although the data showed fairly consistent trends, the drag level was questionable. Subsequently, the same model was tested in free air over a smooth desert floor (reference 6). In this test program, the model was mounted on a truck and operated in close proximity to the desert floor. The data produced tended to confirm those of the wind tunnel program, although the feasibility of this testing technique has not been well established.

The next Lockheed-funded program consisted of a series of simple wing models of various aspect ratios and with numerous end-plate configurations, tested in the low-speed wind tunnel, by the utilization of the "image" technique (reference 7). The test schedule was fairly extensive, with numerous parameters being varied, and produced fairly reliable data with sensible trends. This program formed the basis for the current test series (reference 8).

The current program, the results of which are analyzed in this report, has been funded jointly by the U.S. Army (TRECOM) and Navy (ONR). It is a natural extension of the previous program, but is more extensive in scope. Further refinements in testing techniques were employed, and these produced more consistent results and a positive correlation of data.

MODELS AND TEST PROCEDURE

Sketches of the single-wing models, end plates, and tandem-wing combinations are shown in Figures 1 and 2. Photographs of the test setups are shown in Figure 3. Additional description of the models and test procedure is given under the headings of Single-Wing Image Tests and Tandem-Wing, Ground-Plane Tests.

A limited number of runs were made out of ground effect for all five single wings without end plates and with various end-plate configurations. For general information, Figures 5 and 6 present three-component data O.G.E. for wings without end plates and with the 10% chord depth flat end plates. Figure 7, which represents tests at dynamic pressures of 20, 40, 60, 80 and 100 psf, respectively, shows the effect of Reynolds Number on the skin friction drag coefficient of wing (2-.12-1.0) at Reynolds Number of 1.30, 1.83, 2.07, 2.55 and 2.83×10^6.

SINGLE-WING IMAGE TESTS

The single-wing image tests were run at a dynamic pressure of 80 psf except for the aspect-ratio-4 wing, which was run at 60 psf to minimize deflections. The L/D values shown in this report for the aspect-ratio-4 wing have been adjusted upward to account for the variations of C_D between RN = 2.07×10^6 and 2.55×10^6.

Ten laminated mahogany wings were provided for the image series of tests. Five different wings were evaluated, each with a mirror image. All of the models were Clark Y section wings with 25%-chord plain trailing-edge flaps. Four of the wings were rectangular with a 20-in. chord and three of them, with aspect ratios of 1, 2, and 4, had a maximum thickness of 12% chord (actually 11.7%). The aspect ratio 2 and 4 wings were formed by adding outboard panels to the aspect-ratio-1 wing to increase the span from 20 in. to 40 and 80 in., respectively. The panels were joined with flush-mounted steel splice plates. The fourth rectangular wing had an aspect ratio of 2 and a maximum thickness of 6% chord. (A camber reduction was inherent

with the reduced thickness.) The fifth wing had a taper ratio of 0.60 and a maximum thickness of 12% chord. The mean aerodynamic chord of the tapered wing was 20 in. The 12% thick, aspect-ratio-2 wing was also tested with 15% chord leading-edge flaps deflected 5° and 10°.

A total of 232 end plates, including 168 flat end plates and 64 contoured end plates, was provided for the investigation. The flat end plates were fabricated from 0.05-in.-thick dural and 0.125-in.-thick steel. End-plate depths, d, were 1, 2, and 3 in. or 5, 10 and 15% chord at the trailing edge; the angle between the bottom edge of the end plate and the flat portion of the wing lower surface, τ, varied through -2°, 0°, 2°, 4°, 6° and 10°. The contoured end plates were constructed of mahogany and had a maximum thickness of 8% chord. They had an elliptical planform nose which faired into flat sides at the 15% chord, while the vertical height at the trailing edge varied from 10% (2 in.) to 15% (3 in.) of the wing chord. The 2-in. end plate had a flat bottom and the 3-in. end plate was formed by attaching a 5% chord wedge to the 2-in. end plate. Early in the test program, it was found that the 0.05-in. dural end plates presented a severe "buzz" or vibration problem. This was especially true when the trailing-edge flaps were deflected and, for most cases, when the wings were relatively close together at some positive angle of attack. In certain configurations, the lower forward corner of the end plate vibrated through about $\pm.75$ in. All of the questionable end plates were replaced with 0.125-in. steel plates and the buzz was eliminated.

The force-measuring wing models were supported in an inverted position on a fork through the tunnel floor by a six-component electromagnetic balance system. The image model was mounted above the force model on a similar fork and pitch arm system which was attached to a 2.5-in.-diameter, hydraulically operated piston. The 1500-psi cylinder was mounted vertically on the roof of the tunnel test section with the piston extending down through the ceiling. Hydraulic operating pressure was supplied by a pump actuated by a 3/4-hp electric motor. A precision steel scale was attached to the cylinder case, and a metal pointer was affixed to the piston so that accurate vertical positions could be obtained with the image wing.

At the start of the tests, the force and image wings were installed in the tunnel at zero lift angle of attack, with a spherical yaw-head, flow-survey probe

mounted along the centerline at the image reference plane midway between the two wings. A cursory tunnel flow survey was made at the test dynamic pressure at six different wing-height variations. An average flow angularity variation of only about 0.07° through this vertical translation range was indicated and was considered negligible. A calibration run was made to define the variation of model support deflections with pitching moment and the final data were corrected for effect of support deflections.

Each run was initiated at a desired minimum ground clearance height with a given angle of attack (α). The run was advanced by vertically translating the image wing to successive values of preselected heights, the angle of attack remaining constant. Each run was observed through a transit, and the height settings near "ground" for the wind-on condition were adjusted to the known wind-off settings, insofar as possible, to compensate for any noticeable wing deflections. This ensured the maintaining of a rather uniform height parameter schedule for all test conditions.

No attempt was made to compensate for slight variations in right and left wing-tip gaps between end plates, which may have occurred due to nonuniform spanwise deflection or twist of the wing. It is felt that this effect was negligible except in some instances during the testing of the 80-in. span, aspect-ratio-4 wing.

The 12%-thick, aspect-ratio-2 wing with 10%-chord flat end plates was tested through the vertical translation range at two angles of yaw and two angles of roll. Both the force wing and the image wing could be yawed to the required angles of 5° and 10°. However, only the image wing could be rolled. The image support system was designed so that the image wing could be rolled 10° and 20° to obtain mean roll angles, relative to the ground, of 5° and 10°, respectively. For each vertical height position, the image support structure and wing were translated horizontally to maintain the fixed roll angle relative to the image reference plane. The 12%-thick, aspect-ratio-2 wing with 15%-chord contoured end plates was also tested at 5° and 10° of yaw.

TANDEM-WING GROUND-PLANE TESTS

Because of structural and balance limitations, the tandem-wing tests were run at a dynamic pressure of only 20psf. The tandem-wing test program was mainly exploratory in nature and utilized the 12% thick, aspect ratio 1, 2 and 4 rectangular wings from the image tests. The wings were mounted in varying combinations of

aspect ratio fore and aft on a mahogany fuselage 102 in. long. The following wing-aspect-ratio combinations were tested: 1 fore and aft, 2 fore and aft, 4 fore and aft, 1 forward and 2 aft, 1 forward and 4 aft, and 2 forward and 4 aft. For each of the foregoing wing combinations, the wing gap, or distance from trailing edge of the forward wing to leading edge of the aft wing was varied through 1.0, 1.5, and 2.0 chord lengths or 20, 30, and 40 in. In all cases, the gap was varied by the utilization of removable fuselage sections between the wings and the shifting of the forward wing and fuselage nose section fore and aft as an integral unit. All tandem-wing runs were made with the 15% contoured end plates on the fore and aft wings, with the forward wing at zero incidence and the aft wing at 2° of incidence, and with the forward wing trailing-edge flap deflected 5°.

A 12 ft x 16 ft ground plane was installed on screw-jack supports 40 in. above the floor of the tunnel test section. Each of the configurations was tested through a limited angle-of-attack range at a fixed value of the height parameter above the ground and through a vertical translation at zero angle of attack. Accurate vertical distances above ground were obtained by adjusting the wind-on model position at each point to a previously determined wind-off setting by use of a transit. The actual angle of attack of the model was determined by the use of a Statham Model A5-2-350 accelerometer mounted in the fuselage. This accelerometer was a steady-state reading, strain-gage type, with a range of ± 2 G's. Model base pressure readings were obtained and base pressure corrections were applied to the data. The tandem model was mounted on the 2.5-in., 2500-C internal strain-gage balance and the Lockheed LFL No. 19 sting.

DATA REDUCTION AND PRECISION

The following model dimensions were used to obtain the aerodynamic coefficients presented in this report.

Single Wing

$c = 20$ in. (all models)

$b = 20$, 40, and 80 in. (AR = 1, 2 and 4)

$S = c \times b/144$

Pitching moment reference at quarter chord of MAC

Tandem Wings

c = 20 in. (all models)

S = S (fwd. wing) + S (aft wing)

Pitching moment reference at weighted quarter chord of MAC of forward and aft wings.

All of the image data were corrected for the effect of aerodynamic fork tares, weight tares, and support deflections. Known tunnel-wall corrections were not applicable to the single-wing image-phase runs because the effective cross-sectional area of the tunnel-test section varied constantly during each run. However, tunnel-wall corrections were applied to the out-of-ground-effect runs where the image model was not employed.

All of the tandem-wing data were corrected for the effect of model weight tares, sting deflections, buoyancy, and tunnel-wall effects, modified for ground-plane presence. No aerodynamic sting tares or blockage corrections were applied to the tandem-wing results, nor were fuselage drag and interference drag subtracted.

The accuracies of the aerodynamic coefficients presented in this report for the image models are based upon experimental point scatter and consideration of the processes involved in the measurement and computation of the data. They are believed to be within the following limits:

$C_L = \pm 0.010$ $\quad$ $C_c = \pm 0.002$

$C_D = \pm 0.001$ $\quad$ $C_n = \pm 0.0005$

$C_m = \pm 0.002$ $\quad$ $C_l = \pm 0.0005$

The estimated accuracies of the tandem-wing coefficients are based, primarily, on 0.5% of rated balance loads and consideration of data-point scatter and zero shifts during runs. These estimated limits of precision for each tandem-wing configuration are as follows:

Configuration ($AR_F - AR_A$)	C_L	C_D	C_m
(1-1)	±0.067	±0.013	±0.018
(1-2)	±0.045	±0.009	±0.012
(2-2)	±0.034	±0.007	±0.009
(1-4)	±0.027	±0.005	±0.007
(2-4)	±0.022	±0.004	±0.006
(4-4)	±0.016	±0.003	±0.005

TEST FACILITY

The single-wing image and tandem-wing ground plane tests were conducted in the Lockheed Fluid Dynamics Laboratory Subsonic Wind Tunnel in Burbank, California. The tunnel is of the single-return, closed-throat type, with a test section 8 ft x 12 ft operating at atmospheric pressure. Controlled dynamic pressures range from 1.0 to 150 psf. A 20-channel Giannini digital readout system is used to convert model balance readings to digital form. These digital data are punched out on an IBM summary card punch and also typed out on an electric typewriter. The data for these tests were reduced to coefficient form by means of an IBM 7090 digital computer and automatically plotted on an Electronics Associates data plotter.

DISCUSSION

SCOPE AND FORM OF DATA

The primary purpose of this wind-tunnel program was to provide an aerodynamic perspective of low-aspect-ratio wings flying in ground effect. The test variables were selected so as to gain some understanding of the effects of: aspect ratio (1, 2 and 4); thickness ratio (6% and 12% aspect ratio 2); taper ratio (1.0 and 0.6 at aspect ratio 2); leading-edge flap deflection (5° and 10° at aspect ratio 2); trailing-edge flap deflection (-5°, $+5^{\circ}$ and $+15^{\circ}$ at all aspect ratios), end-plate height (5%, 10% and 15% chord); and end-plate contour shape.

Tests of single wings were conducted at various ground clearance heights and angles of attack by the use of the image technique with end plates off, lower edge of end plates parallel to the lower wing surface, and lower edge of end plates parallel to the ground. A limited number of tests of the single wings were conducted out of ground effect (O.G.E.) including Reynolds Number variation. The aspect-ratio-2 wing was tested in sideslip and roll, and a limited number of runs were conducted with various combinations of wings in tandem over a ground plane.

A run tabulation is shown in Table I. The run numbers are listed to indicate the scope of the test variables and are not referred to elsewhere in this report. The original data for the various runs are presented in a formal wind-tunnel data report prepared by the Wind Tunnel Department of the Lockheed-California Company (see reference 8).

Consideration has been given to the designer in the presentation of aerodynamic data in this report. For example, the ground clearance height parameter used in this report is $h/\sqrt{S}$, where h is defined as the minimum structural clearance height and S is the total wing area. It is assumed that the designer starts with a wing area in mind dictated by gross weight and take-off and cruise-speed considerations, and a ground height dictated by sea state or terrain considerations, and thus

$h/\sqrt{S}$ is an immediately useful parameter. A chart is shown in Figure 4 for quick reference to $h/\sqrt{S}$ as a function of gross weight, wing loading, and ground clearance. A relation of wing loading, sea-level velocity, and lift coefficient is also shown for convenience. In the example shown on Figure 4 for a wing loading of 18, a gross weight of 40,000 lb, and a ground clearance height of 3.7 ft, $h/\sqrt{S} = .08$ and at 130 knots, $C_L = 0.3$. Single-wing data in this report are presented at $h/\sqrt{S}$ values of .01, .02, .04, .08, .16, .32, and O.G.E. Tandem-wing pitch runs are presented at $h_o/\sqrt{S} = .06$.

In general, performance data for single wings tested by the image method are shown for tests conducted with the lower edge of the end plates maintained parallel to the ground, whereas stability data are presented for runs where the lower edge of the end plates are fixed, in this case, parallel to the lower wing surface. These are referred to in this report as the ($\tau = \alpha$) mode and the ($\tau = K = 0^o$) mode, respectively. An empirical method (referred to as the common-data pivot concept) has been developed which allows both performance and stability data to be modified to include any arbitrary end-plate tilt angle. An empirical approach to performance data is suggested. This approach uses an effective aspect ratio; however, a generalized parameter that would account for both aspect ratio and chordal effects has not yet been found. A simple empirical approach to rolling moment due to bank angle is suggested, although no simple relation for rolling moment due to sideslip is apparent.

LIFT/DRAG RATIO FOR ($\tau = \alpha$) MODE

The L/D ratio is plotted vs lift coefficient (C_L) for various values of the height parameter, $h/\sqrt{S}$, and test values of angle of attack (α) on Figures 8 to 24 for all single-wing configurations tested by the image method. Data are presented at $h/\sqrt{S}$ values of .01, .02, .04, .08, .16, .32, and O.G.E., where data are available. Summary curves of $(L/D)_{max}$ are shown on Figures 25 through 36.

On Figures 8 to 24, a "limiting line" radiating from the origin is labeled $1/C_{D_{min}}$. This represents the L/D with zero induced drag, where $C_{D_{min}}$ is obtained from O.G.E. data (Figures 6 and 7). It should also be noted that a radial line at half the limiting-line slope theoretically represents $(L/D)_{max}$ where $C_D = 2C_{D_{min}}$.

TABLE I (1 OF 3)

SINGLE-WING IMAGE-TEST RUNS

FLAPS		END PLATES			I.G.E. RUNS NOMINAL VALUES α - DEG.						YAW	BANK	O.G.E. RUNS
δ_F DEG	δ_N DEG	TYPE	d	τ	-2	0	2	4	6	10	ψ DEG	ϕ DEG	τ = 0
					WING (1-.12-1.0)								
0	0	OFF		α	33	34	35	36			0	0	13
0	↓	FLAT	1	α	37	38	39	41	79	42	↓	↓	
-5		↓	2	α	47	48	49	50					
0			↓	α	43	44	45	46	78	204			
0				0	74	44	73	71	72				15
+5				α	54	53	52	51	77	207			
15			2	α	55	56	75	76	59	208			
0		FLAT	3	α	62	61	60	206	205	203			
0		CONT	2	α	63	65	67	69					18
0	0	CONT	3	α	64	66	68	70			0	0	17
					WING (2-.12-1.0)								
0	0	OFF			80	81	82	83			0	0	8
15	↓	OFF		α	103	102	101	100	104	105	↓	↓	
0		FLAT	1	α	84	85	169	166	165	163			
0		↓	1	0	86	85	87	88	89				
15			1	α	144	146	145	143	142	141			
-5			2	α	122	125	123	124					
0			↓	α	110	111	109	108	107	106			
↓				0	112	111	113	114	115		↓	↓	9
				0		192					5	0	
				0		193					10	0	
				0		201					0	-5	
0				0		202					0	-10	
5				α	117	116	118	119	120	121	0	0	
15	↓			α	94	95	93	92	90	91	↓	↓	
15	0			0	96	95	97	98	99				
-5	5			α		126	127	128	129	130			
0	5			α		135	134	133	132	131			
5	5			α		136	137	138	139	140			
-5	10		↓	α		158	159	160	161	162			
0	10			α		157	156	155	154	153			
15	10		2	α		147	148	149	150	151			
0	0		3	α	176	171	170	168	164	167			
0	↓		3	0	173	171	172	174	175				
15		FLAT	3	α	188	189	190	185	186	187			
0		CONT	2	α	177	179	181	183			↓	↓	11
↓		↓	3	α	178	180	182	184					12*
↓	↓	↓	3	0		195					5	0	
0	0	CONT	3	0		194					10	0	

* ALSO, AT DIFFERING R.N., RUNS (196 - 200)

TABLE I (2 OF 3)

SINGLE-WING IMAGE-TEST RUNS

FLAPS		END PLATES			I.G.E. RUNS NOMINAL VALUES α - DEG.						YAW	BANK	O.G.E. RUNS
δ_F DEG	δ_N DEG	TYPE	d	τ	-2	0	2	4	6	10	ψ DEG	ϕ DEG	τ = 0
					(-1)	WING (4-.12-1.0)							
0	0	OFF			302	301	303	304			0	0	20
0		FLAT	1	α	324	323	308	305	317	320			
-5			2	α	336	335	337	338					
0				α	313	312	309	306	318	321			
0				0	313	312	314	315	316				21
5				α	344	343	342	339	340	341			
15			2		345	346	347	348	349	350			
0			3	α	326	325	311	307	319	322			
0		CONT	2	α	330	327	331	333					23
0	0	CONT	3	α	329	328	332	334			0	0	22
						WING (2-.06-1.0)							
0	0	OFF		α	295	263	293	294			0	0	28
0		FLAT	1	α	247	244	250	256	257	261			
-5			2	α	285	284	283	282					
0				α	248	245	251	254	258	260			
0				0	264	245	265	266	267				29
5				α	276	277	278	279	280	281			
15			2	α	287	288	289	290	291	292			
0			3	α	249	246	252	255	259	262			
0		CONT	2	α	274	272	270	268					30
0	0	CONT	3	α	275	273	271	269			0	0	32
						WING (2-.12-0.6)							
0	0	OFF			213	212	214	236	215	216	0	0	25
-5		FLAT	2	α	240	241	242	243					
0				α	239	231	238	237	218	217			
0				0	235	231	234	233	232				26
5				α	227	230	229	228	219	220			
15	0	FLAT	2	α	226	225	224	223	222	221	0	0	

TABLE I (3 OF 3)

TANDEM WING GROUND PLANE TESTS

CONFIG.	g/c	TYPE	RUN	CONFIG.	g/c	TYPE	RUN
1 - 1	1	P	405	1 - 4	1	P	375
		VT	406			VT	377
	1.5	P	402		1.5	P	373
		VT	403			VT	374
	2	P	399		2	P	370
		VT	400			VT	371
1 - 2	1	P	390	2 - 4	1	P	361
		VT	391			VT	362
	1.5	P	393		1.5	P	364
		VT	394			VT	365
	2	P	396		2	P	367
		VT	397			VT	368
2 - 2	1	P	387	4 - 4	1	P	357
		VT	388			VT	359
	1.5	P	384		1.5	P	355
		VT	385			VT	356
	2	P	381		2	P	351
		VT	382			VT	353

The fact that in many cases $(L/D)_{max}$ does not fall on this line shows that the drag polar cannot be represented by a simple parabola.

Effect of Angle of Attack

With zero trailing-edge flap deflection, $(L/D)_{max}$ in ground effect occurs at near $+1.0^{\circ}$ for all five basic wings; at negative angles of attack L/D falls off sharply as it approaches the limiting line. With $+5^{\circ}$ trailing-edge flap deflection, the angle of attack for $(L/D)_{max}$ in ground effect occurs at α near -1.0° for all five basic wings and L/D holds up well at the lower angle-of-attack limit of -2°. With -5° trailing-edge flap deflection, the angle of attack for $(L/D)_{max}$ in ground effect occurs at α near $+3^{\circ}$ for all five basic wings and L/D falls off sharply at angles below 0° where L/D approaches the limiting line. In general, C_L and consequently L/D, fall off rapidly at negative angles of attack as the surface is approached. This phenomenon is commonly described as the "Venturi effect."

Effect of Flap Deflection

Very little data are available to aid in the selection of an optimum airfoil contour operating in close proximity to the ground. To this end, all wings were provided with trailing-edge flaps. Wing (2-.12-1.0) was provided with leading-edge flaps as well to investigate basic camber influences. The $(L/D)_{max}$ plots of Figures 25 through 31 show that, for best L/D with end plates, the trailing edge should be cambered and not reflexed. The $(L/D)_{max}$ in ground effect for $\delta_F = +5^{\circ}$ is distinctly better than no flap for all wings, and the $(L/D)_{max}$ for $\delta_F = -5^{\circ}$ is distinctly worse than no flap. This conclusion is somewhat modified for the thin wing where the benefit of $+5^{\circ}$ flap is small compared with the penalty of -5° flap. For the tapered wing, it appears that the benefit of $+5^{\circ}$ flap is large compared with the penalty of -5° flap. For a given wing, the C_L at L/D_{max} in ground effect is relatively unoffected by trailing-edge flap deflections between $\pm 5^{\circ}$.

At large lift coefficients, it can be noted that better L/D can be obtained with 15° trailing-edge flap than with 5° flap. The approximate crossover C_L values

are 1.0 for wing (1-.12-1.0), 1.1 for wing (2-.12-1.0), 1.3 for wing (4-.12-1.0), 0.8 for wing (2-.06-1.0), and 0.9 for wing (2-.12-0.6). Of possible interest for future camber studies is the high value of L/D at high C_L for wing (2-.06-1.0) with 15° flap in ground effect, as noted on Figure 22.

Effect of Nose Droop

Whereas trailing-edge camber appears to have a significant influence on L/D, reference to Figures 14, 15 and 27 would indicate that, at least for wing (2-.12-1.0), leading-edge camber effects are small and detrimental. The L/D loss in ground effect is about the same as O.G.E., indicating very little ground effect influence. The most noticeable influence is seen by comparing Figures 13 and 15, where 10° nose droop improved C_L and L/D at large angle of attack with 15° flap deflection.

Effect of Aspect Ratio

The variations of $(L/D)_{max}$ and C_L at $(L/D)_{max}$ with the height parameter $h/\sqrt{S}$ is shown in Figures 31 and 32 for all wings tested with flat end plates having a depth of 10% chord. The influence of aspect ratio on $(L/D)_{max}$ for the 12% thick wings without taper is noted to be quite pronounced at all values of $h/\sqrt{S}$. The C_L at $(L/D)_{max}$ increases as the ground is approached and also increases with aspect ratio.

From Wieselsberger's theory (reference 1) and recent experimental data (reference 3), it was expected that the best correlation of aspect-ratio effects without end plates could be shown in a plot of $\left\{(L/D)_{max\ I.G.E.}\right\} \Big/ \left\{(L/D)_{max\ O.G.E.}\right\}$ or $\sqrt{(AR_e)/(AR)}$ vs. h_o/b where, in this case, h_o is the distance from the quarter chord of the non-end-plated wing to the ground and b is the span. This plot is shown in Figure 33 and is to be compared with a plot of the same ratio vs. $h_o\sqrt{S}$ in Figure 34. It can only be concluded that, over the limited range of the parameters covered in this report, a height parameter based on $\sqrt{S}$ correlates data equally as well as that based on b. The $(L/D)_{max}$ ratio with various end plates is plotted in Figures 35 and 36 vs. $h/\sqrt{S}$. It is noted, for example, that with d/c = .05, flat end plates

correlation is good down to $h/\sqrt{S} = .04$ where $(L/D)_{max}$ is essentially doubled for all aspect ratios.

At lower values of $h/\sqrt{S}$ the correlation deteriorates, and it is proposed that no universal correlating parameter should be expected since a combination of lifting-line and chordal influences is present. On a purely lifting-line basis, h/b is predominant; on a chordal influence basis h/c is predominant, and $(h/\sqrt{S})$ falls somewhere in between.

An effective aspect ratio must be determined to estimate L/D at all values of lift coefficient. This can be determined from the expression

$$AR_e = C_L^2 \left/ \left(\frac{C_L}{L/D} - C_{D_{min}} \right) \right. \text{ at } (L/D)_{max}$$

or,

$$AR_e = AR \left\{ \frac{(L/D)_{max\ I.G.E.}}{(L/D)_{max\ O.G.E.}} \right\}^2 .$$

Use of either method of predicting L/D vs. C_L shows good agreement with data obtained from ($\tau = \alpha$)-mode testing.

Effect of End Plates

The influence of end plates on the $(L/D)_{max}$ of the five basic wings tested is summarized in Figures 25 through 31. Data are shown with end plates off; with flat end plates of three depths, d/c = .05, .10, and .15; and for two contoured end plates, flat bottom d/c = .10 and wedge bottom d/c = .15. The end-plate geometry is shown in Figure 1. In reviewing Figures 25 through 31, it should be remembered that h is defined as the minimum structural clearance height to the wing trailing edge in the case of end plates off, and to the bottom of the end plate with end plates on. Since the main preoccupation with end plates is to allow larger clearance for the wing structure proper, it may be of interest to compare L/D for a given trailing-edge height. In making this comparison, L/D for the configuration with end plates should be read at an incrementally lower $h/\sqrt{S}$ given by $\frac{d/c}{\sqrt{AR}}$.

For a given value of $h/\sqrt{S}$, it can be said, in general, that for aspect-ratio 1, end plates show an increase of $(L/D)_{max}$ compared with end plates off, whereas little difference is noted at aspect-ratio 2. The reverse is true at aspect-ratio 4. For example, compare a flat end plate of d/c = .05 with end plate off at $h/\sqrt{S}$ = .04, $\Delta(L/D)_{max}$ = 4 for AR = 1, 0 for AR = 2 and -1.5 for AR = 4. At lift coefficients larger than C_L at $(L/D)_{max}$, the L/D for a given $h/\sqrt{S}$ falls off much more rapidly with end plates off than with end plates on. A physical explanation of these phenomena can be seen if the height of the emanating tip vortex is assumed to be at the lower structural height at the quarter chord (lifting line theory). With 15° flap deflection, a very striking influence of end plates is noticed. From Figure 16 at $h/\sqrt{S}$ = .02 and C_L = 1.2, for example, L/D = 9 with end plates off and 22.5 with flat end plates at d/c = .15. In this case, L/D is increased by a factor of 2.5, while the height of the wing trailing edge is increased by a factor of 4.

Concerning the effects of end-plate geometry, it is noted that L/D drops off with increased depth of end plate, and, in general, the small-depth (d/c = .05) flat end plate produced the highest $(L/D)_{max}$ of all end plates tested. However, for d/c = .10 the flat-bottom, contoured end plate is better than the flat end plate, and for d/c = .15 the wedge-bottom, contoured end plate is much better than the flat end plate. It is also noticed that there is little difference in $(L/D)_{max}$ between the contoured flat-bottom (d/c = .10) end plate and the contoured wedge-bottom (d/c = .15) end plate, whereas flat end plates show a noticeable reduction of L/D with height. This would indicate that a wedge-bottom, contoured end plate of minimum height consistent with structural clearance requirements is desirable.

The loss in L/D with depth of flat end plate at low values of $h/\sqrt{S}$ is larger than would be expected from skin friction drag only; this fact indicates more fundamental effects on flow distribution. On the other hand, at aspect-ratios 1 and 2, the difference between contoured end plates is so small that beneficial effects must be attributed to the wedge bottom on the deeper end plate. For aspect-ratio 4, the difference in L/D between the two contoured end plates is of the order expected because of skin friction drag.

The importance of end-plate tilt angle, τ, on L/D at a given value of $h/\sqrt{S}$ is shown in Figure 37. On this figure, L/D is plotted vs. C_L for three aspect

ratios from the ($\tau = \alpha$) mode and the ($\tau = 0^{\circ}$) mode. It is apparent that end plates with bottom edges inclined to the ground always have lesser values of L/D than those with bottom edges parallel to the ground. This appears reasonable from the fact that the trailing vortices shed along the bottom edge are further removed from their image counterpart. This points out the importance of selecting the proper end-plate tilt angle to optimize L/D in the C_L range of interest or of providing for variable-tilt angle in the initial design.

Effect of Thickness

Reference 3 states that, in the comparison of L/D of two wings of aspect-ratio 5 in ground effect, the thin wing (11.7% Clark Y-H) has higher L/D at low-lift coefficients and the thicker wing (12% mod. Glenn Martin) has higher L/D at high-lift coefficient. The same effect is noted here in comparing aspect-ratio-2 wings with Clark Y sections at 6% and 11.7% thickness ratios. For zero trailing-edge flap deflection and all end-plate configurations, L/D for the 6% section is larger at C_L's below 0.8. With $+5^{\circ}$ flap deflection the crossover C_L is about 1.0, and with 15° flap deflection the crossover is at the stall C_L for the 6% wing. The stall C_L for the 6% thick wing with 15° flap (Figure 22) is a function of ground height and is 1.2 at $h/\sqrt{S} = .32$ ($\alpha = 10^{\circ}$) and 1.4 at $h/\sqrt{S} = .01$ ($\alpha = 4^{\circ}$). For the 12%-thick wing with 15° flap no stall is evident at $\alpha = 10^{\circ}$ except at $h/\sqrt{S}$ below .02 where stall occurs at $C_L = 1.6$ (Figure 13). Comparison of wing thickness effects on $(L/D)_{max}$ for the aspect-ratio-2 wings is shown in Figure 31. The influence is quite significant as compared with aspect-ratio effects, for example.

Effect of Taper

Both taper and sweep can have practical benefits for ground-effect machines. There is a storage and structural advantage in providing thicker root sections, and smaller chord end plates might prove as effective. Sweep can help problems of balance and might improve static stability margin in ground effect. The (2-.12-0.6) wing tested has a taper ratio of 0.6 and 26° leading edge sweep since the trailing edge is straight (Figure 1).

Whereas O.G.E. characteristics show taper to have beneficial effects on drag and stall (Figure 7), this is not necessarily true in ground effect. With end plates off, L/D for the tapered wing is slightly better than that of the straight wing at all C_L's. With flat end plates at d/c = .10, however, L/D for the tapered wing is worse for 0°, +5° and 15° trailing-edge flap deflection. At large C_L's and +15° flap deflection the reduction of L/D with taper is quite apparent. No direct evidence of stall is noted at $\alpha = 10°$ (Figure 24); however, at all ground heights the C_L is somewhat lower than that of the straight wing. Comparison of taper effects on $(L/D)_{max}$ and C_L at $(L/D)_{max}$ for the aspect-ratio-2 wings is shown in Figures 31 and 32. The influence is small compared to thickness effects, for example.

THREE-COMPONENT DATA FOR ($\tau = K = 0°$) MODE

Drag coefficient (C_D), angle of attack (α), and pitching moment coefficient at the quarter chord (C_m) are plotted vs. lift coefficient (C_L) on Figures 38 to 45 for all model configurations tested by the image method with end plates parallel to the flat bottom side of the Clark Y airfoil. This method of testing with a fixed-end-plate geometry is referred to as the ($\tau = K$) mode as differentiated from the ($\tau = \alpha$) mode, where the end plates are maintained parallel to the surface at all angles of attack. A method of converting ($\tau = \alpha$) mode data to ($\tau = K$) mode data by means of a common-data pivot concept is discussed in a separate section of this report.

The three-component data of Figures 38 to 45 are plotted vs. C_L for values of $h_o/\sqrt{S}$ of .04, .08, .16, .32, and O.G.E. (where data are available). In this case, it should be noted that h_o is defined as the structural clearance height (half the distance between image models) measured at the quarter chord. At any angle of attack other than zero, the leading or trailing edge of the end plate is closer to the ground and represents a lower value of $h/\sqrt{S}$.

Drag

The ($\tau = 0$) mode drag data shown on Figures 38 to 45 are plotted at con-

stant values of $h_o/\sqrt{S}$ and are not considered to have the significance of data plotted vs. $h/\sqrt{S}$. The effect of end-plate tilt angle at constant values of $h/\sqrt{S}$ for three representative configurations is shown on Figure 37. The effect shows the importance of selecting the proper end-plate tilt angle for the C_L range of interest or providing variable-tilt angle if the design C_L range is large.

Lift Curve Slope and C_L at $\alpha = 0$

The lift-curve slope and C_L at $\alpha = 0$ increase with aspect ratio and with ground effect. The variation of lift curve slope with aspect ratio O.G.E. is predictable by lifting-line theory; however, the ground effect indicates the presence of other influences. For example, at $h_o/\sqrt{S} = .04$, the lift-curve slope of all three aspect ratios (1, 2, and 4) is about the same and is greater than 2τ.

For the 6%-thick wing the lift curve slope for a given value of $h/\sqrt{S}$ is no different from the thicker 12% wing; however, the C_L at zero α is reduced by about 0.2. This is primarily a camber influence, however, and is not necessarily attributed to thickness effects. The lift characteristics for the tapered wing are essentially the same as for the straight wing.

Static Stability and C_{m_o}

The static stability margin in pitch as measured by a negative slope of dC_m/dC_L increases as the ground is approached. Whereas at $C_L = 0.5$ the aspect-ratio-1, -2, and -4 wings all show an instability of about 2% O.G.E., stable slopes of 11%, 9%, and 5%, respectively, are indicated in ground effect at $h_o/\sqrt{S} = .04$. The pitching moment coefficient at $C_L = .5$ is about -.07 for all three aspect ratios at $h_o/\sqrt{S} = .04$. The effect of thickness and taper on static stability margin in ground effect appears to be small. However, there is a noticeable shift in C_{m_o}. At $C_L = 0.5$ and $h_o/\sqrt{S} = .04$, for example, $C_m = -.05$ for the thin wing, -.07

for the straight wing, and -.08 for the tapered wing. With 15° flap deflection on wing (2-.12-1.0) at zero angle of attack at $h/\sqrt{S} = .04$, $C_L = 1.1$, $dC_m/dC_L = -.02$ and $C_m = -.20$. Since the static stability margin for a given ground height is less with flap deflection, it may govern c.g. limits from stability considerations.

Static stability in plunge as measured by dC_L/dh is noticeable at all positive angles of attack.

COMMON-DATA PIVOT CONCEPT

The preceding discussion of performance data has dealt primarily with the ($\tau = \alpha$)-testing mode where the bottoms of the end plates are maintained parallel to the ground. The discussion of stability data has dealt with the ($\tau = K$) mode (in this case, $K = 0°$), where the end plates are fixed parallel to the bottom (reference line) of the airfoil. As noted previously, the bulk of the data were run in the ($\tau = \alpha$) mode. Hence, the question arises as to whether a method is available which could convert these data into the ($\tau = K$) mode. If this can be done, it would reduce considerably the number of test runs.

At first glance, this would appear to be a rather formidable task, since the correlation would have to include effects of height from ground, angle of attack, and end-plate tilt angle. Fortunately, the data generally appear to relate in such a manner that all three variables are correlated by a simple geometric strategem. The authors choose to call it the "common-data pivot" (CDP) concept.

The concept can best be explained by referring to Figure 46. Geometries differing only as a consequence of functional mode are compared, i.e., ($\tau = 0°$) and ($\tau = \alpha$) modes. Wing geometry, end-plate depth, angle of attack, and testing reference station (X_o) are the same between modes.

In the simplest terms, the CDP may be regarded as another common reference station (X_L), from which the height (h_L) from the ground to the bottom edge of the end plate is measured. On this basis, a comparison of C_L data between modes will appear practically identical, independent of height from ground, angle of attack, and end-plate tilt angle. In the same manner, $C_{m_{.25}}$ data can be correlated by the

use of the corresponding reference station (X_m) and height (h_m). Lift/drag-data correlation is also possible.

Another way of visualizing the CDP concept is to imagine a wing with end plates, disposed at any given angle of attack and height above the ground. Further, imagine the artifice of an end-plate bottom edge free to rotate about the common data pivot at X_L. If constant end-plate depth is maintained, the CDP concept states that no change in C_L will occur due to the angular displacement of the end-plate bottom edge. Or, $\left(\frac{\partial C_L}{\partial \tau}\right)_{d,\, h_L,\, X_L} = 0$. The same type of argument applies to the other parameters, $C_{m_{.25}}$ and L/D.

The CDP concept was developed from the observation that test data (plotted against h_o/b) at constant angle of attack could be made to coincide between functional modes by a shift of $\Delta h/b$. After it was noted that the essential difference between modes was the difference in end plate tilt angle ($\Delta \tau$), working graphs were constructed by plotting ($\Delta h/b$) vs. ($\Delta \tau$). It turned out that such plots could be approximated by straight lines. On the assumption of small angles, the slope of these lines could be expressed as a shift in reference station (ΔX) to what may be described as the "common-data pivot."

In Figure 46, the heights h_v and h_p correspond to test-data values at the same C_L of the ($\tau = \alpha$) mode and the (τ = K)-mode configurations, respectively. The testing reference station (X_o) was held constant at the tip-end chord position, $c_t/2$. End-plate, bottom-edge tilt angles τ_v and τ_p are also similarly distinguished. The CDP is assumed to exist at the point (X_L, h_L).

A more direct comparison is afforded by superimposition of the two functional modes, as shown in the inset. The CDP is made coincident, and only portions of the bottom edges of the end plates are shown.

By utilizing the following definitions:

$$\Delta h = h_p - h_v \qquad (1)$$

$$\Delta\tau = \tau_p - \tau_v \tag{2}$$

$$\Delta X = X_L - X_o \tag{3}$$

and converting the inset into an analytical model as shown in the figure, the fundamental relationship is simply derived, as follows:

$$-\frac{\Delta\tau}{57.3} = \frac{\Delta h}{X} \text{ (assumption of small angles)} \tag{4}$$

$$\frac{\Delta X}{c_t} = -57.3\,(b/c_t)\,\frac{\Delta(h/b)}{\Delta\tau} \tag{5}$$

$$\frac{\Delta h}{b} = \frac{.01745}{(b/c_t)}\left(\frac{\Delta X}{c_t}\right)\Delta\tau \tag{6}$$

Equation (5) is useful in determining the CDP from test data. The slope $\frac{\Delta(h/b)}{\Delta\tau}$ represents the best linear approximation of the adjusted test data. Equation (6) is the final expression used to demonstrate correlation on the basis of the common-data-pivot concept and to translate data about any other reference point.

Correlations are shown in Figures 47 to 51, where test data from the ($\tau = \alpha$) mode configurations adjusted according to Equation (6) (shaded symbols) are compared with original data from the ($\tau = 0^\circ$)-mode configurations, (open symbols and faired curves). The correlation appears to hold for the data parameters α, C_L, $C_{m_{.25}}$ and L/D, and for all geometries tested. It is not expected to apply to large angles of α or τ, nor when "venturi" effects are present.

It appears from this empirical method, for the data analyzed, that the CDP is located at about the three-fourths chord for C_L, unit-chord for $C_{m_{.25}}$, and half-chord for L/D. In the case of L/D, the test data are compared directly without adjustment. In some instances a small adjustment would give more consistent agreement.

CHARACTERISTICS IN YAW

The effects of yaw in ground effect at zero angle of attack are shown for

wing (2-.12-1.0) in Figure 52, with both the flat end plates at d/c = 0.10 and with contoured wedge bottom end plates at d/c = .15. There is no appreciable difference between the end-plate configurations, except what appears to be a distinct ground influence on yawing moment in the case of the contoured end plates. Otherwise, for either geometry, side force and yawing moment do not seem to be affected significantly by ground proximity.

An interesting dihedral effect is noted, greatly pronounced in ground proximity. The most likely explanatian of this phenomenon is that the end plates produce circulatian that is additive to that of the basic wing on the downstream wing panel and subtractive on the upstream panel. Thus, when the wing is yawed "nose" left, the left wing panel experiences a higher wing loading than the right one. A positive rolling mament (i.e., a tendency to bank right wing down) ensues.

Out of ground effect, the end plates are of extremely low aspect ratia. Hence, the roll moment induced by yaw is very small. At the other extreme, when the real and image wing end plates are just shart of touching, the end plate effective aspect ratio is somewhere between twice the O.G.E. value and infinite. This produces a large asymmetrical wing loading in yaw, resulting in a vastly increased roll moment.

Unlike the roll moment due to bank case, the roll moment due to yaw case is not readily amenable ta analysis from the unyawed condition. This is mainly because of the very law aspect ratio of the end plates, which must now be considered as "wings" at angle of attack, whereas, in the banked wing case, the end plates can be visualized essentially as an extension of the main wing extremities. This is discussed subsequently.

CHARACTERISTICS IN ROLL

The thesis that the most powerful influence of ground effect is associated with the wing tip extremities is again in evidence in the roll characteristics at zero angle of attack for wing (2-.12-1.0) with flat end plates at d/c = .10, as shown in Figures 53 and 54. At first glance, there appears to be no appreciable difference between the -5° and -10° bank angle lift and rolling moment characteristics in ground effect. However, the real significance is that these characteristics can be

reasonably approximated from the zero bank angle characteristics by consideration of the heights at the wing tip extremities.

Consider Figure 53, where C_L is plotted against the testing height parameter, h/b. If the wing proper were the dominant factor in the influence of ground effects, then an average height between wing tips would tend to correlate unbanked-wing data with banked-wing data. As the corresponding dotted curve shows, this is not a plausible assumption. However, if the wing tip extremities play the dominant role in ground effect, then an average C_L depending on the heights at the wing tips might conceivably facilitate correlation. Such is the case for both banked-wing cases as shown by the dashed curve. Though not exact, the trend is remarkably the same.

Having established the dominance of the wing-tip extremities in determining the trend in C_L for banked wing cases from the unbanked wing case, it is natural to attempt to apply this information to the prediction of rolling moment, C_l (see Figure 54). First of all, the fact that an average C_L yielded reasonable correlation suggests that the change in lift distribution over the left-wing panel is equal and opposite to that over the right wing panel. If this is the case, then we can expect the rolling moment to be proportional to the difference in C_L, obtained from the unbanked-wing data at the local wing tip heights.

As can be seen in Figure 54, correlation is thus achieved at both -5° and -10° bank angles by use of the factor of 0.1. The tendency is toward increased prediction accuracy as the unbanked condition is approached. This is particularly encouraging, since a means is provided for extending the test information and for determining initial roll-stability derivatives.

In Figure 55, the roll moment coefficient is plotted against bank angle for values of the minimum ground-clearance height parameter (lowest wing tip). The curves are completed by use of the preceding empirical method. As indicated by the curve slopes, roll stability is assured in ground proximity, particularly at shallow bank angles.

CHARACTERISTICS OF TANDEM WINGS

Six combinations of rectangular 11.7% thick Clark Y wings of aspect-ratio 1, 2 and 4 were tested in tandem over a ground plane. The basic model details are shown

in Figure 2. Three-inch contoured end plates ore used, and the forward wing incorporates +5° flap deflection ond is mounted with zero incidence, whereas the aft wing has no flap deflection ond is mounted at 2° incidence. This selection was based on data observed from the single-wing image tests and was intended to optimize L/D, stability and trim.

The results of the tests of the tondem wings are summarized in Figures 56, 57, and 58. The vertical traverse runs ore all at the reference angle-of-attock of zero. L/D ratio and C_L are plotted vs. the minimum cleorance height parameter $h/\sqrt{S}$ for all test configurations and gap-chord ratios (g/c). The pitch runs are all at c.g. height above the ground board of $h_o/\sqrt{S} = .06$. The c.g. locations are determinable from wing-area weighted moments from the quarter-chord station of each wing. Values are noted in Figure 58. The pitch ongles were run at 1° intervals covering the range from -3° to +3°. The pitch run data are plotted as L/D vs. C_L and as pitching moment coefficient (C_m) vs. C_L.

One thing oppears common to all tandem-wing configurations -- an inconsistent effect of gop-chord rotio. This may be due, in part, to the testing technique. However, in the main, it is believed that this points up the complicated flow interaction between the wings and fuselage. This, then, suggests more detailed future studies of the flow mechanism of tandem wings.

It is encouraging to note that for this exploratory-type program, the trends of C_L and L/D in ground effect as well as the C_m vs. C_L curves ure smooth and show no spurious discontinuities. It is noted that static stability improves with C_L and, in general, is positive at C_L's greoter than 0.3 for all configurations. In oddition, the out-of-trim moment coefficient is smoll, and this fact justifies the selection of incidence ond camber. The presence of static stability at the weighted c.g., in spite of the body instobility contribution ond possible downwash effects, substontiotes the idea that plungo effects con make a large contribution to stability of tandem wings in ground effect.

CONCLUSIONS

1. The image technique appears to be a satisfactory method for testing basic wings in ground effect and it has been possible to isolate the influences of camber and end-plate changes on five basic wings.

2. It has been shown that at aspect ratios of 1, 2 and 4 the maximum L/D in ground effect is associated with small down trailing-edge flap deflection and zero nose droop. Aspect-ratio-1 and -2 wings should employ end plates which have small depth, a contoured section, and a wedge bottom. At a given ground-clearance height, a better L/D is obtained on the aspect-ratio-4 wing with end plates off; however, the difference in absolute clearance of the wing trailing edge should be noted.

3. Maximum L/D at the ground-clearance parameter $h/\sqrt{S} = 0.04$ is approximately double the O.G.E. value of $(L/D)_{max}$ for all five basic wings tested (5% chord depth end plates and zero flap deflection). No correlation of $(L/D)_{max}$ exists at lower values of $h/\sqrt{S}$ where the ratio is higher for the lower-aspect-ratio wings.

4. The 6% thickness ratio aspect-ratio-2 wing has improved L/D over the 11.7% thickness ratio aspect-ratio-2 wing at all lift coefficients below 0.8. The 0.6 taper ratio aspect-ratio-2 wing has slightly higher L/D than the straight wing with end plates off, and slightly lower L/D with end plates on.

5. Tests by the ($\tau = K = 0$) mode show that static stability, lift curve slope, and plunge stability improve as the ground is approached, except at negative angles of attack. A method has been developed

which will allow ($\tau = K = 0$) testing data to be converted to ($\tau = \alpha$) mode data.

6. Ground effect has little influence on characteristics in yaw except for dihedral, which increases as the ground is approached. Rolling moment due to bank angle can be closely estimated from lift data at zero bank.

7. The ground-plane technique appears better suited for development testing of complex configurations. The tandem investigation reported herein was of an exploratory nature and better data could be obtained by utilizing a lighter weight model, higher dynamic pressure, and a more sensitive balance.

8. The tandem wings show large static stability at the ground height parameter $h/\sqrt{S} = 0.06$, in spite of downwash and body instability contributions.

RECOMMENDATIONS

The results obtained in the subject test program have extended the state of the art of wings operating in close proximity to the surface. However, a review of the technology reveals that several other areas of investigation would be highly useful, and the following are recommended:

1. Test the same simple wings over a ground plane to obtain correlation between the image and ground-plane testing techniques.
2. Conduct an investigation of flap configurations and other methods of optimizing maximum lift coefficient of a wing in ground effect.
3. Continue and expand end-plate configurations to optimize the lift/drag ratio.
4. Investigate camber, wing thickness, and thickness distribution effects promoting high L/D, as indicated by results of the present test program.
5. Investigate effects of the propeller slipstream on wing characteristics.
6. Conduct flow visualization, wake surveys and pressure distribution testing to aid in better understanding of the ground-effect phenomenon.
7. Extend the investigation to include wings of conventional aspect ratios, thickness ratios and taper ratios, utilizing the same testing techniques.

8. Test in the (τ = K) mode for values of K other than 0^{o} to extend the application of the CDP concept.

BIBLIOGRAPHY

1. Wieselsberger, C., Wing Resistance Near the Ground, NACA TM 77, 1922.
2. Serebrisky, Y. M. and Biachuev, S. A., Wind Tunnel Investigation of the Horizontal Motion of a Wing Near the Ground, NACA TM 1095, 1946.
3. Fink, M. P. and Lastinger, J. L., Aerodynamic Characteristics of Low Aspect Ratio Wings in Close Proximity to the Ground, NASA TN D-926, July 1961.
4. Carter, Arthur W., Effect of Ground Proximity on the Aerodynamic Characteristics of Aspect Ratio 1 Airfoils With and Without End Plates, NASA TN D-970, October 1961.
5. King, R. W., Low Speed Wind Tunnel Tests of an Aspect Ratio 2 Wing in Ground Effect: Ground Plane Technique, L-47, L-48, Phase II (unpublished Lockheed report).
6. East, A. W., Report on a Research Program on a Low Aspect Ratio Wing in Ground Effect, Lockheed-California Company Report 15484, February 1963.
7. King, R. W., Low Speed Wind Tunnel Tests of Low Aspect Ratio Wings in Ground Effect: Image Technique (unpublished Lockheed report).
8. Onspaugh, C. M., Wind Tunnel Investigation of Single and Tandem Low Aspect Ratio Wings in Ground Effect (U), Lockheed Fluid Dynamics Laboratory Report L-53, May 1963.

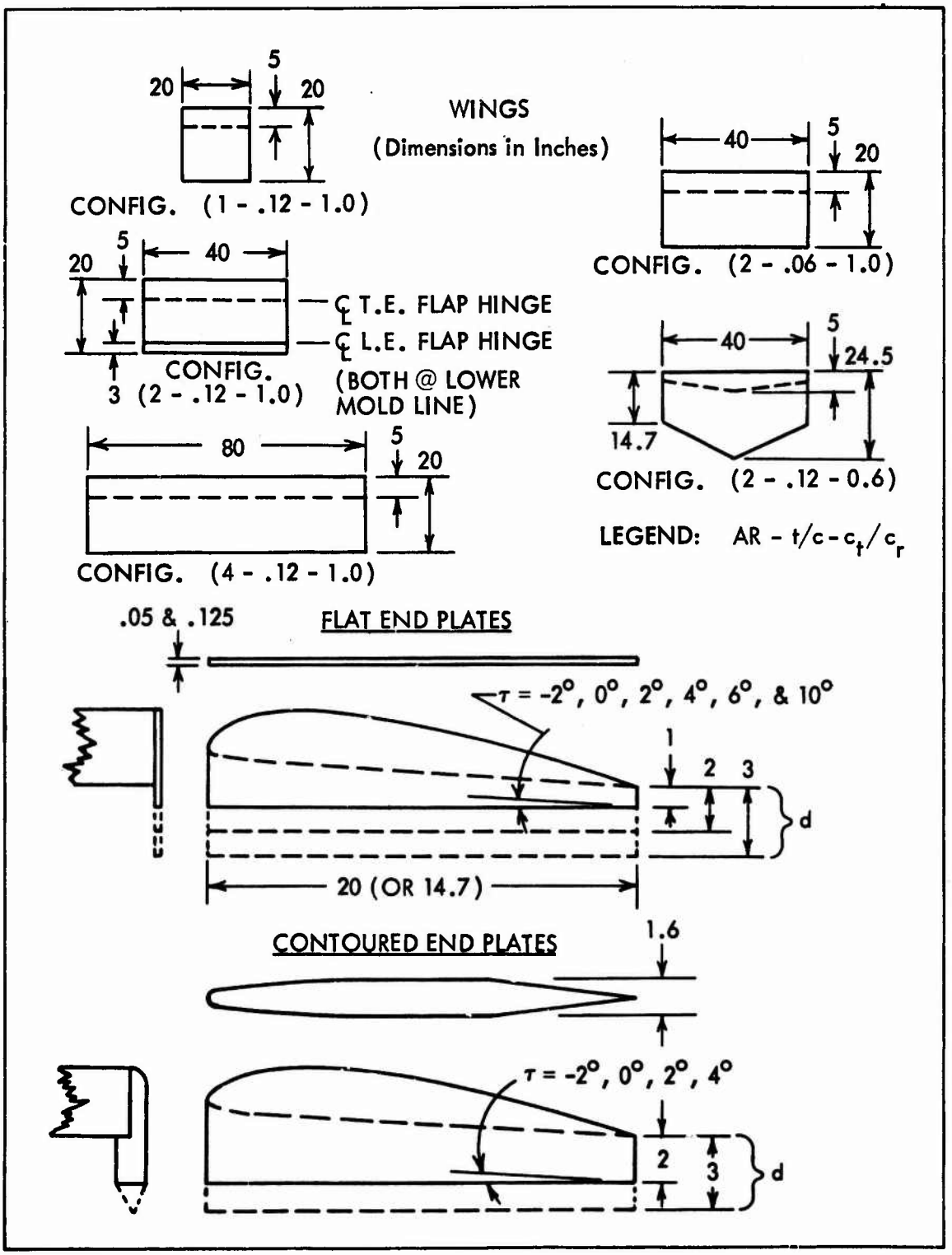

FIGURE 1. WING AND END PLATE CONFIGURATIONS, SINGLE WING.

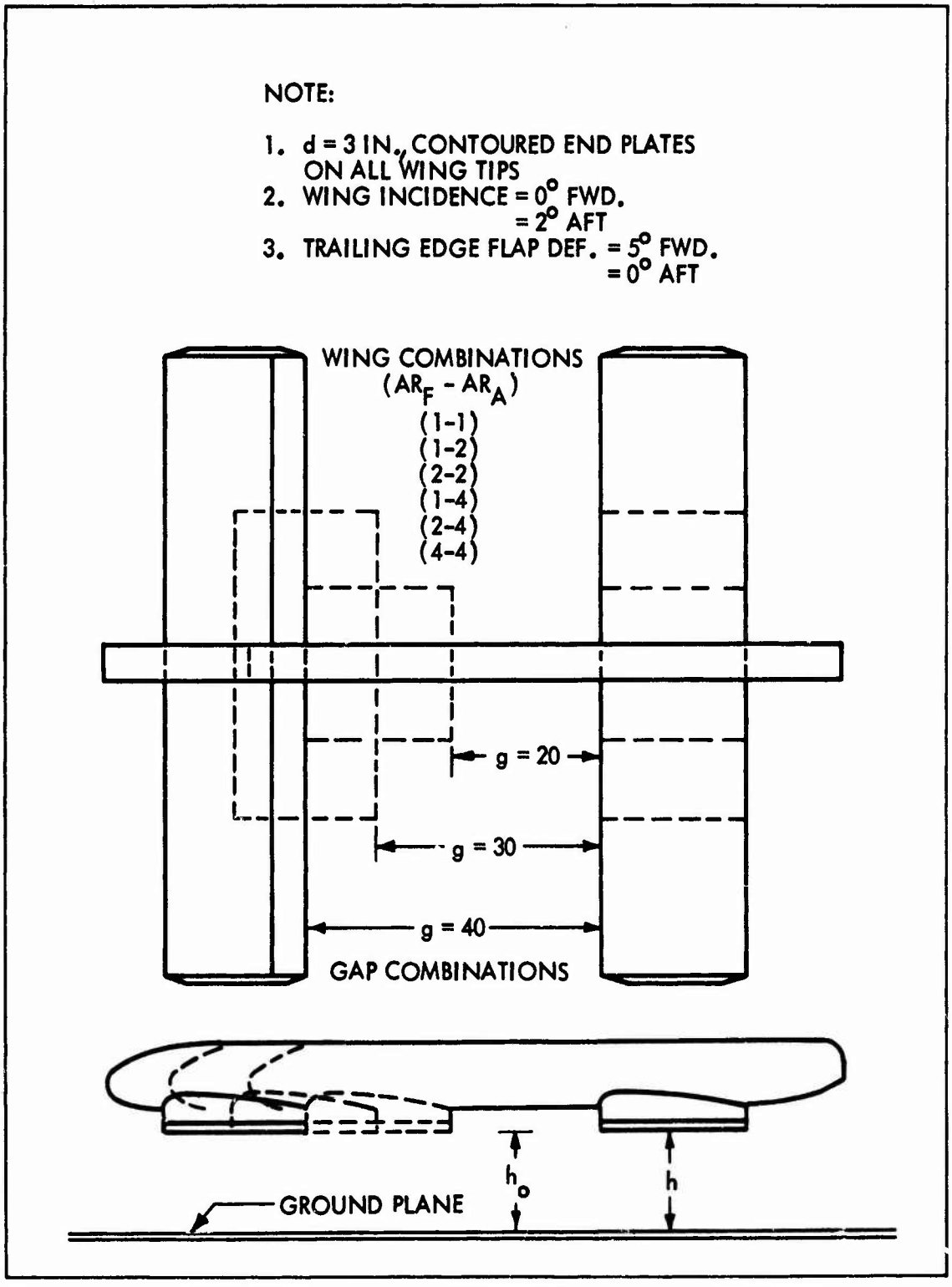

FIGURE 2. TANDEM WING CONFIGURATIONS.

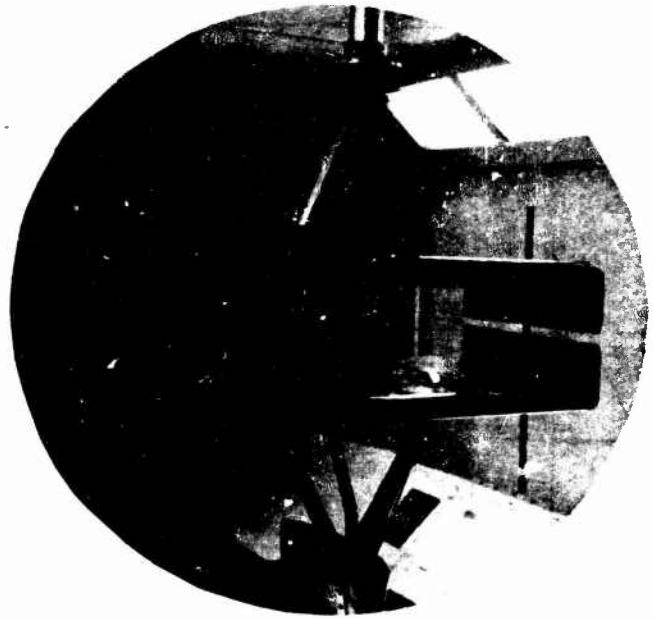

SINGLE WING (IMAGE)

Upper "image" wing support is vertically (and sideways) translatable. Lower wing is mounted to regular tunnel balance support system. Model shown is wing (2- .12- 1.0) with contour plus wedge end plates.

TANDEM WINGS (GROUND PLANE)

Model is supported by sting support and is poised over false tunnel floor serving as ground plane. Model shown is configuration (2 - 4) with gap ratio, g/c=2.0.

FIGURE 3. TYPICAL MODEL-TEST INSTALLATIONS

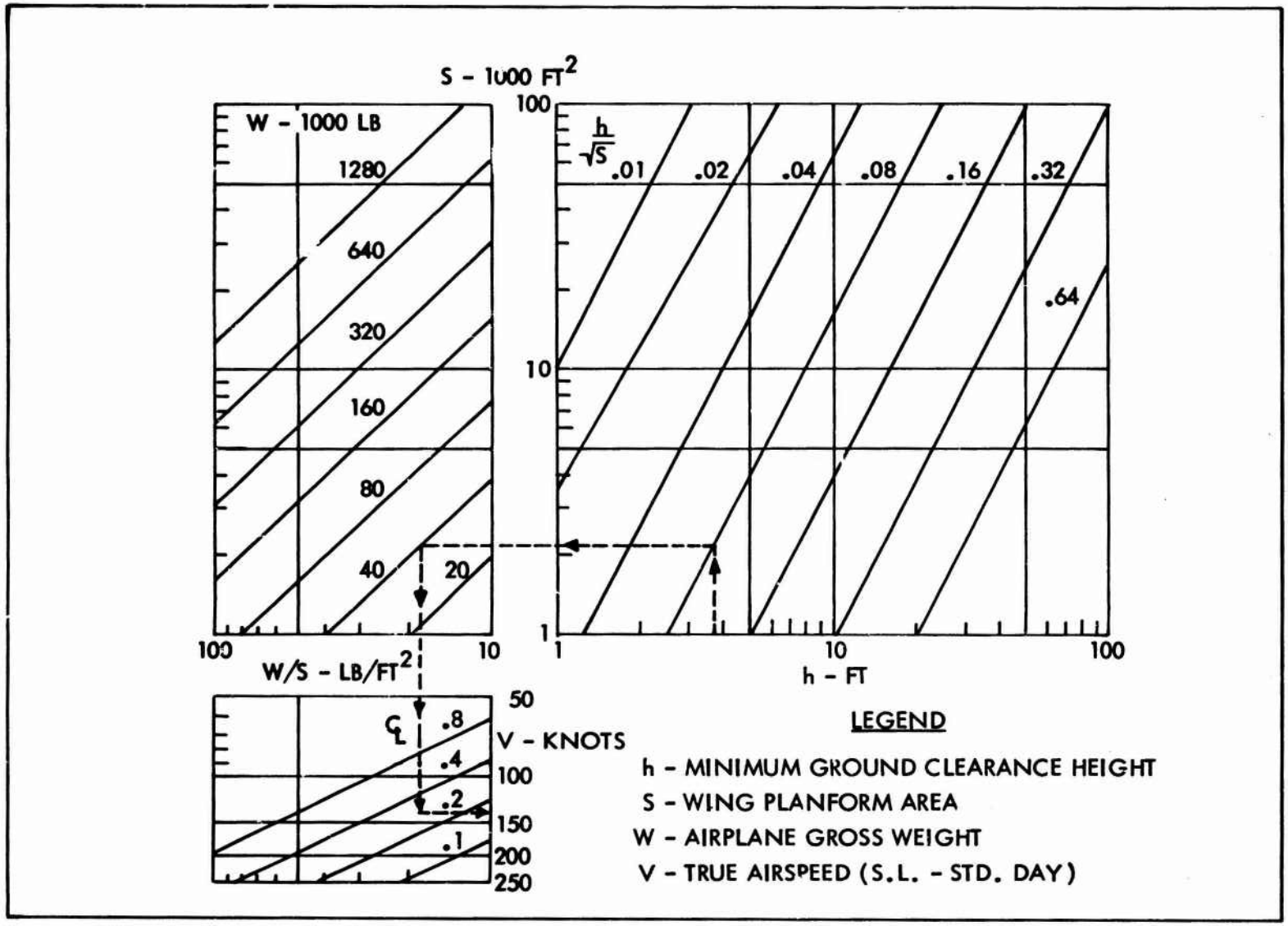

FIGURE 4. OPERATIONAL DESIGN CHART FOR C_L AND $h/\sqrt{S}$.

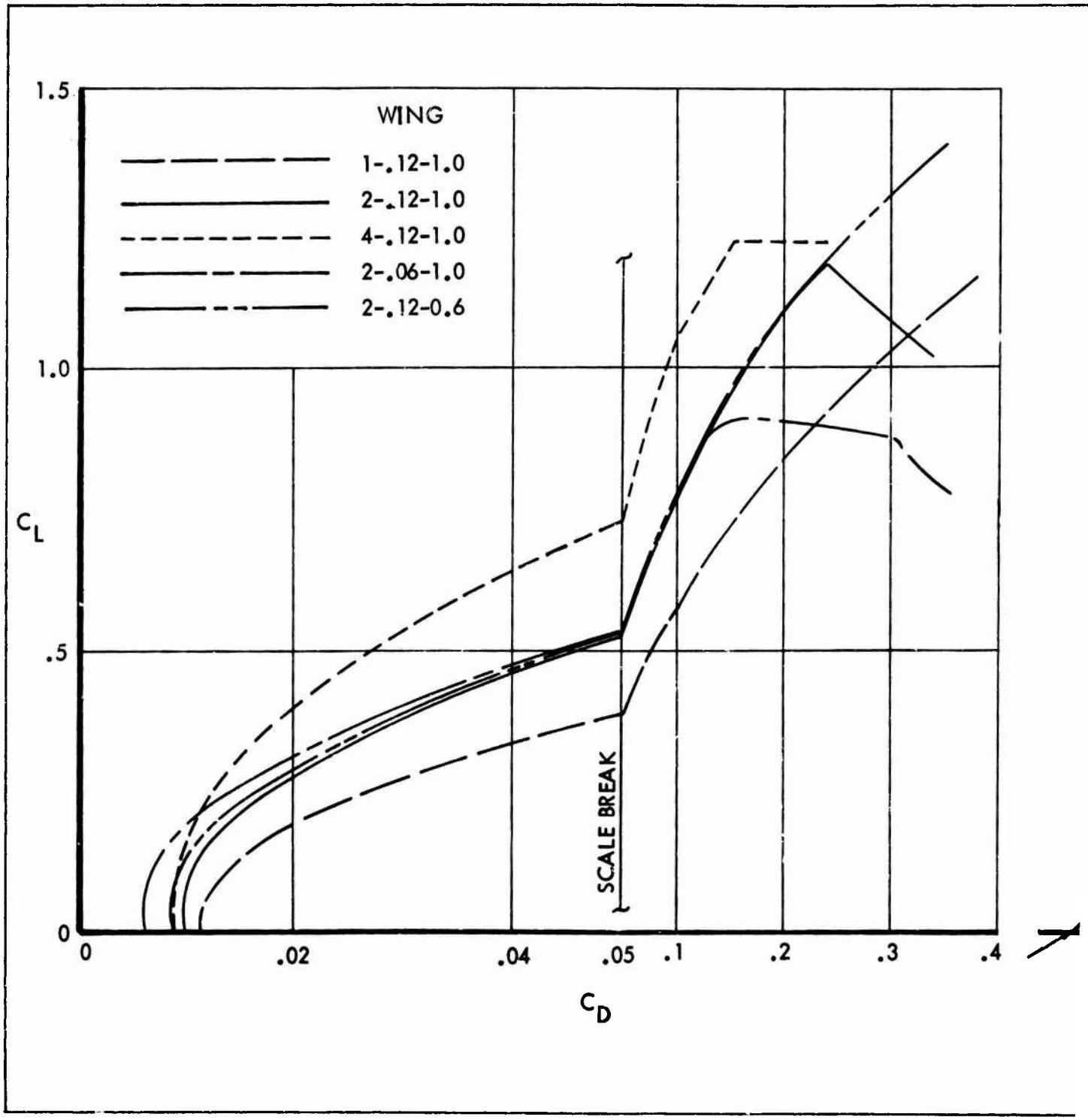
WING
1-.12-1.0
2-.12-1.0
4-.12-1.0
2-.06-1.0
2-.12-0.6
1.5
1.0
.5
0
C_L
0
.02
.04
.05
.1
.2
.3
.4
C_D
SCALE BREAK

FIGURE 5.

A

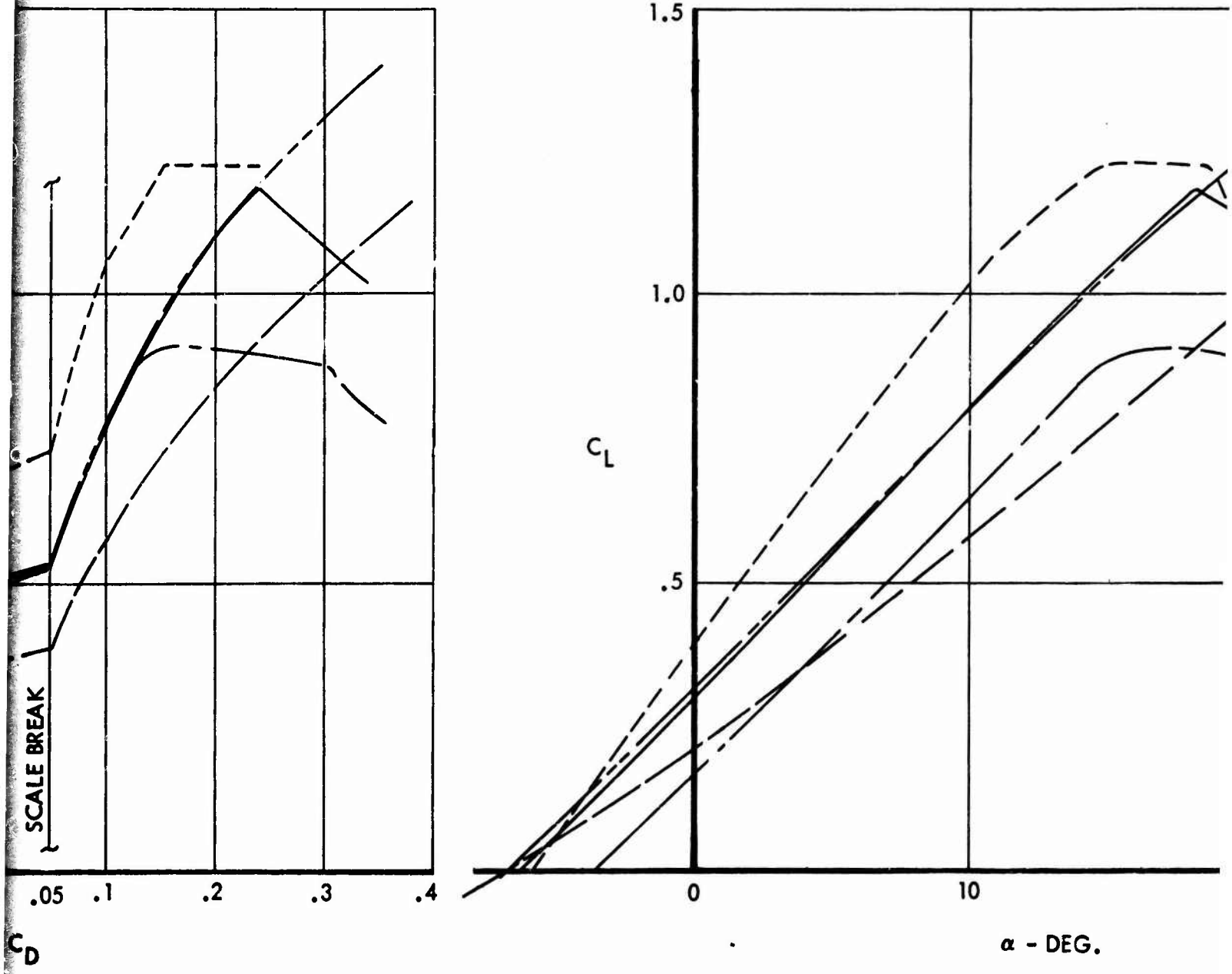

FIGURE 5. WINGS WITHOUT END PLATES, O. G. E.

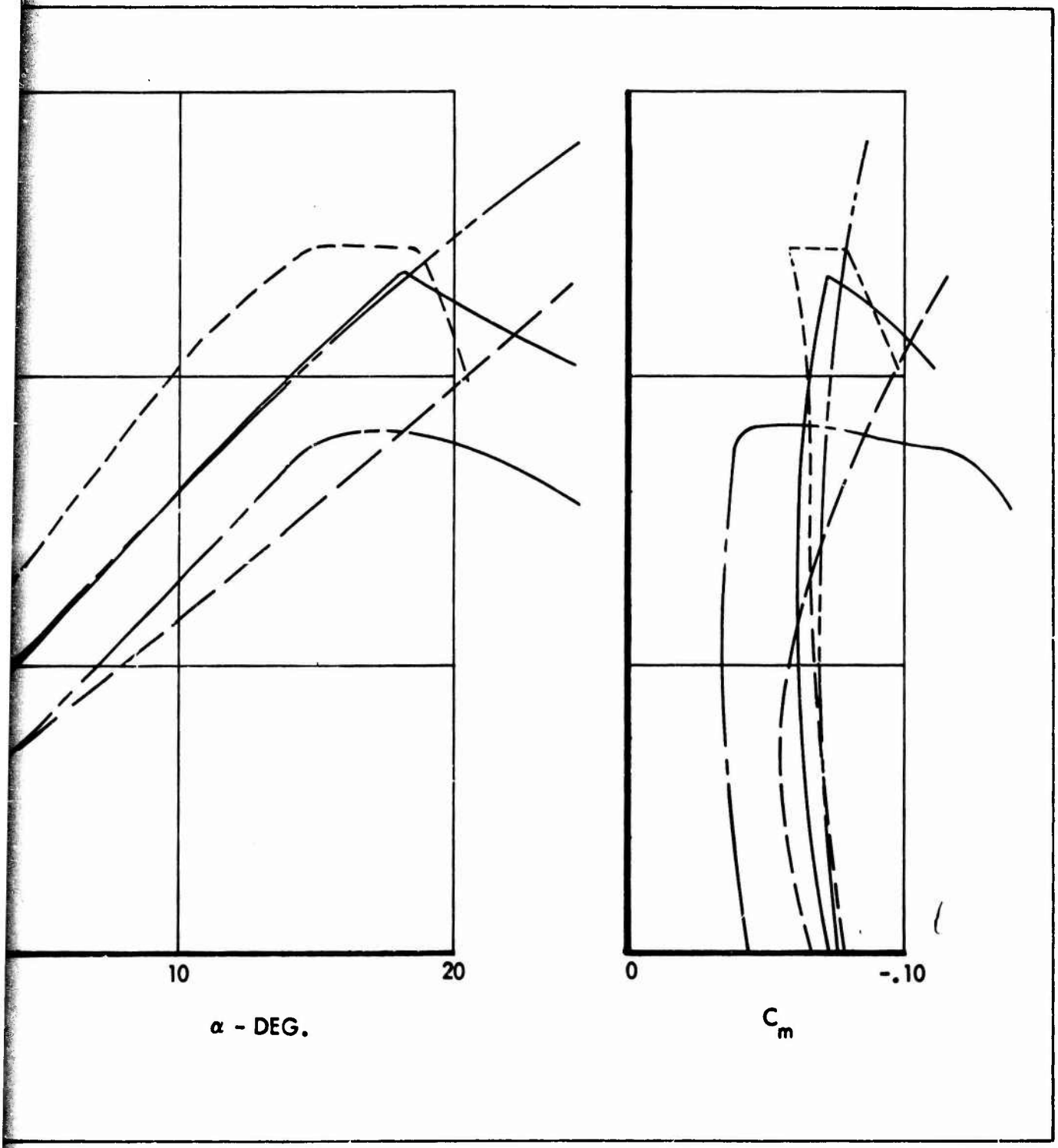

LATES, O.G.E.

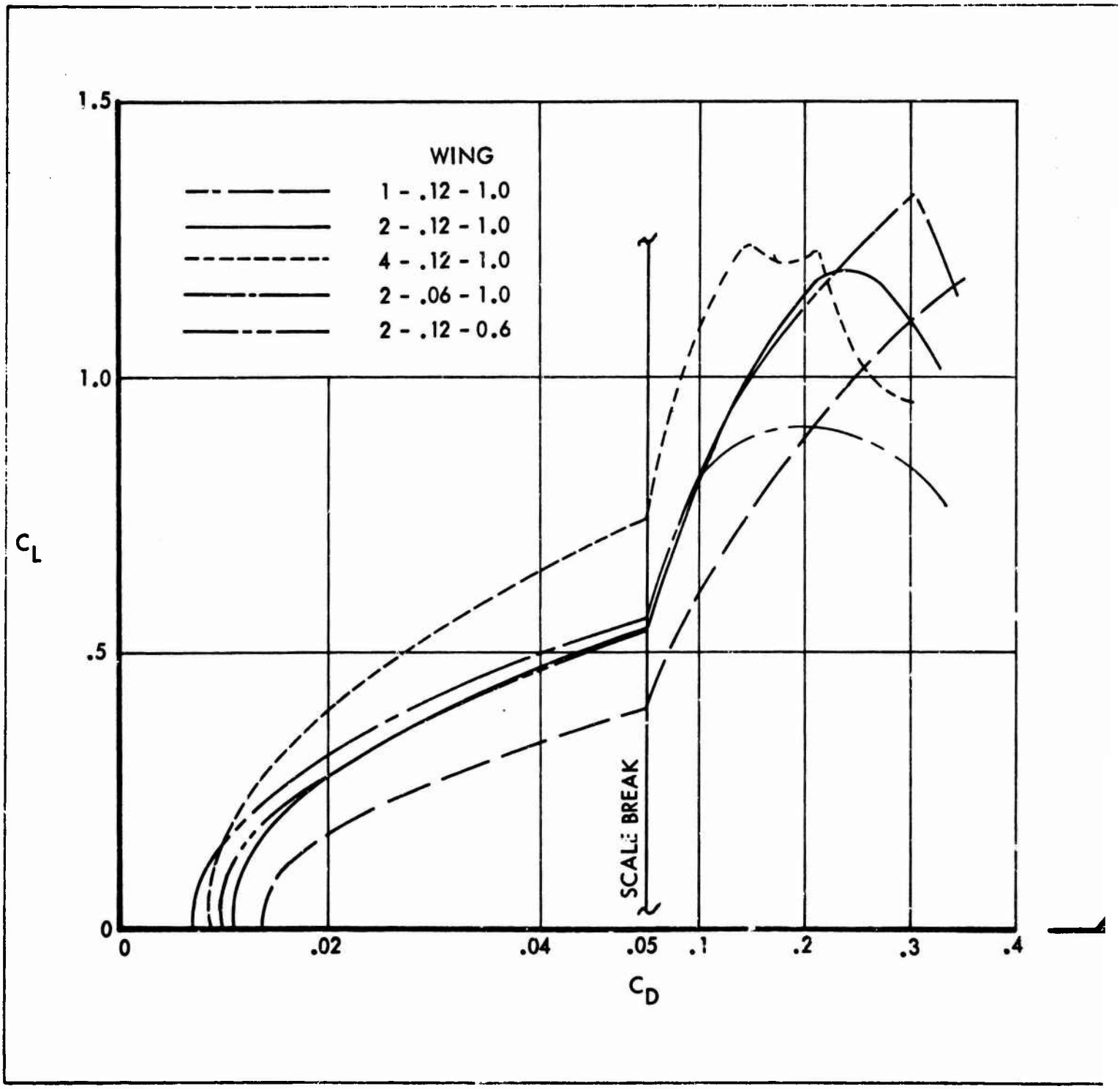

FIGURE 6. WINGS WIT

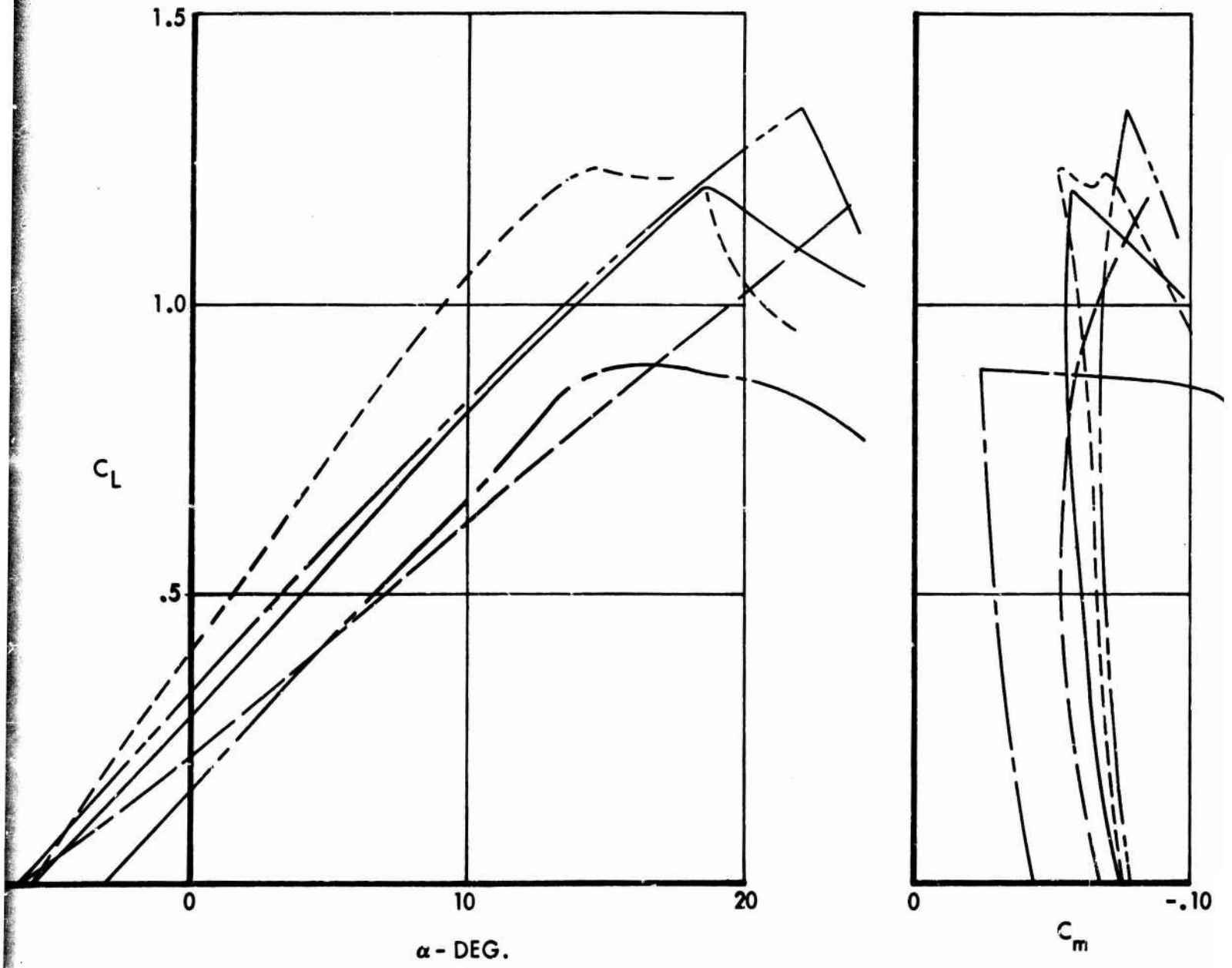

TH FLAT END PLATES (d/c = .10), O. G.E.

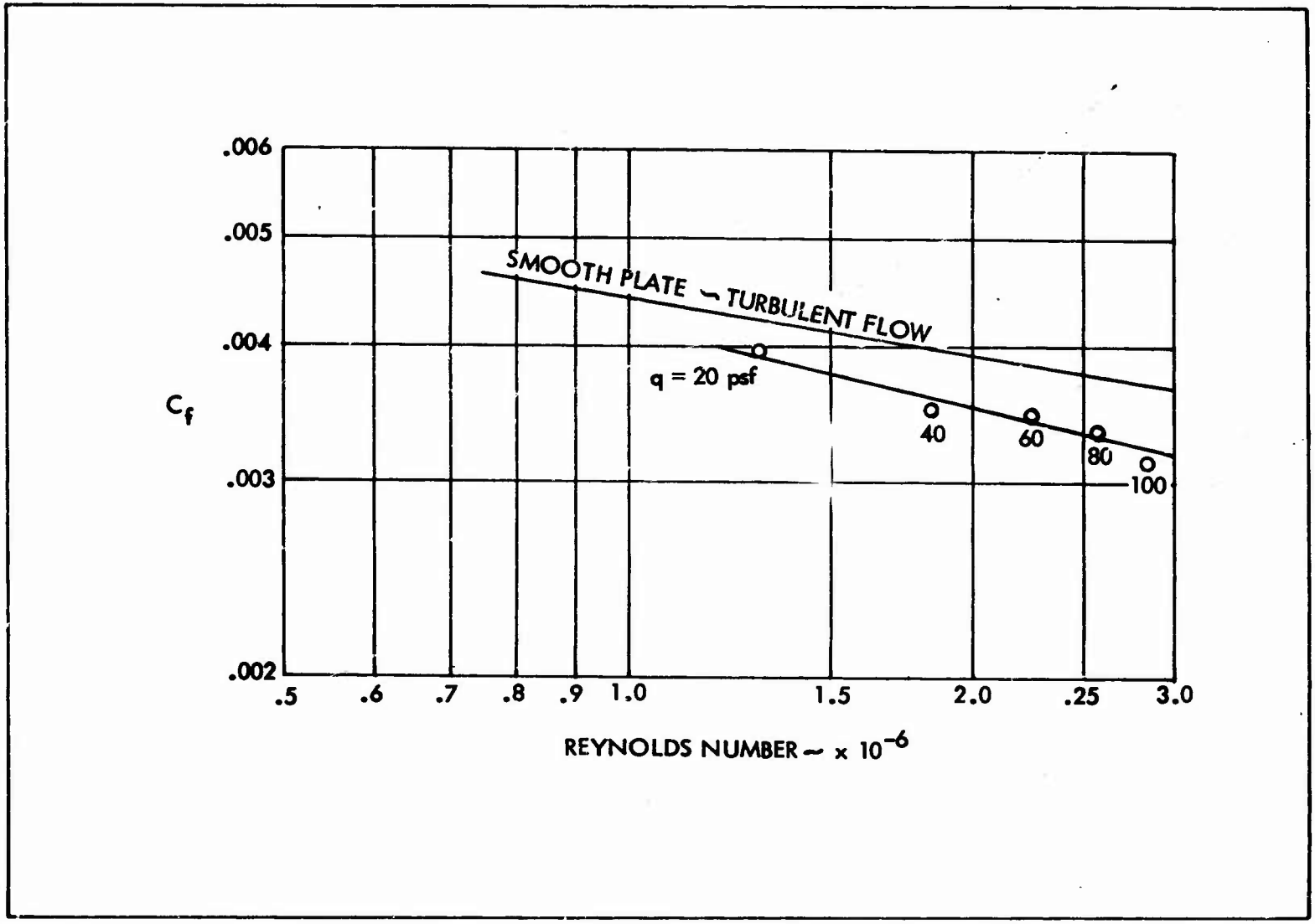

FIGURE 7. EFFECT OF REYNOLDS NUMBER ON SKIN FRICTION DRAG, WING (2-.12-1.0) WITH CONTOURED END PLATES (d/c = .15).

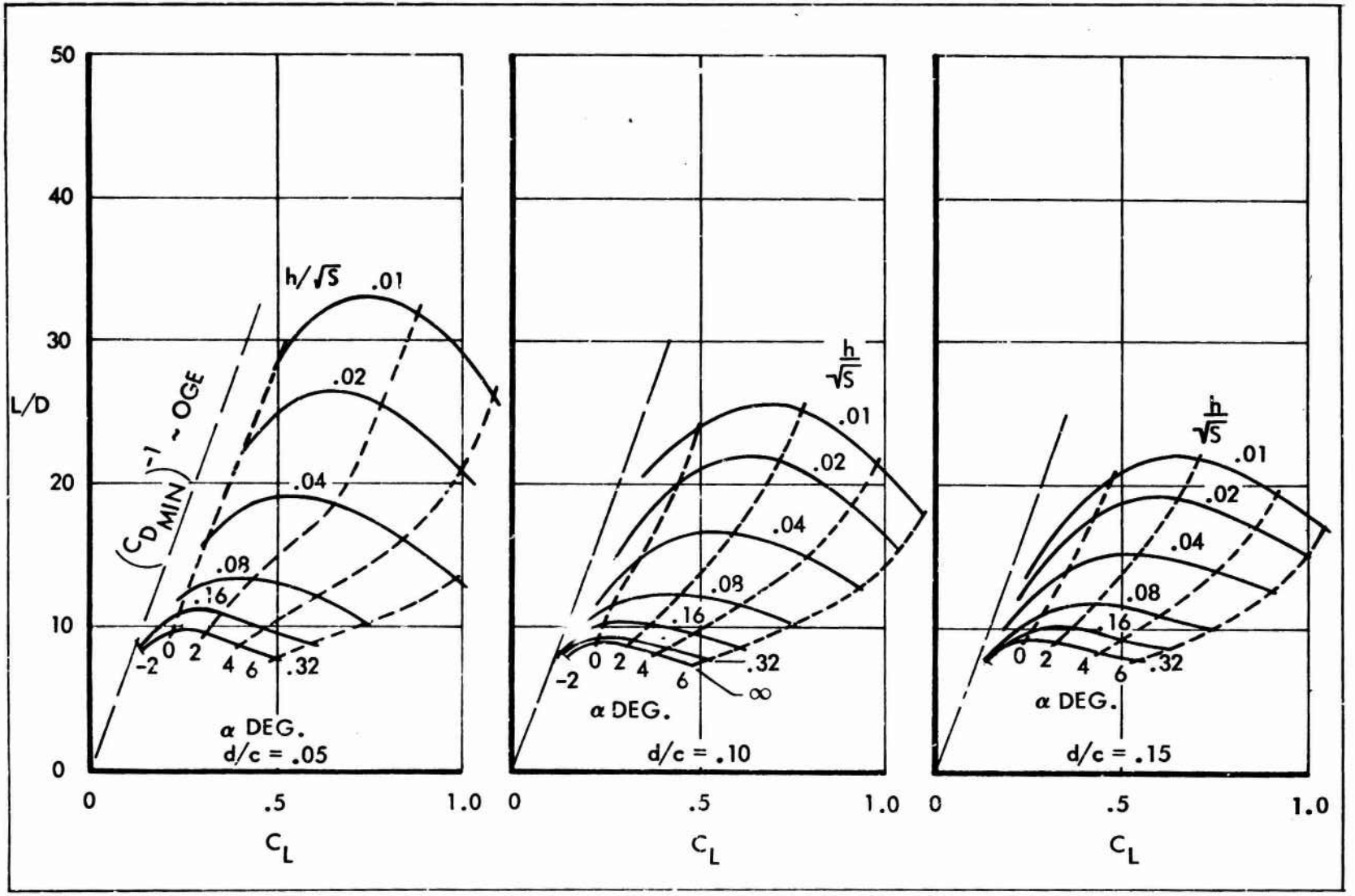

FIGURE 8. WING (1-.12-1.0), DEPTH OF FLAT END PLATES.

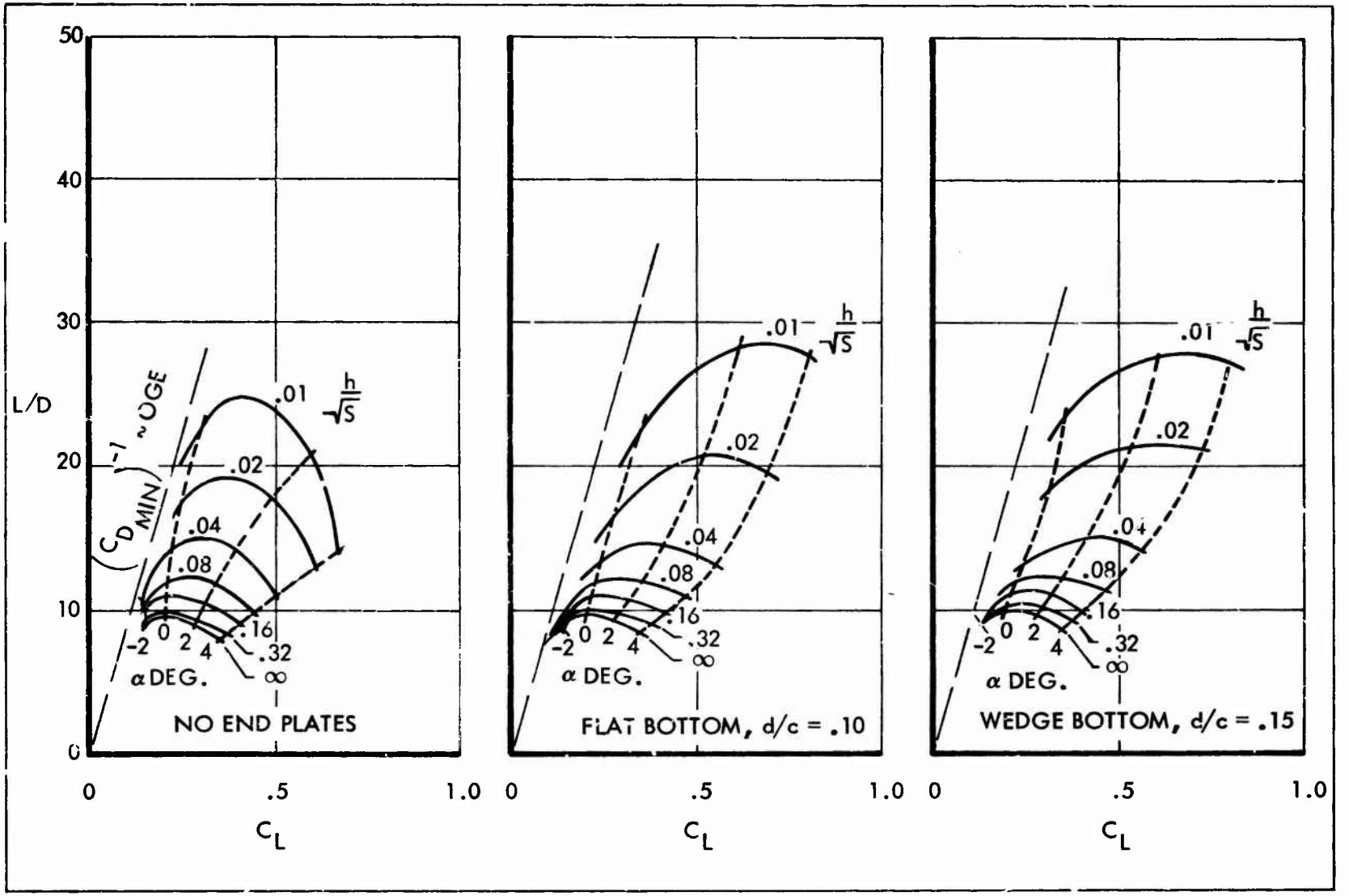

FIGURE 9. WING (1-.12-1.0), NO END PLATES & CONTOURED END PLATES.

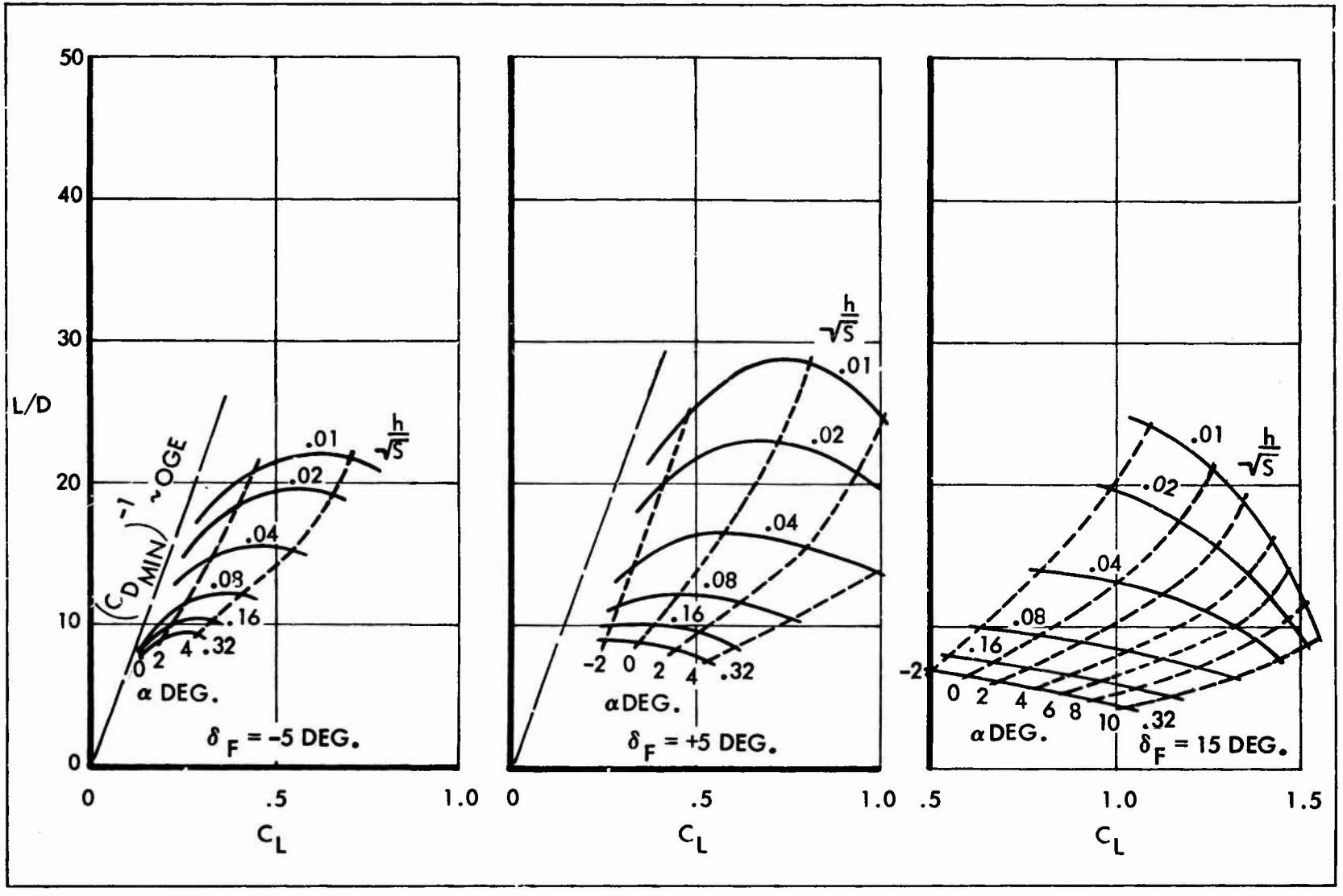

FIGURE 10. WING (1-.12-1.0) FLAP DEFLECTION, FLAT END PLATES (d/c = .10).

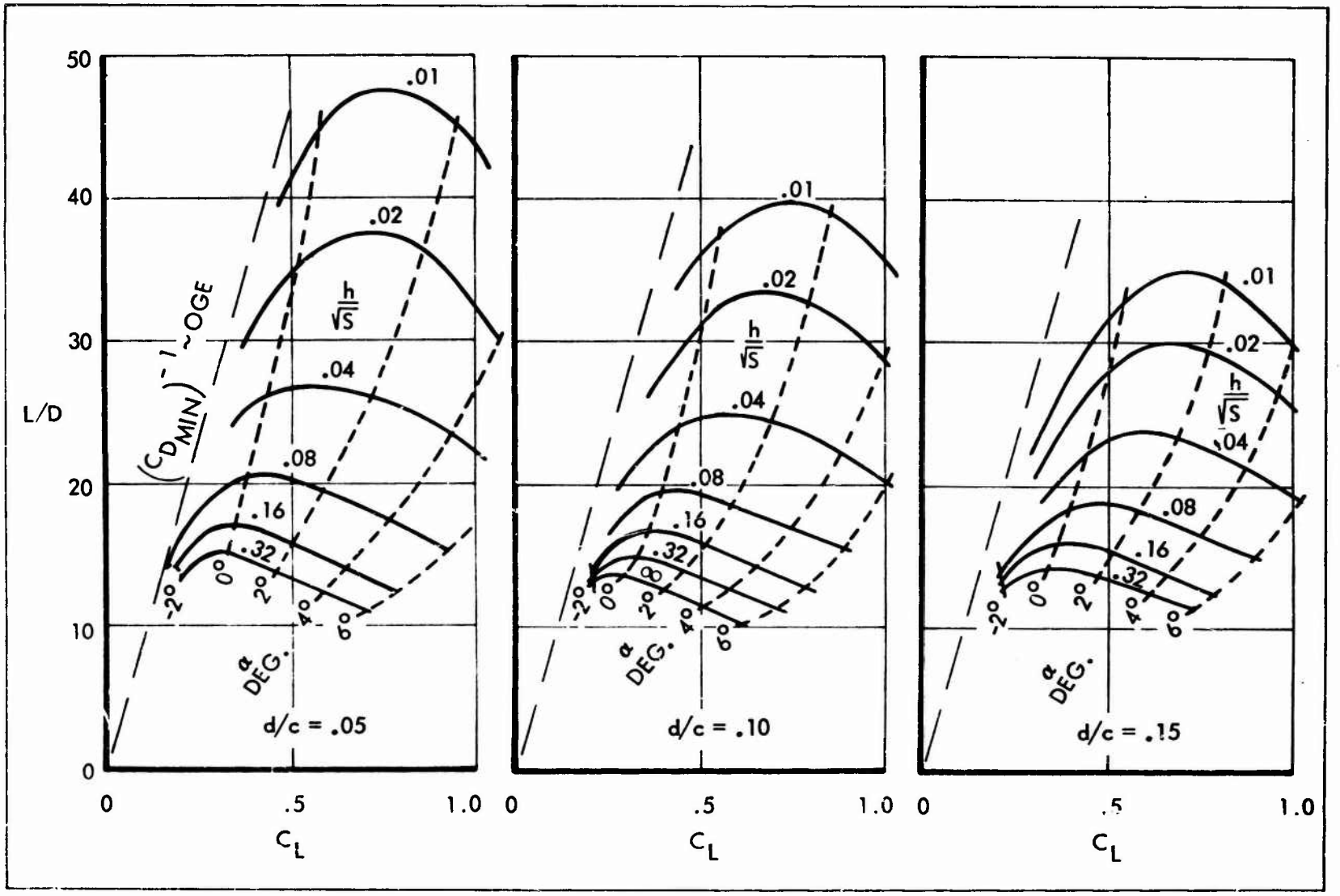

FIGURE 11. WING (2-.12-1.0), DEPTH OF FLAT END PLATES.

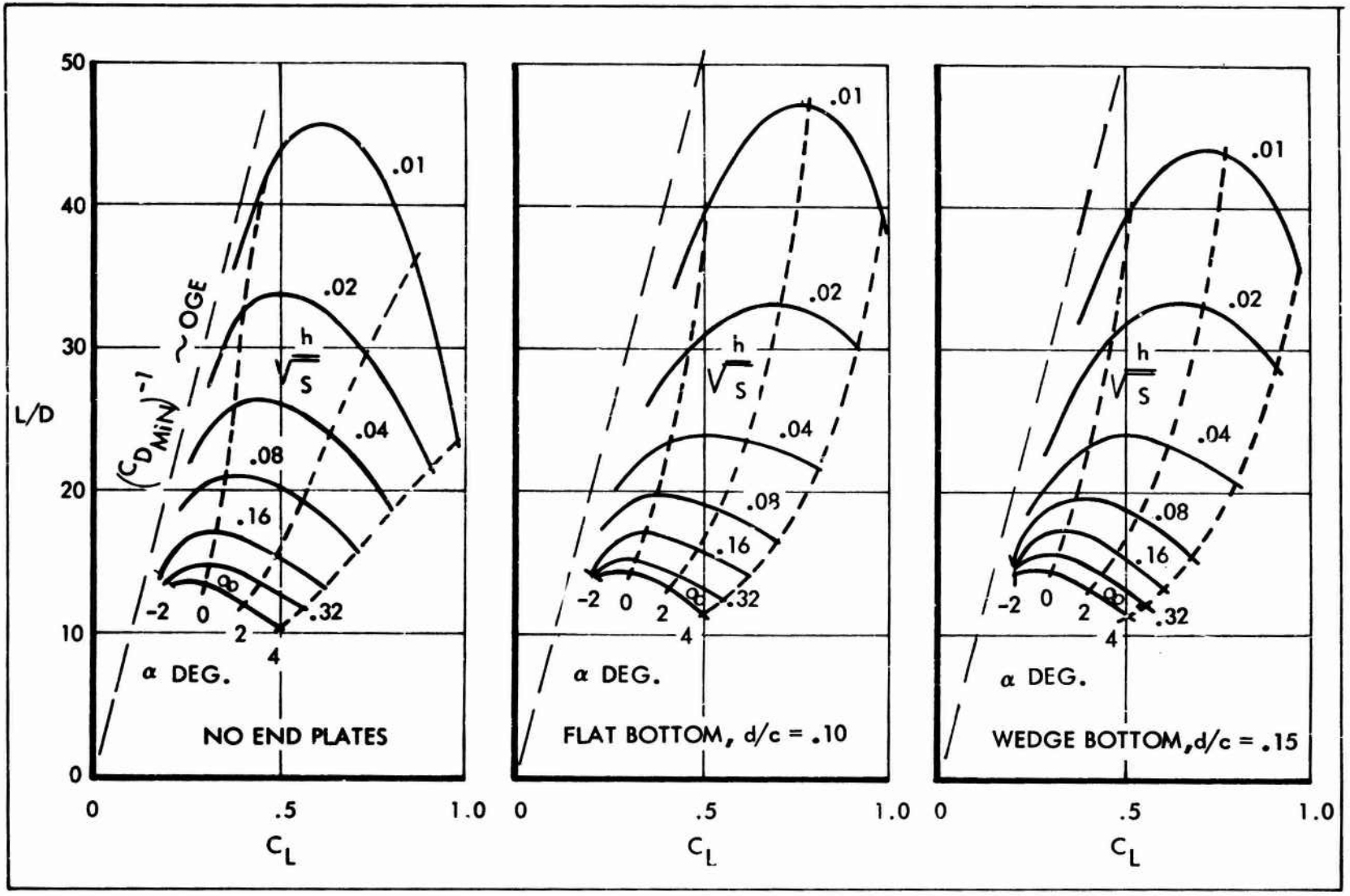

FIGURE 12. WING (2-.12-1.0), NO END PLATES & CONTOURED END PLATES.

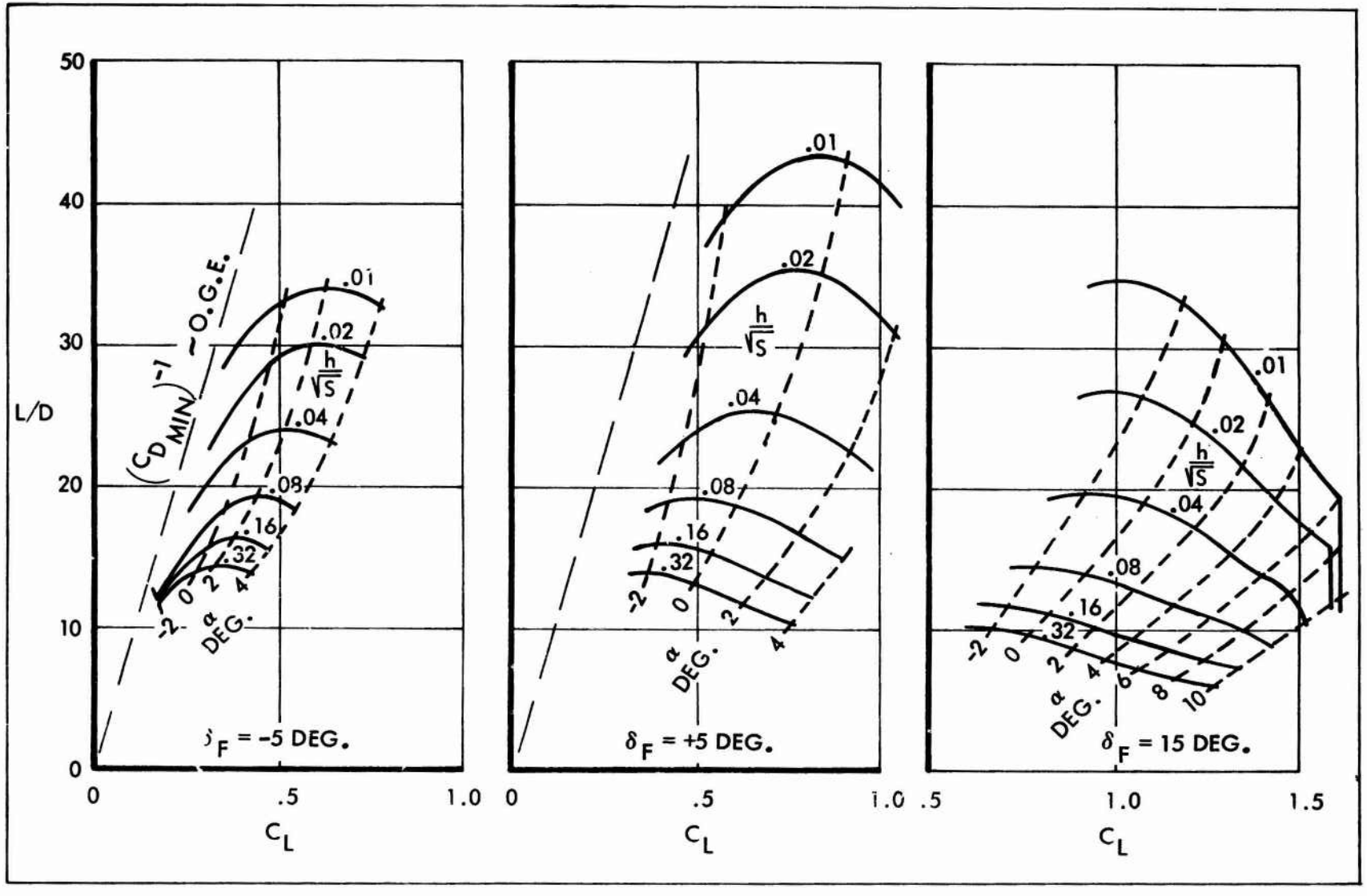

FIGURE 13. WING (2-.12-1.0), FLAP DEFLECTION, FLAT END PLATES (d/c = .10).

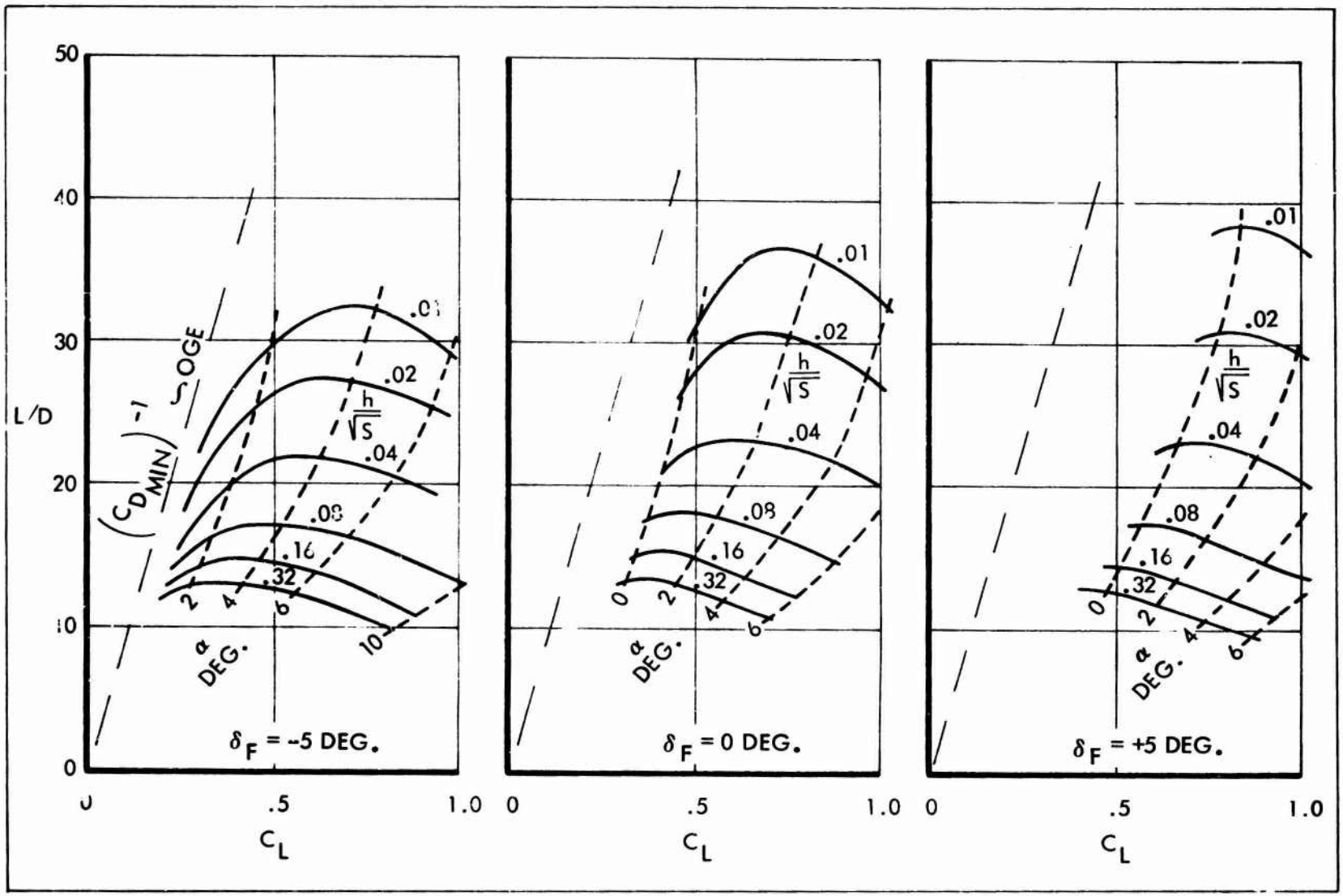

FIGURE 14. WING (2-.12-1.0), FLAP DEFLECTION, FLAT END PLATES (d/c = .10), 5° NOSE DROOP.

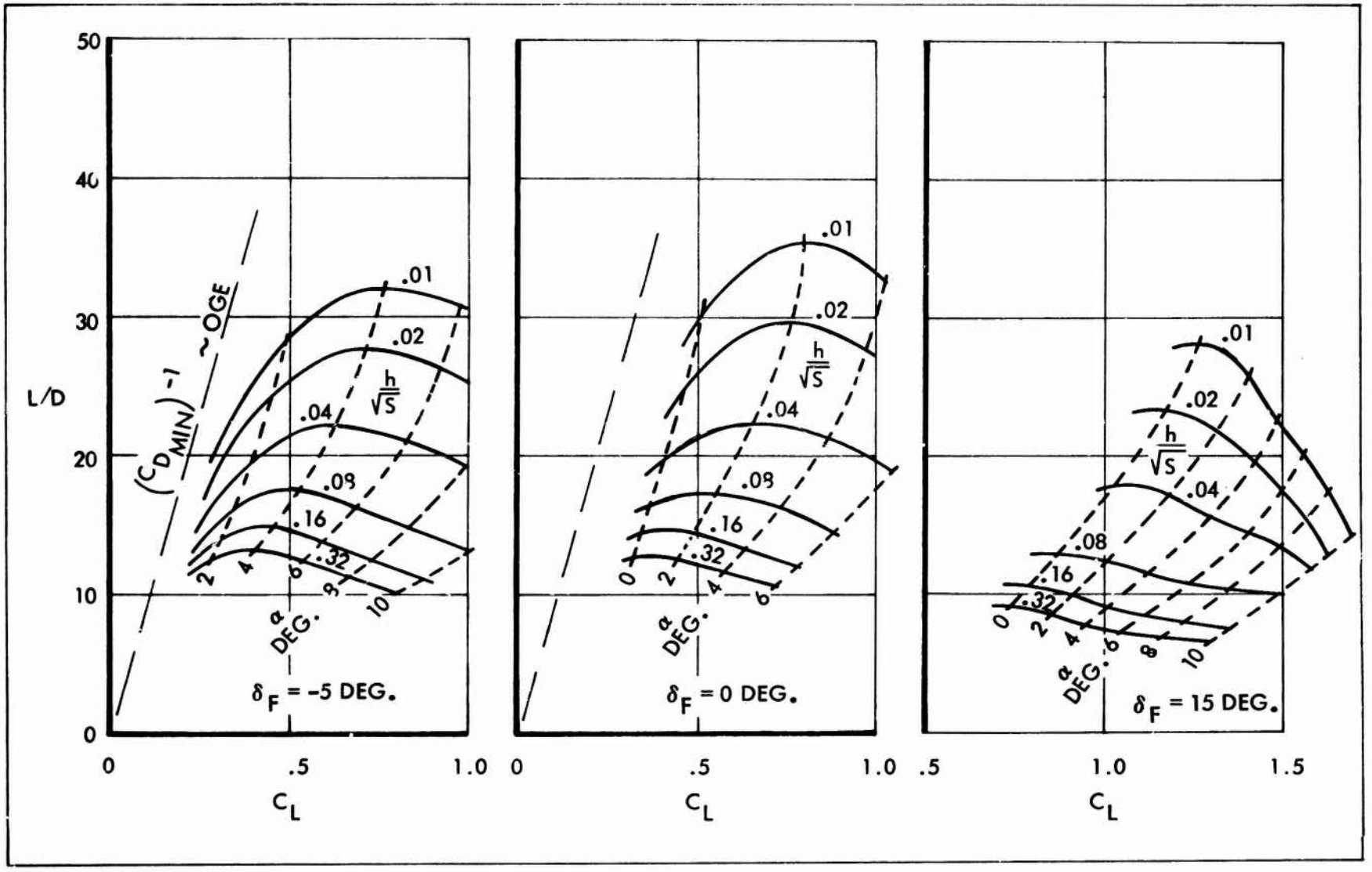

FIGURE 15. WING (2-.12-1.0), FLAP DEFLECTION, FLAT END PLATES (d/c = .10), 10° NOSE DROOP.

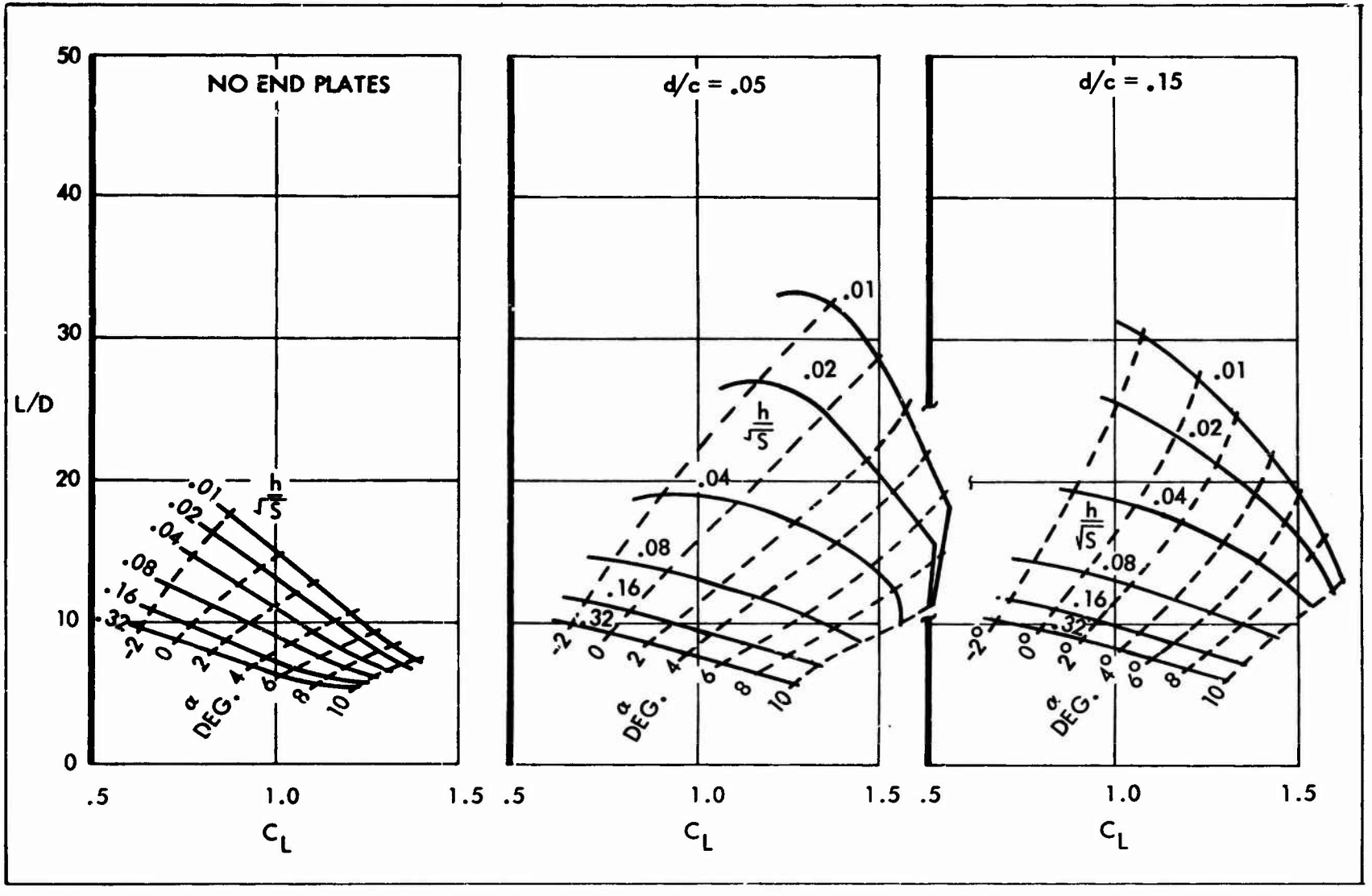

FIGURE 16. WING (2-.12-1.0), DEPTH OF FLAT END PLATES, 15° FLAP DEFLECTION.

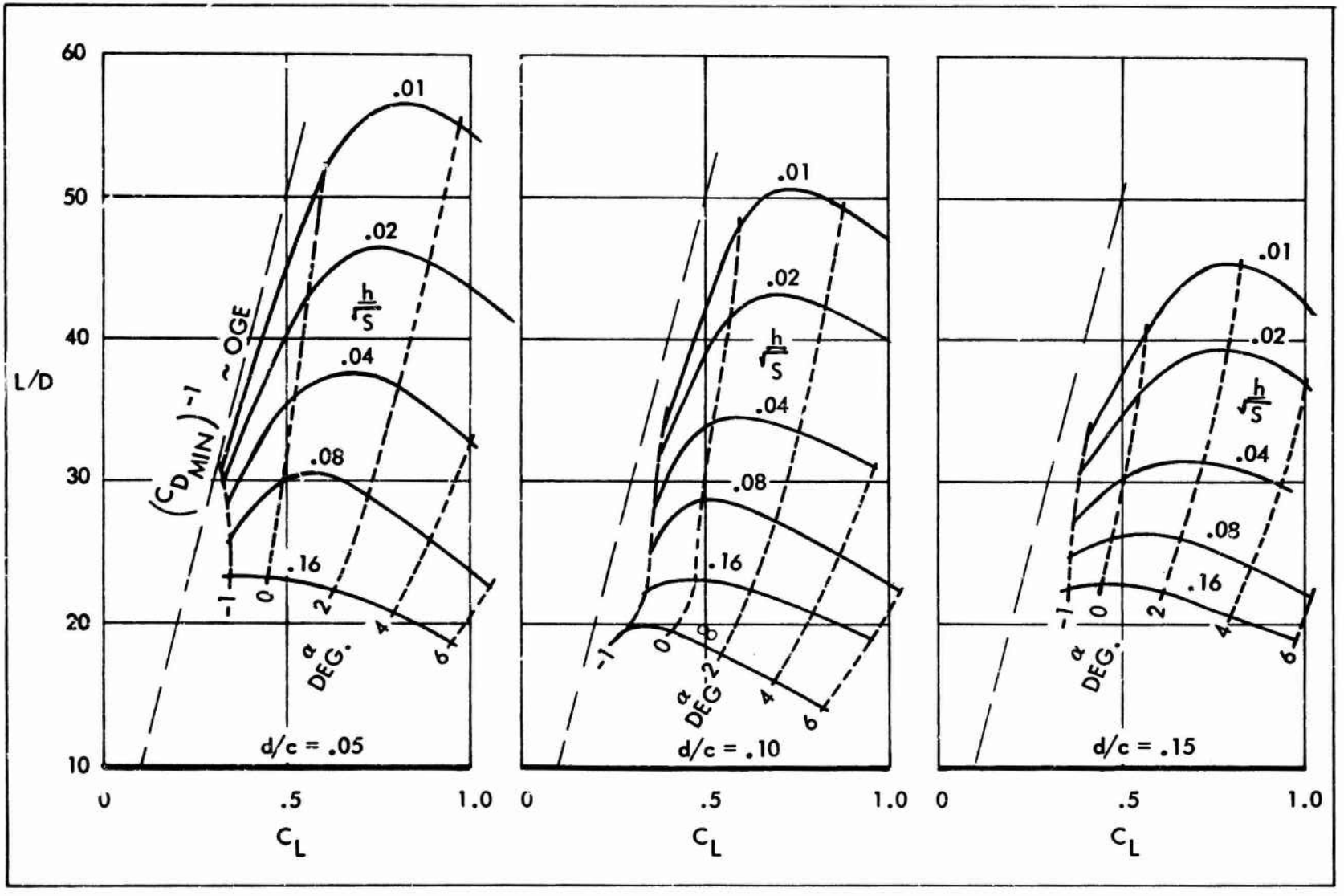

FIGURE 17. WING (4-.12-1.0), DEPTH OF FLAT END PLATES.

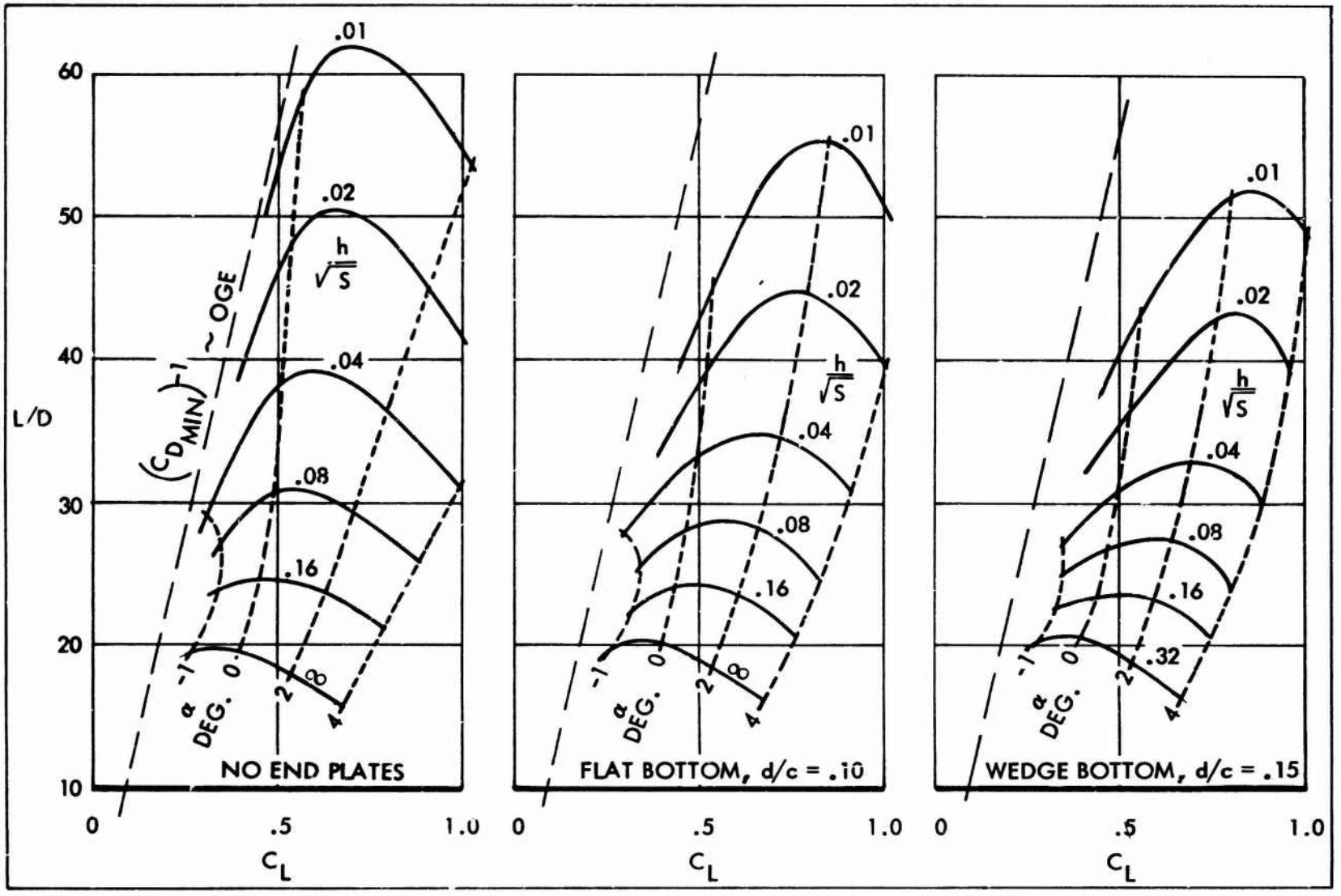

FIGURE 18. WING (4-.12-1.0), NO END PLATES & CONTOURED END PLATES.

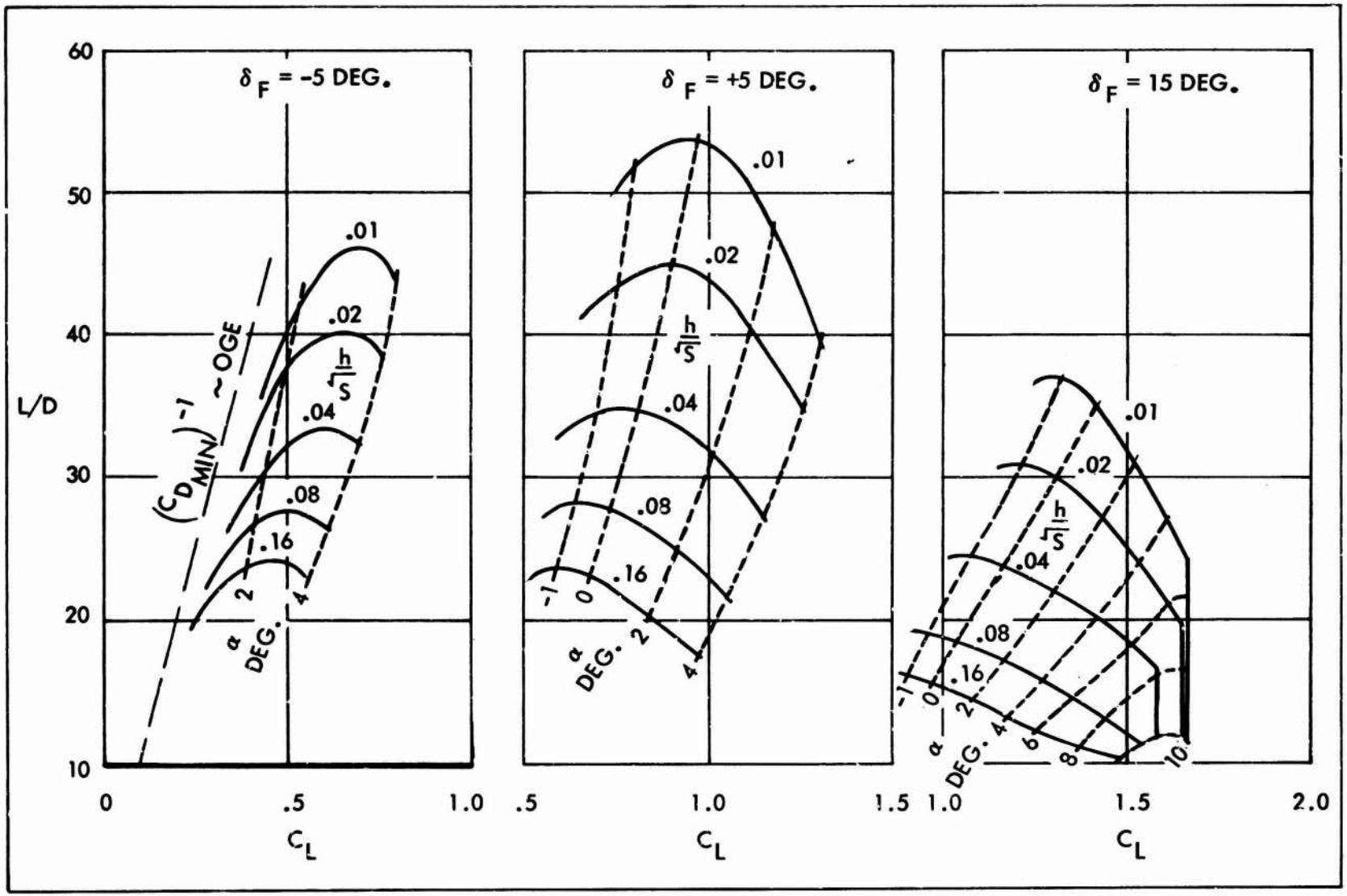

FIGURE 19. WING (4-.12-1.0), FLAP DEFLECTION, FLAT END PLATES (d/c = .10).

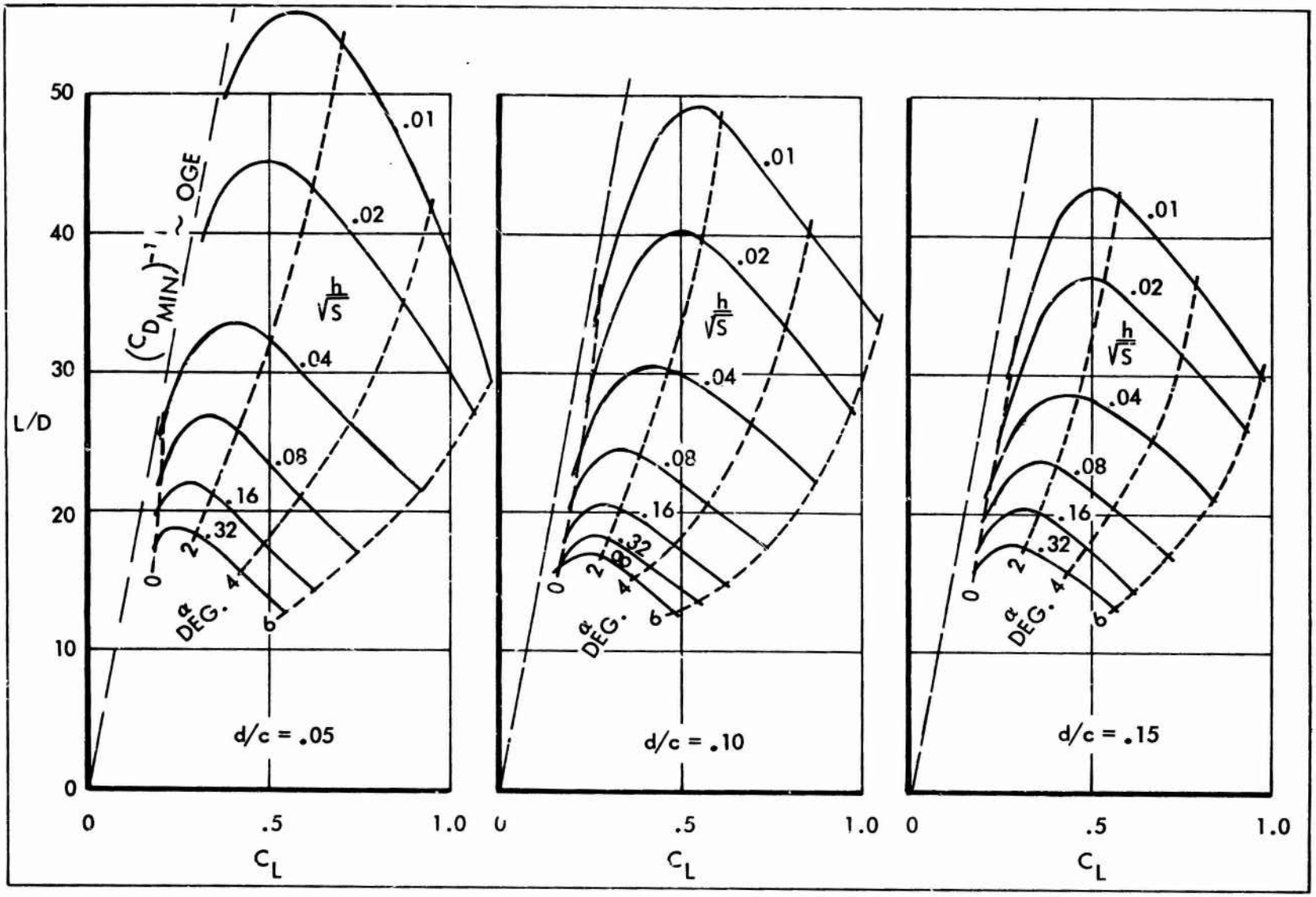

FIGURE 20. WING (2-.06-1.0), DEPTH OF FLAT END PLATES.

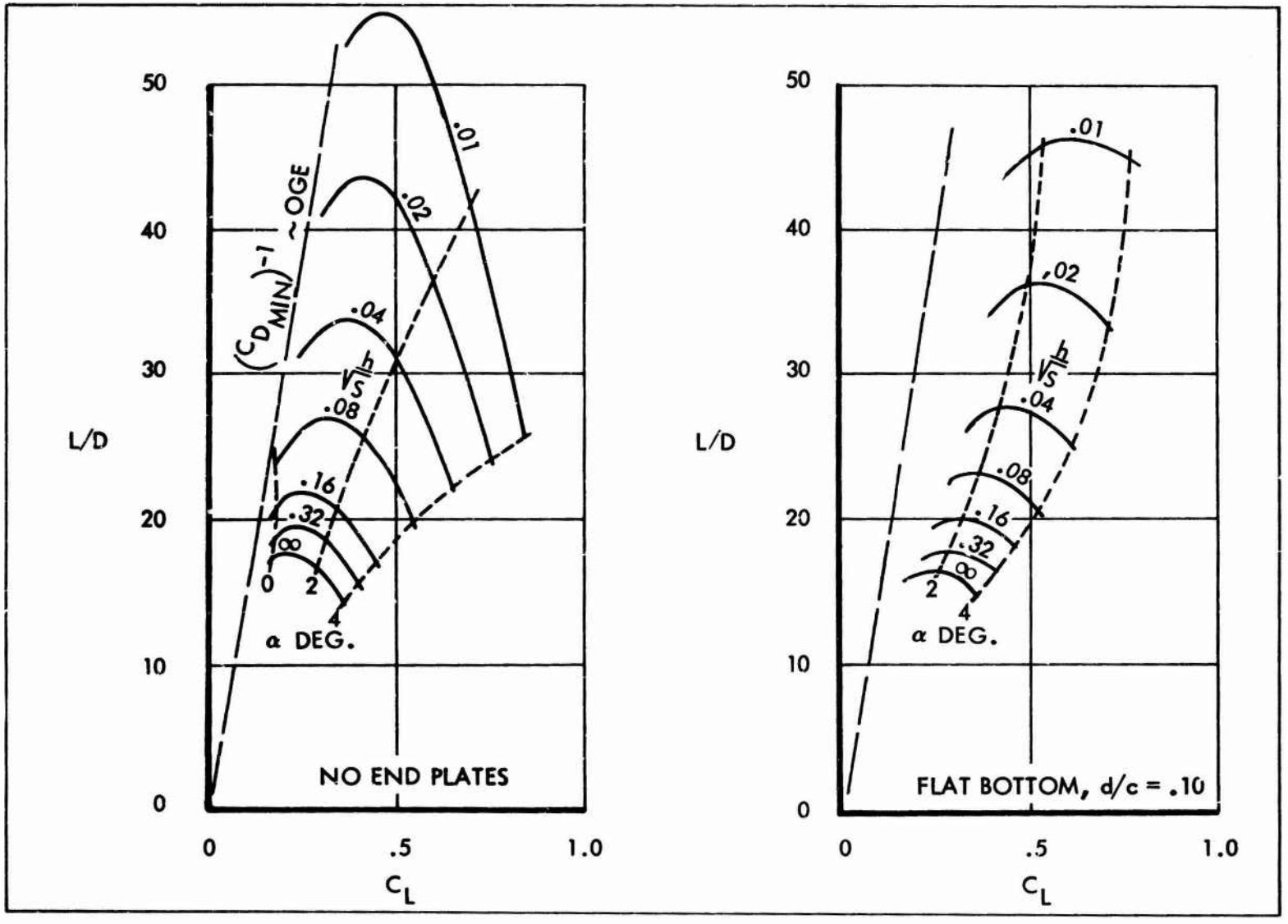

FIGURE 21. WING (2-.06-1.0), NO END PLATES & CONTOURED END PLATES.

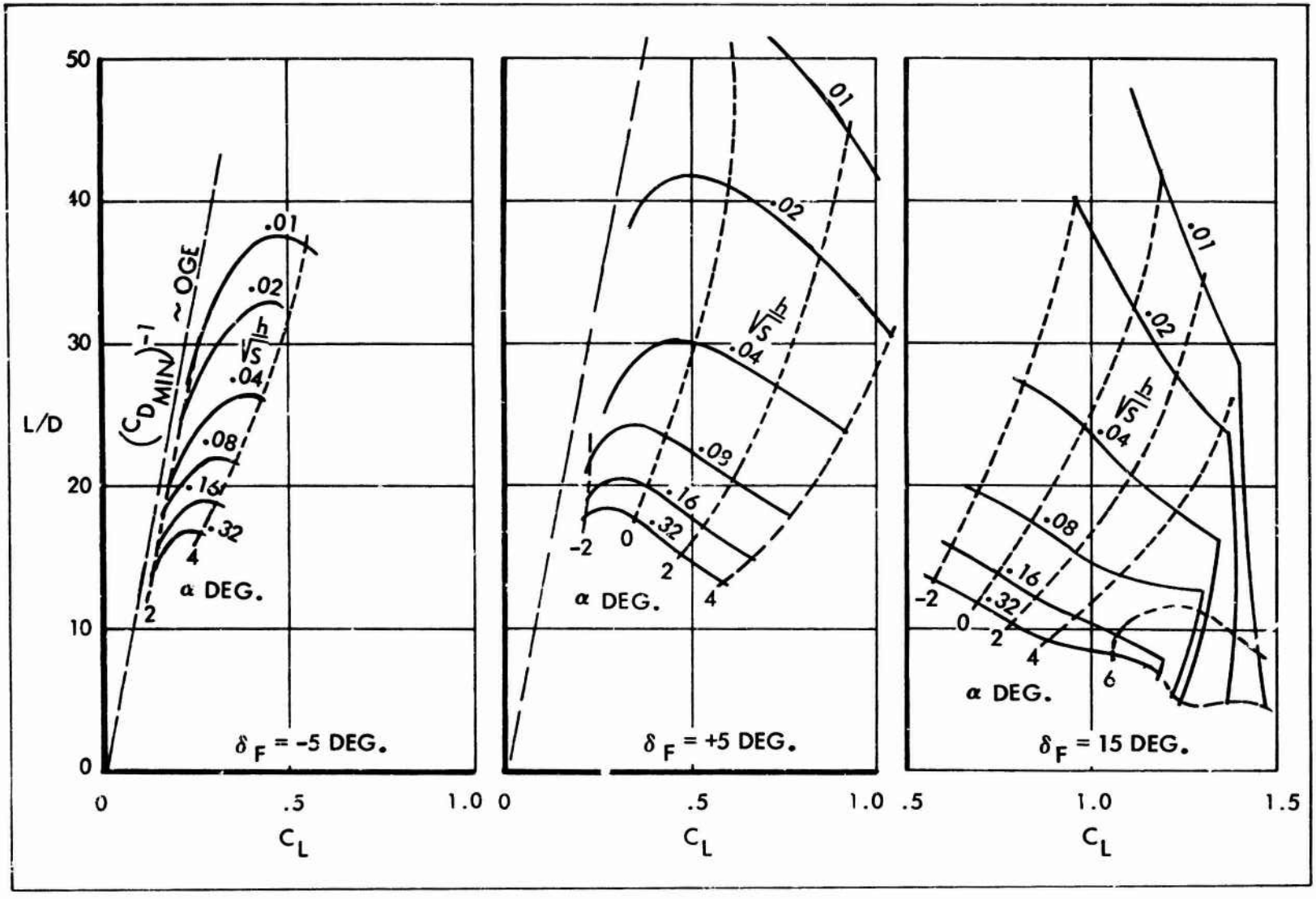

FIGURE 22. WING (2-.06-1.0), FLAP DEFLECTION, FLAT END PLATES (d/c = .10).

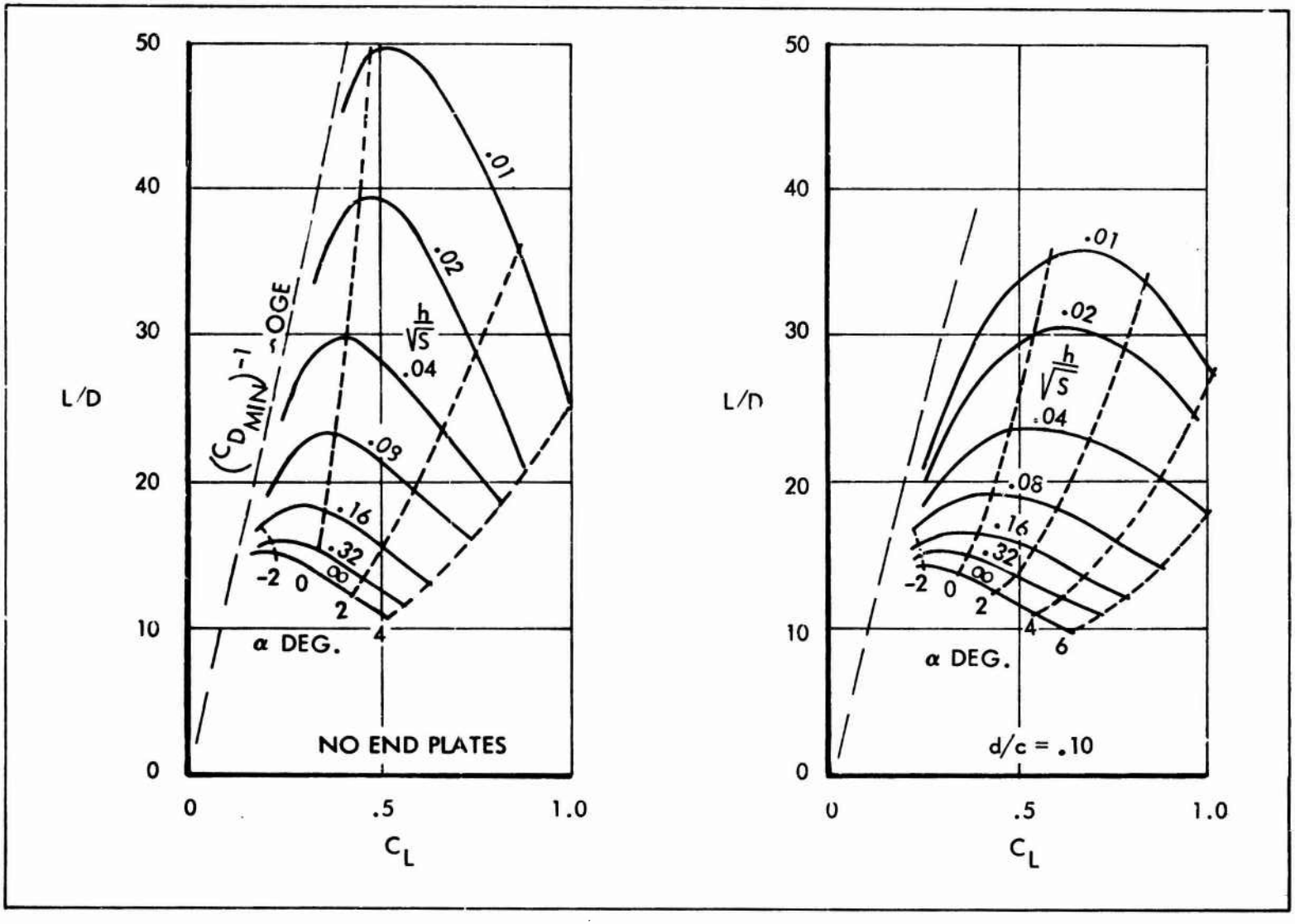

FIGURE 23. WING (2-.12-0.6), NO END PLATES, FLAT END PLATES.

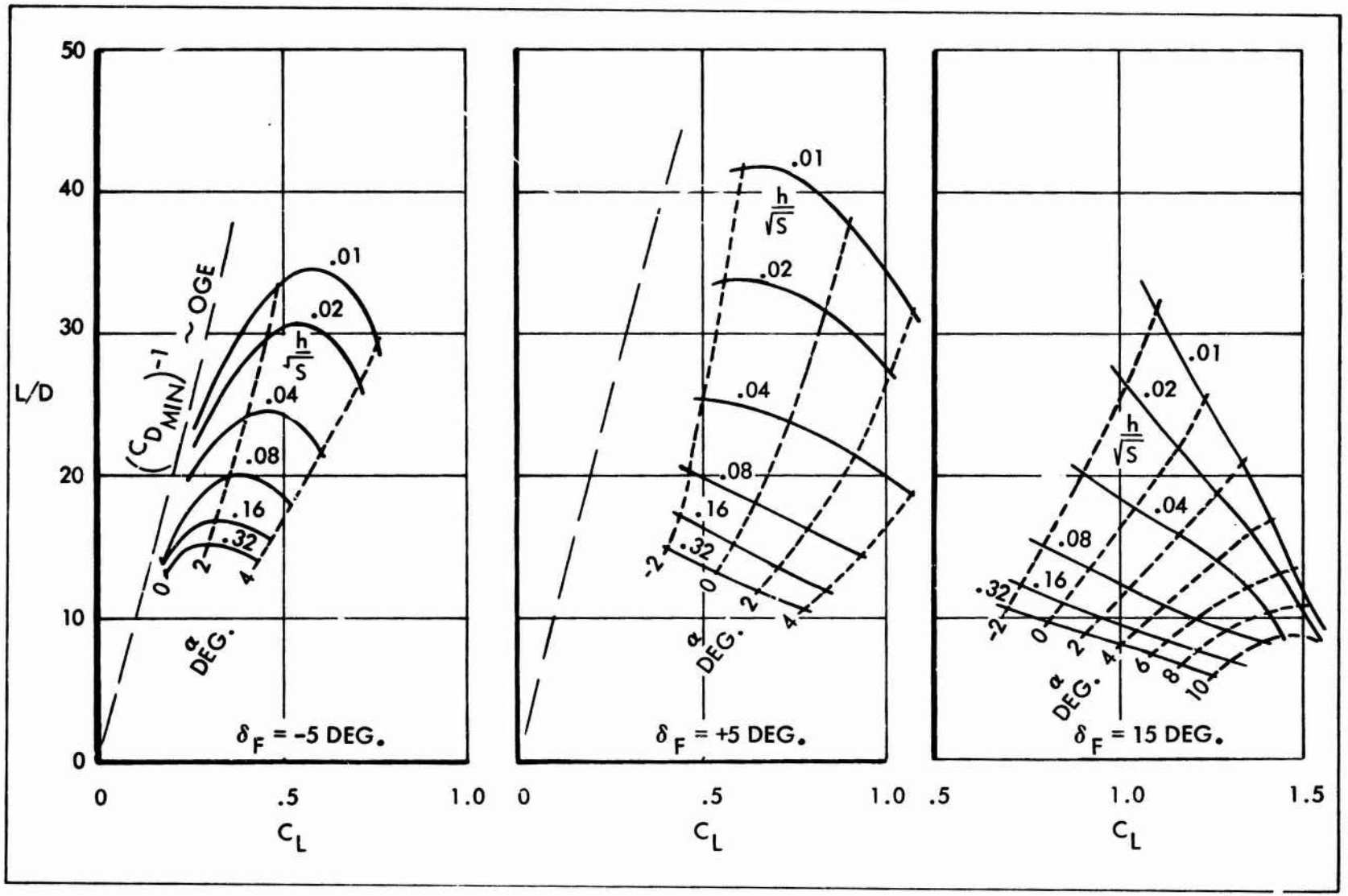

FIGURE 24. WING (2-.12-0.6), FLAP DEFLECTION, FLAT END PLATES (d/c = .10).

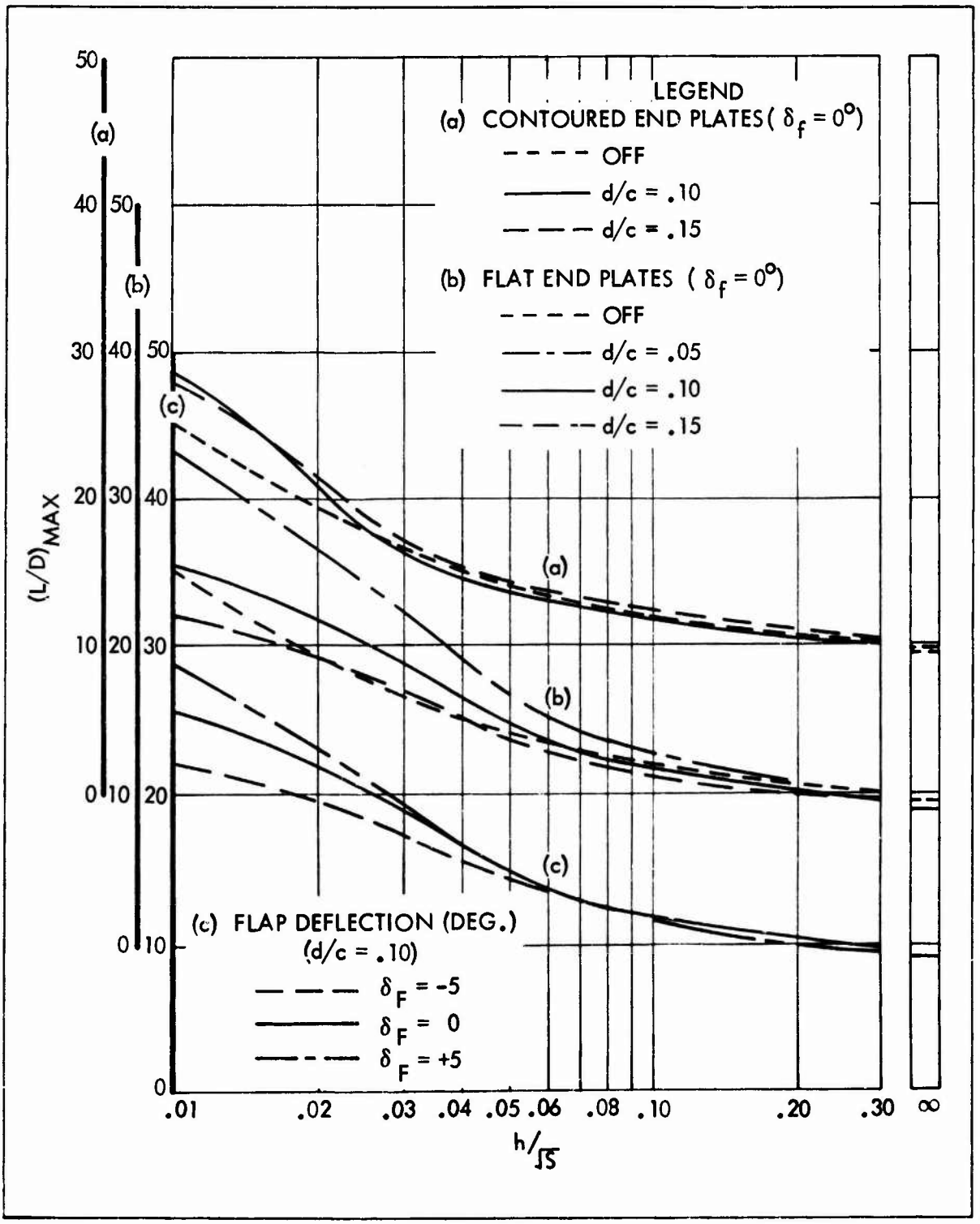

FIGURE 25. WING (1-.12-1.0), END PLATES, FLAP DEFLECTION.

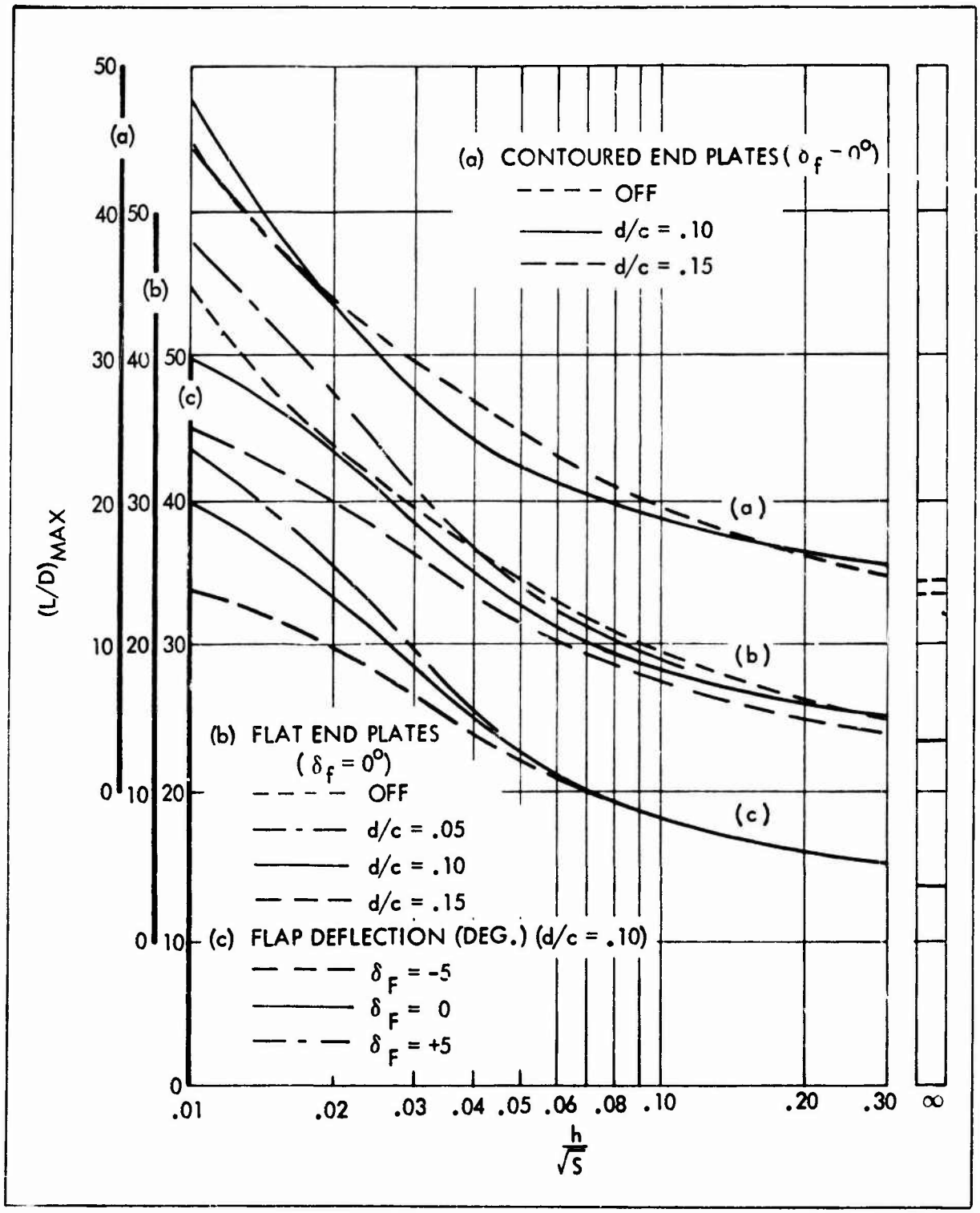

FIGURE 26. WING (2-.12-1.0), END PLATES, FLAP DEFLECTION.

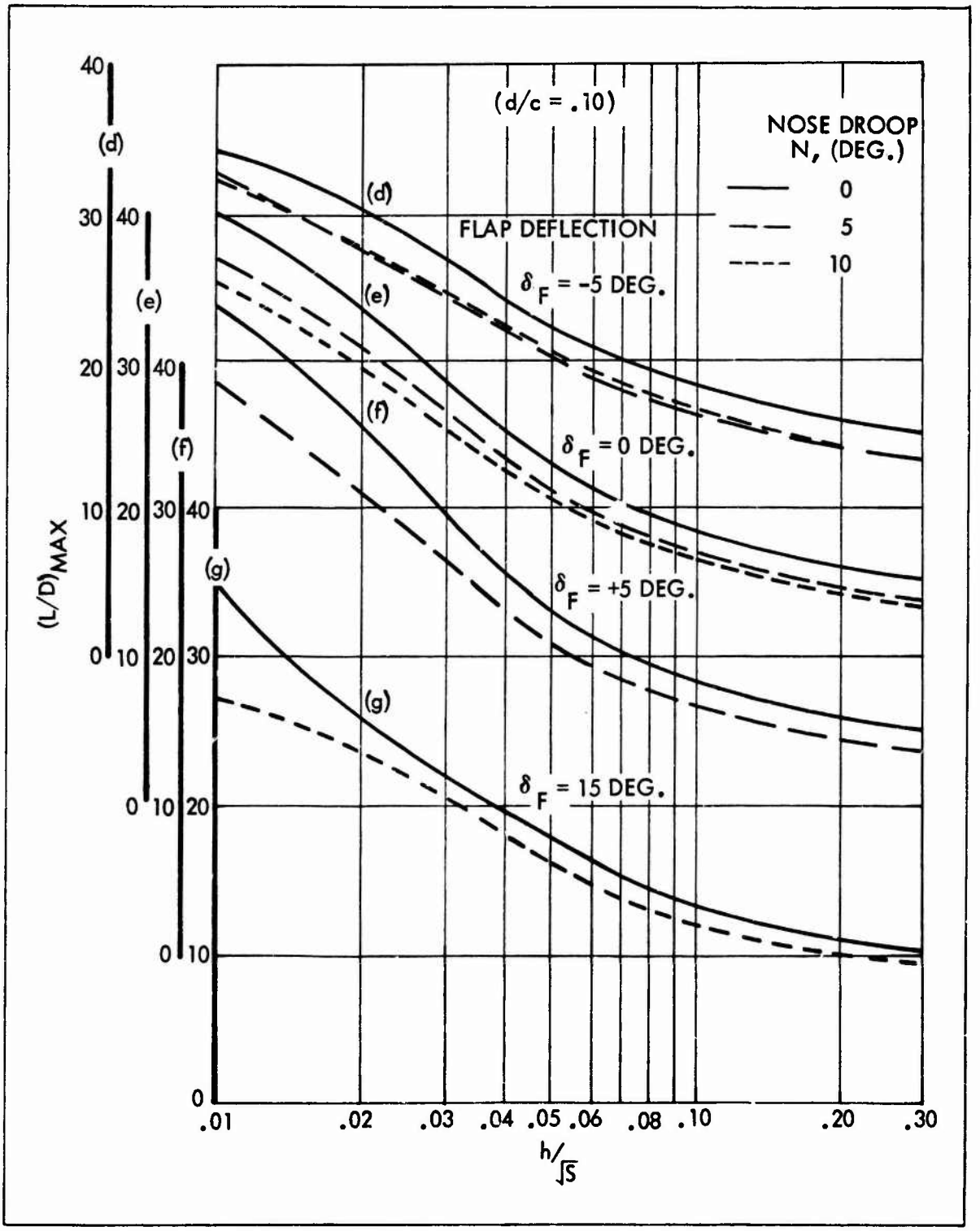

FIGURE 27. WING (2-.12-1.0), NOSE DROOP, FLAP DEFLECTION, FLAT END PLATES

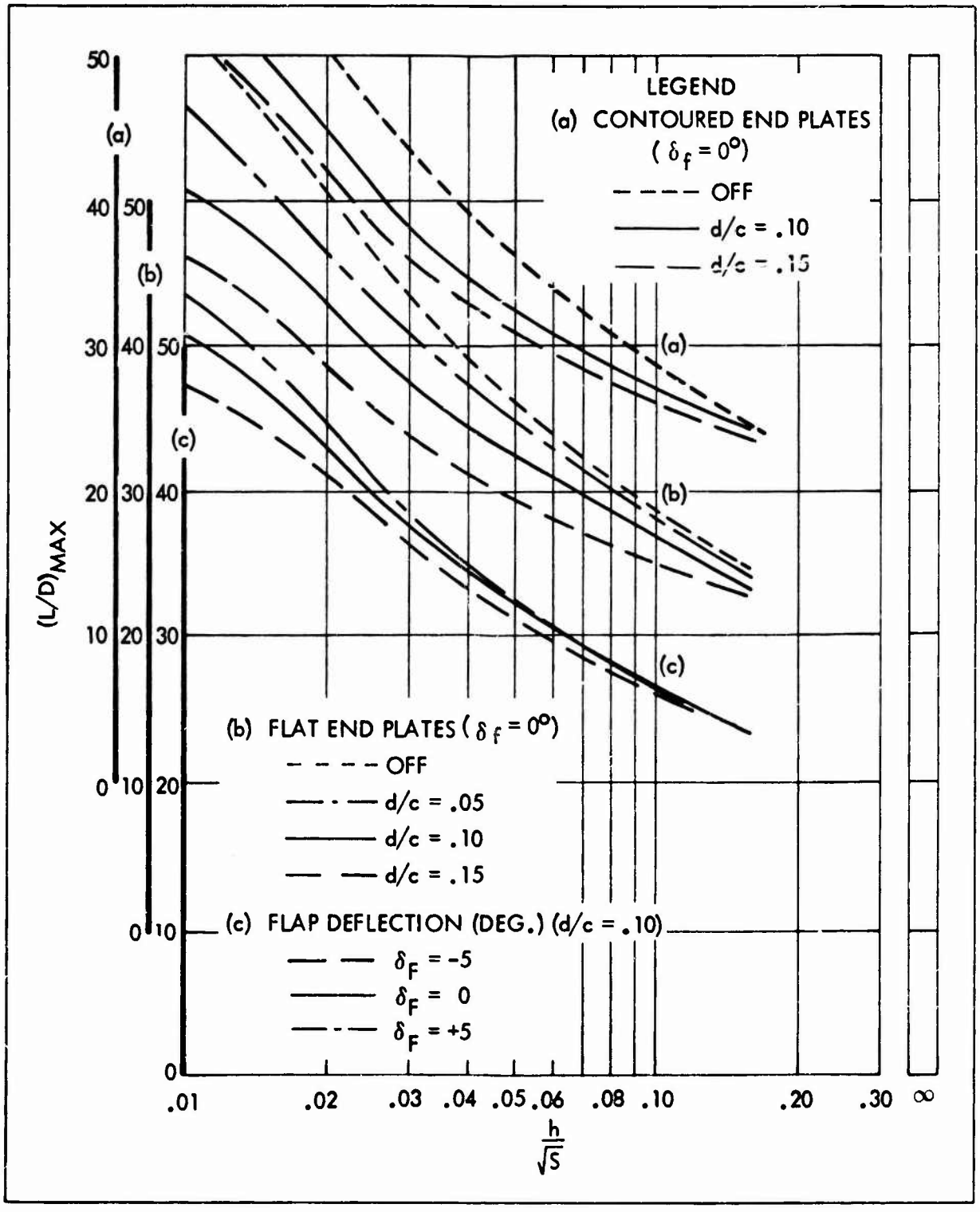

FIGURE 28. WING (4-.12-1.0), END PLATES, FLAP DEFLECTION.

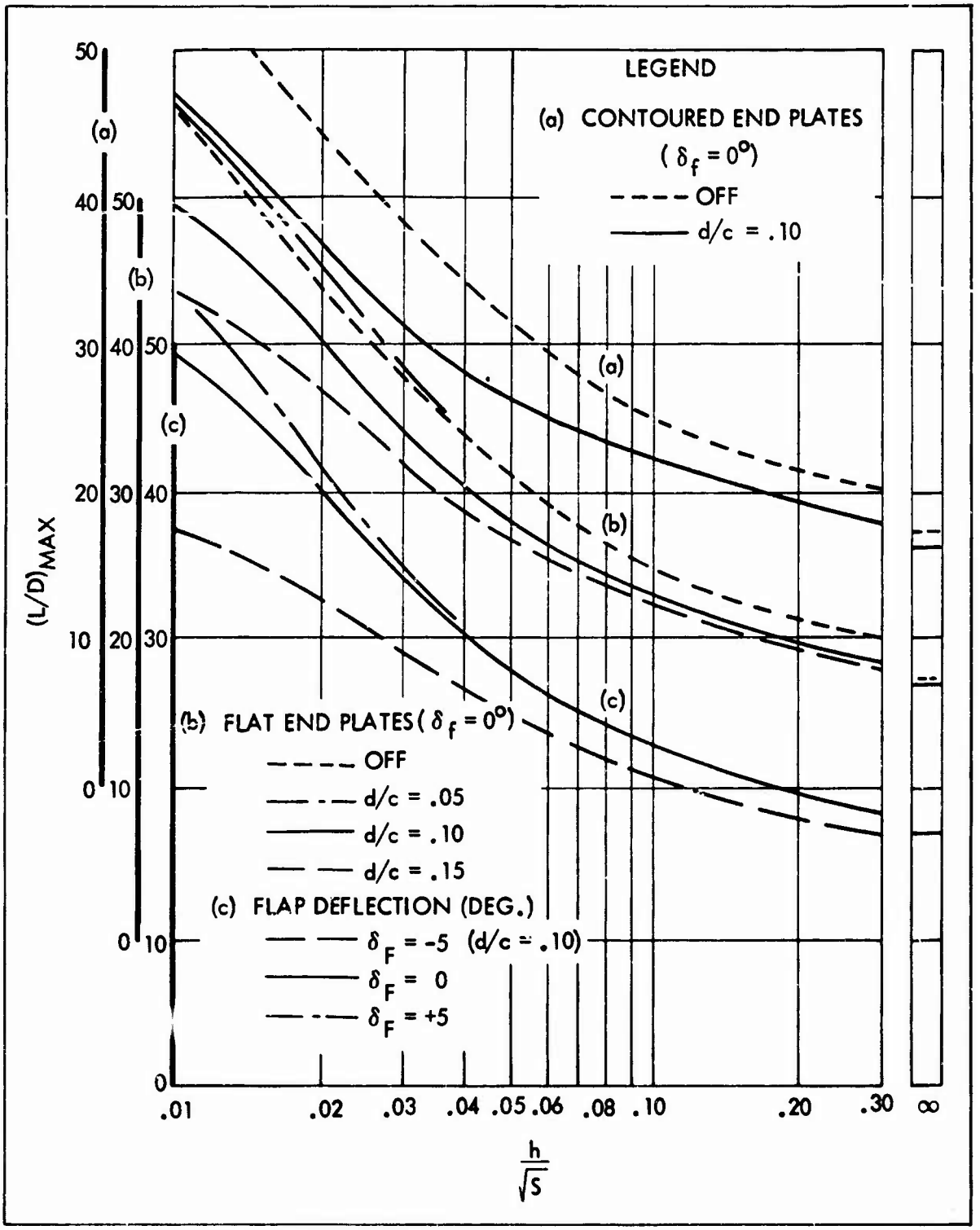

FIGURE 29. WING (2-.06-1.0), END PLATES, FLAP DEFLECTION.

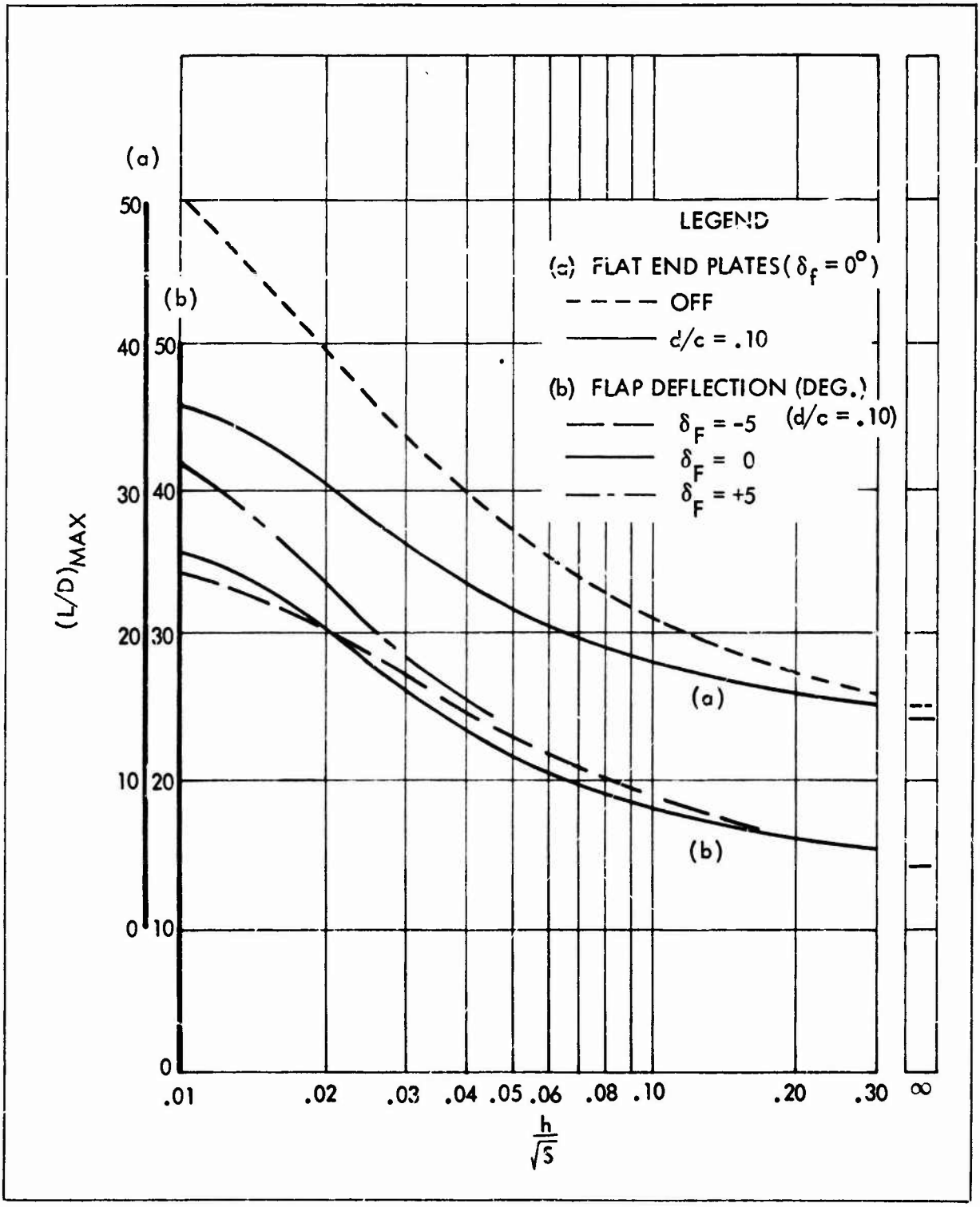

FIGURE 30. WING (2 -.12 -0.6), END PLATES, FLAP DEFLECTION.

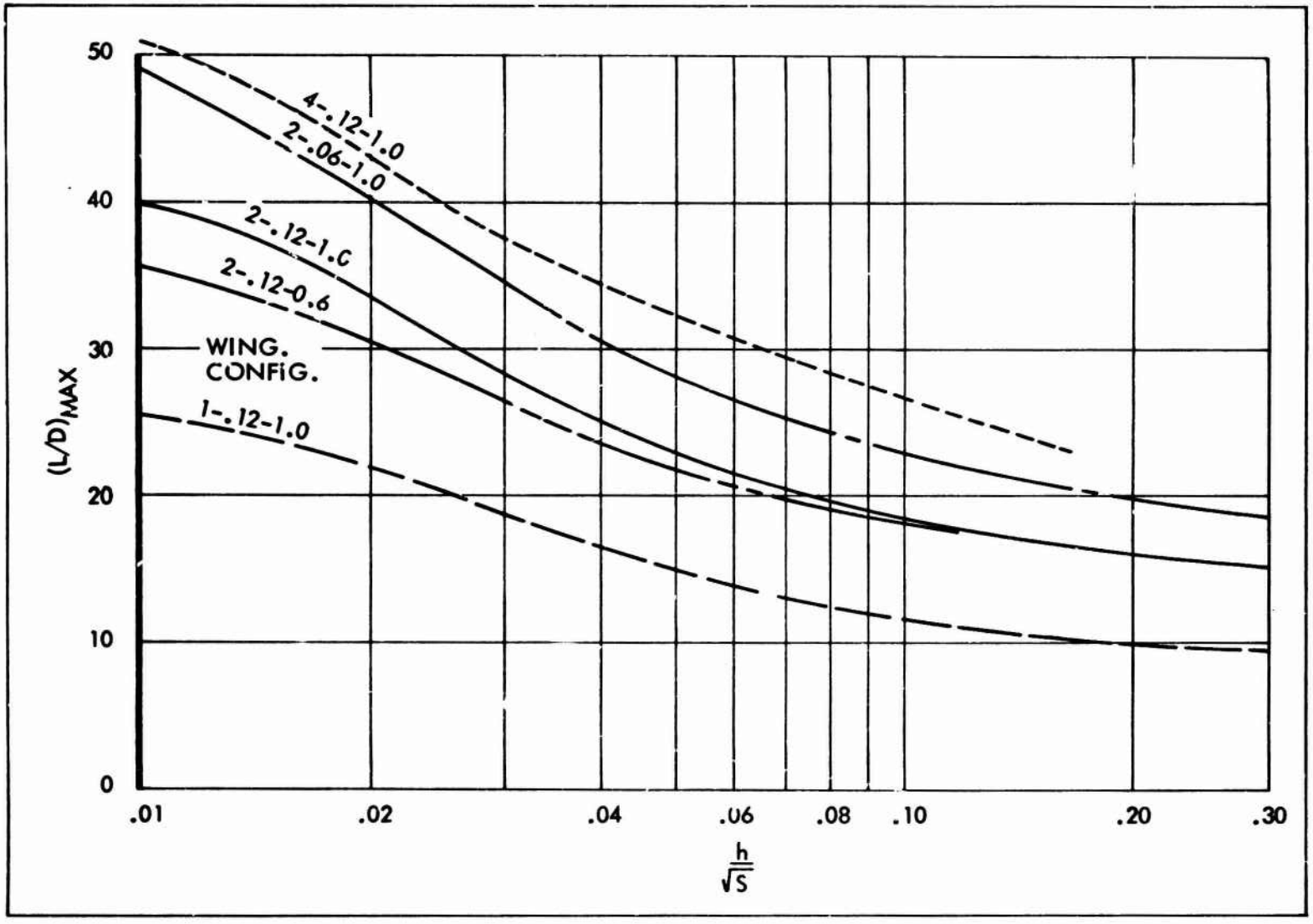

FIGURE 31. VARIOUS WINGS, FLAT END PLATES (d/c = .10).

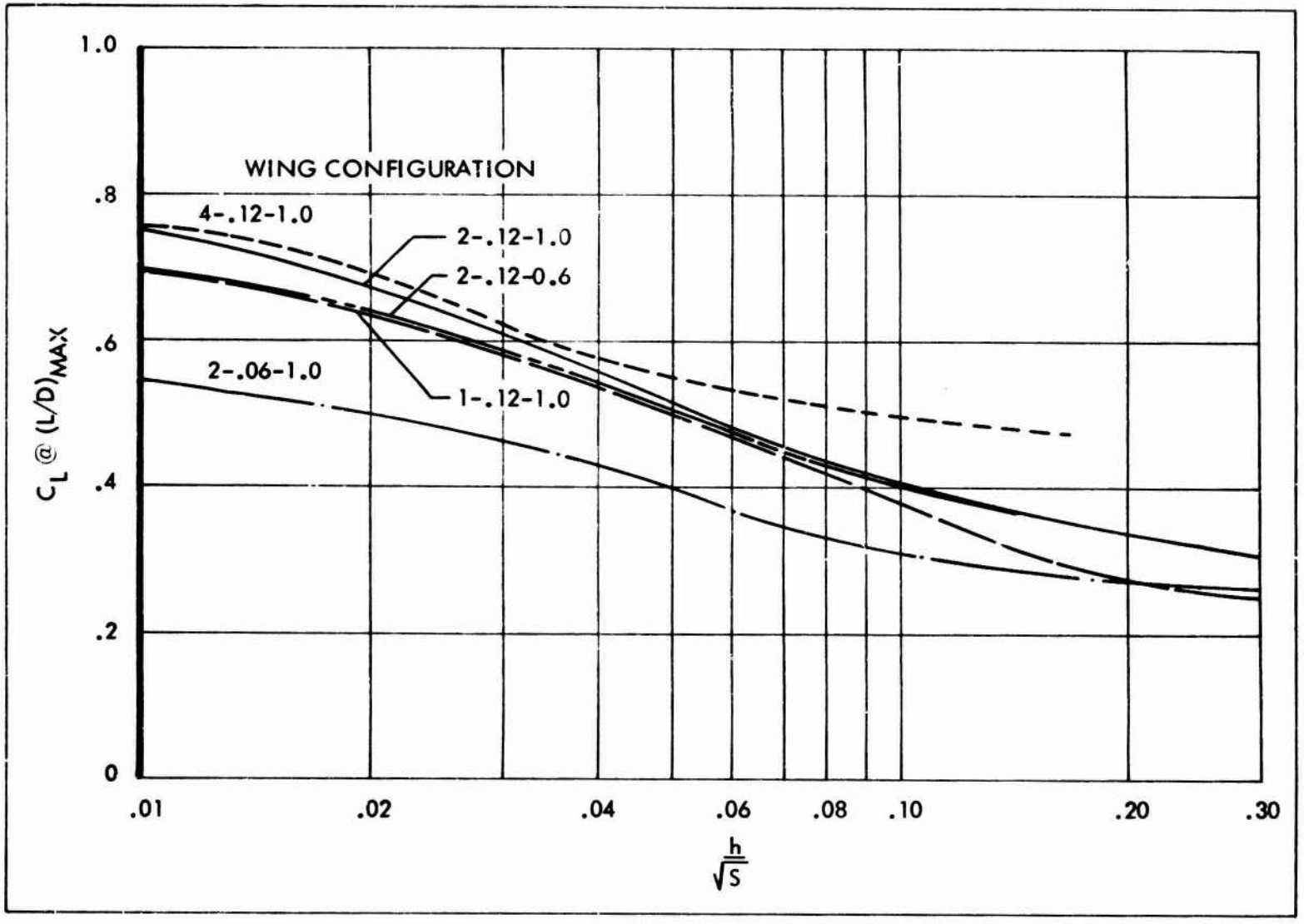

FIGURE 32. SUMMARY OF C_L CORRESPONDING TO $(L/D)_{MAX}$.

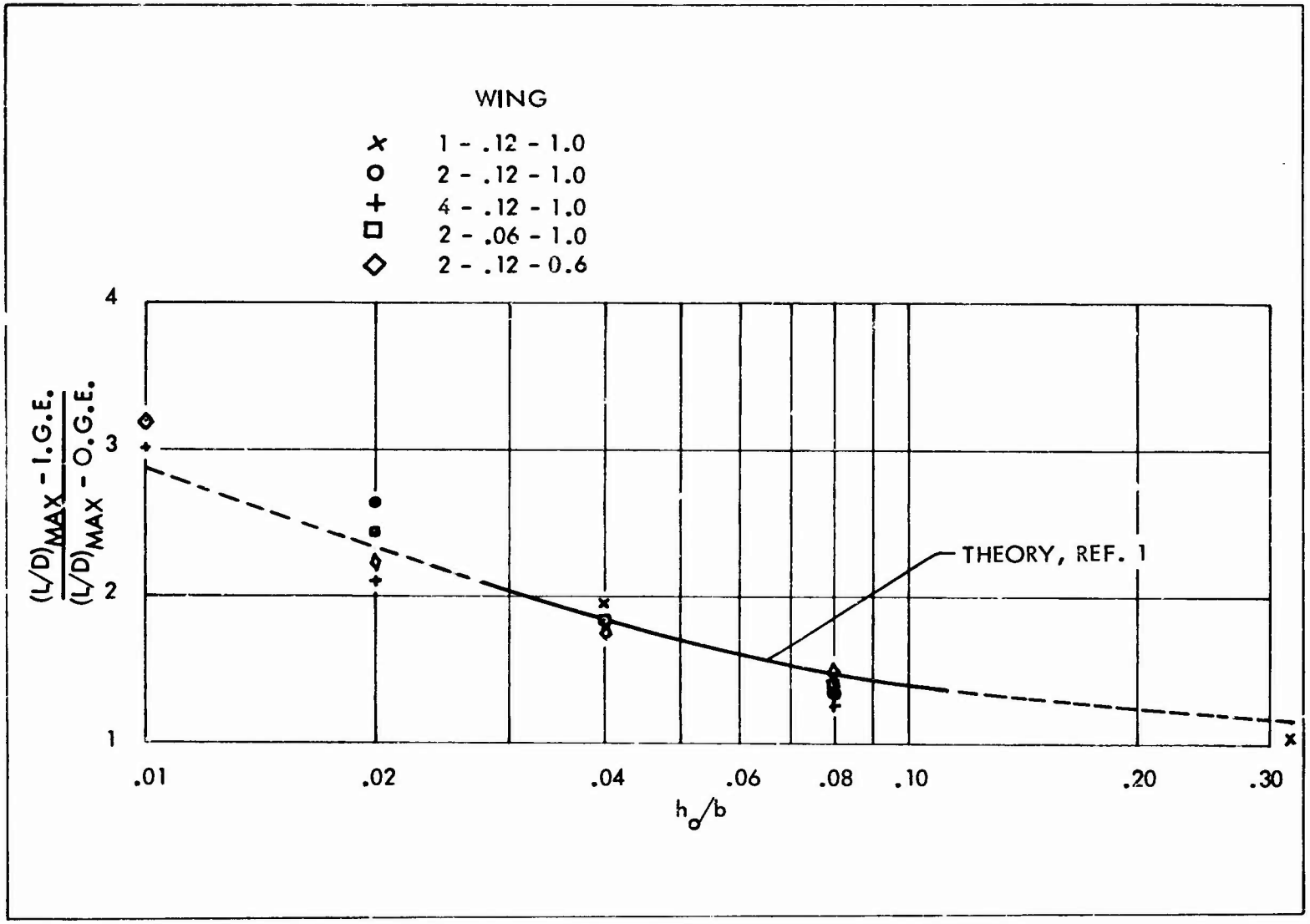

FIGURE 33. $(L/D)_{MAX}$, GROUND PROXIMITY RATIO VS. h_o/b, NC END PLATES.

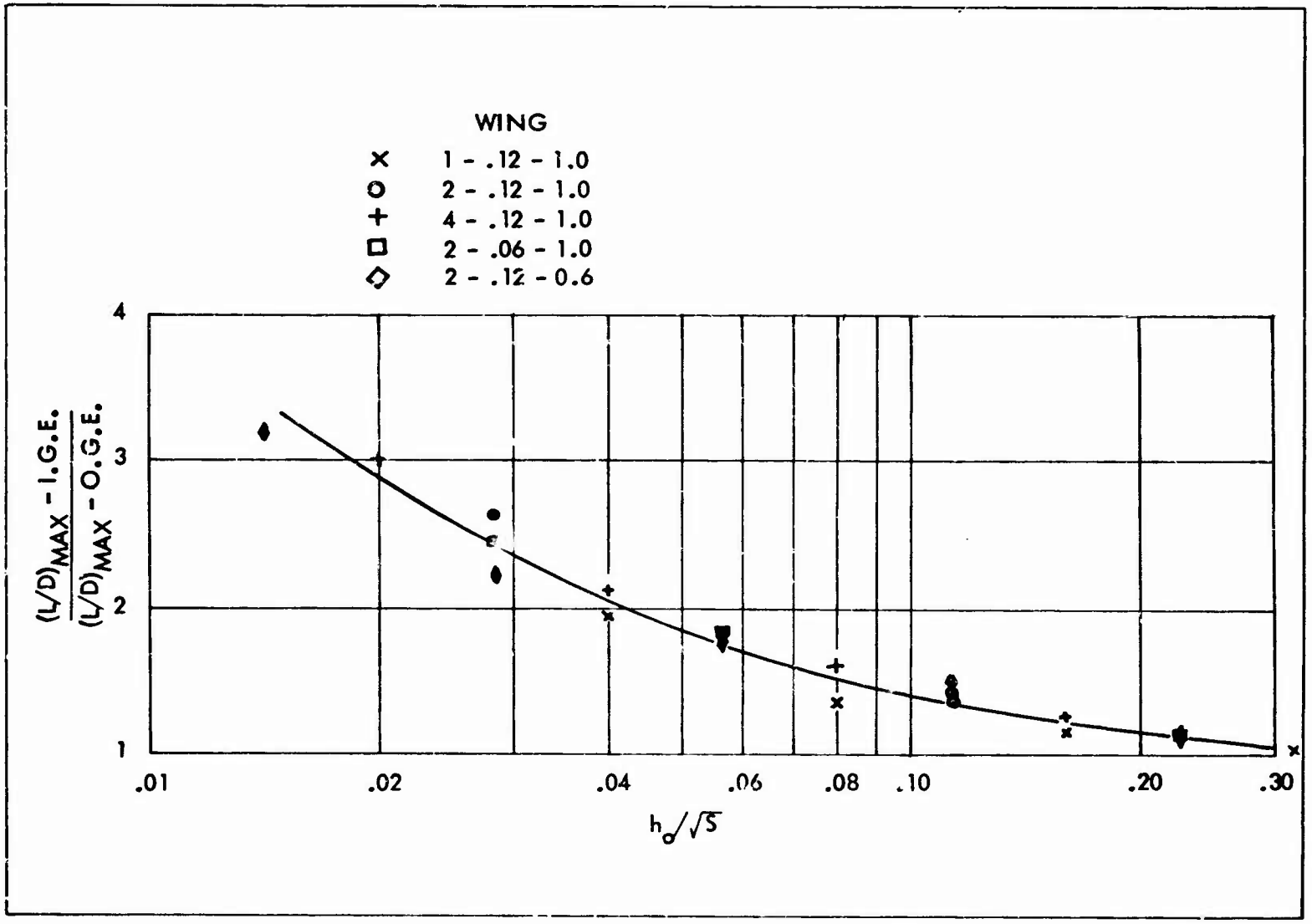

FIGURE 34. $(L/D)_{MAX}$ GROUND PROXIMITY RATIO VS $h_o/\sqrt{S}$, NO END PLATES.

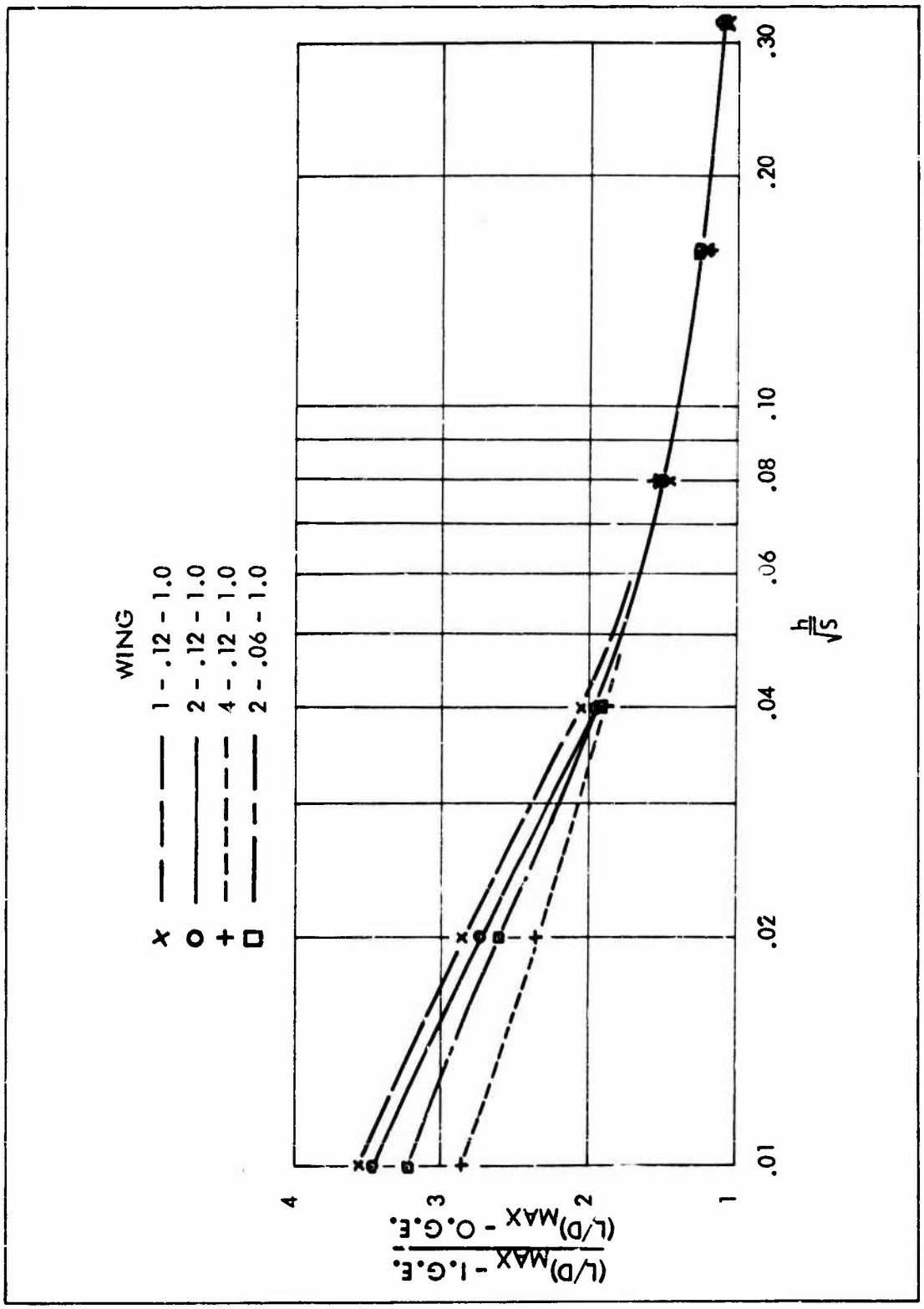

FIGURE 35. $(L/D)_{MAX}$, GROUND PROXIMITY RATIO VS. $h/\sqrt{S}$, FLAT END PLATES ($d/c = .05$).

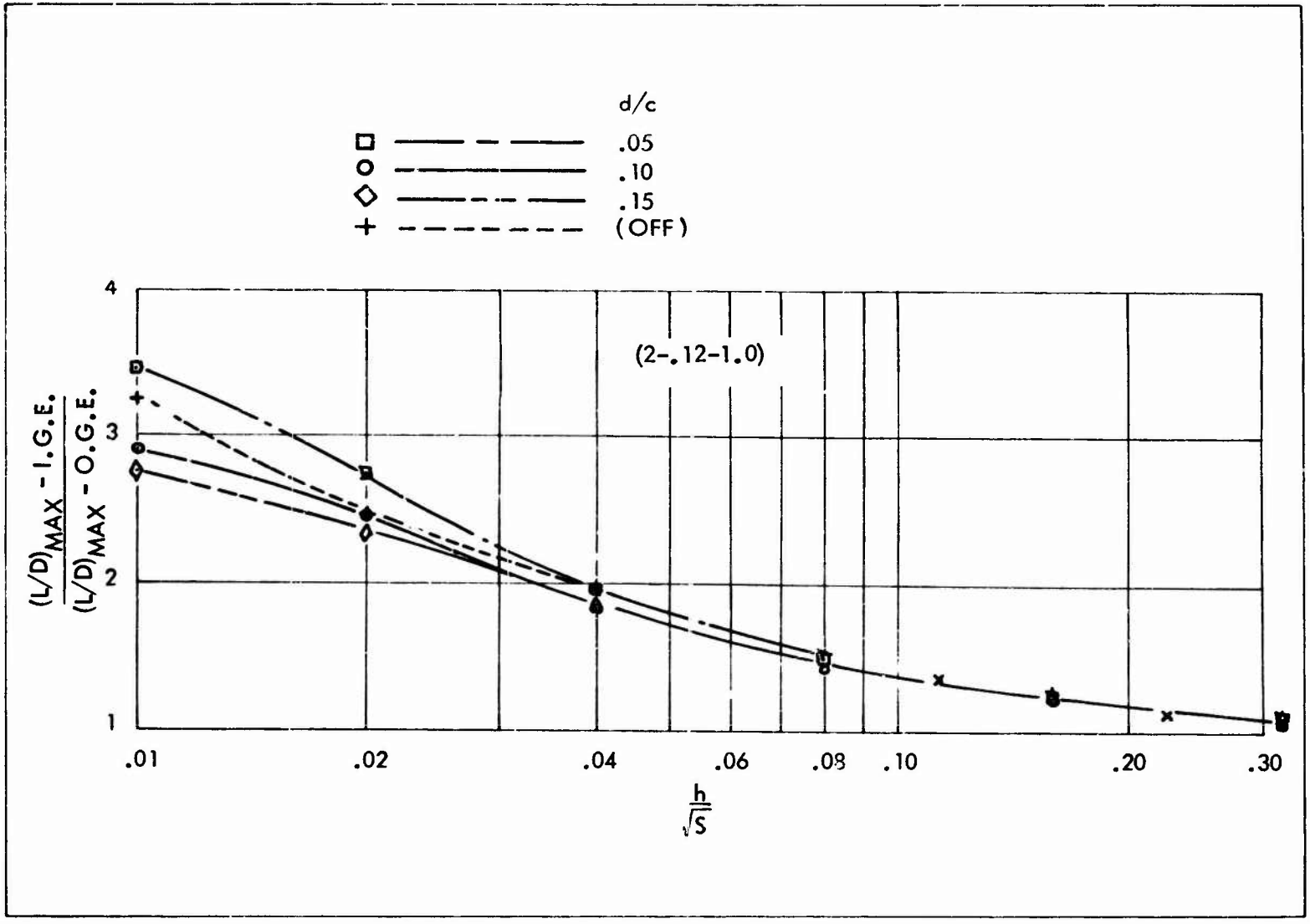

FIGURE 36. $(L/D)_{MAX}$, GROUND PROXIMITY RATIO VS. $h/\sqrt{S}$, DEPTH OF FLAT END PLATES ON WING.

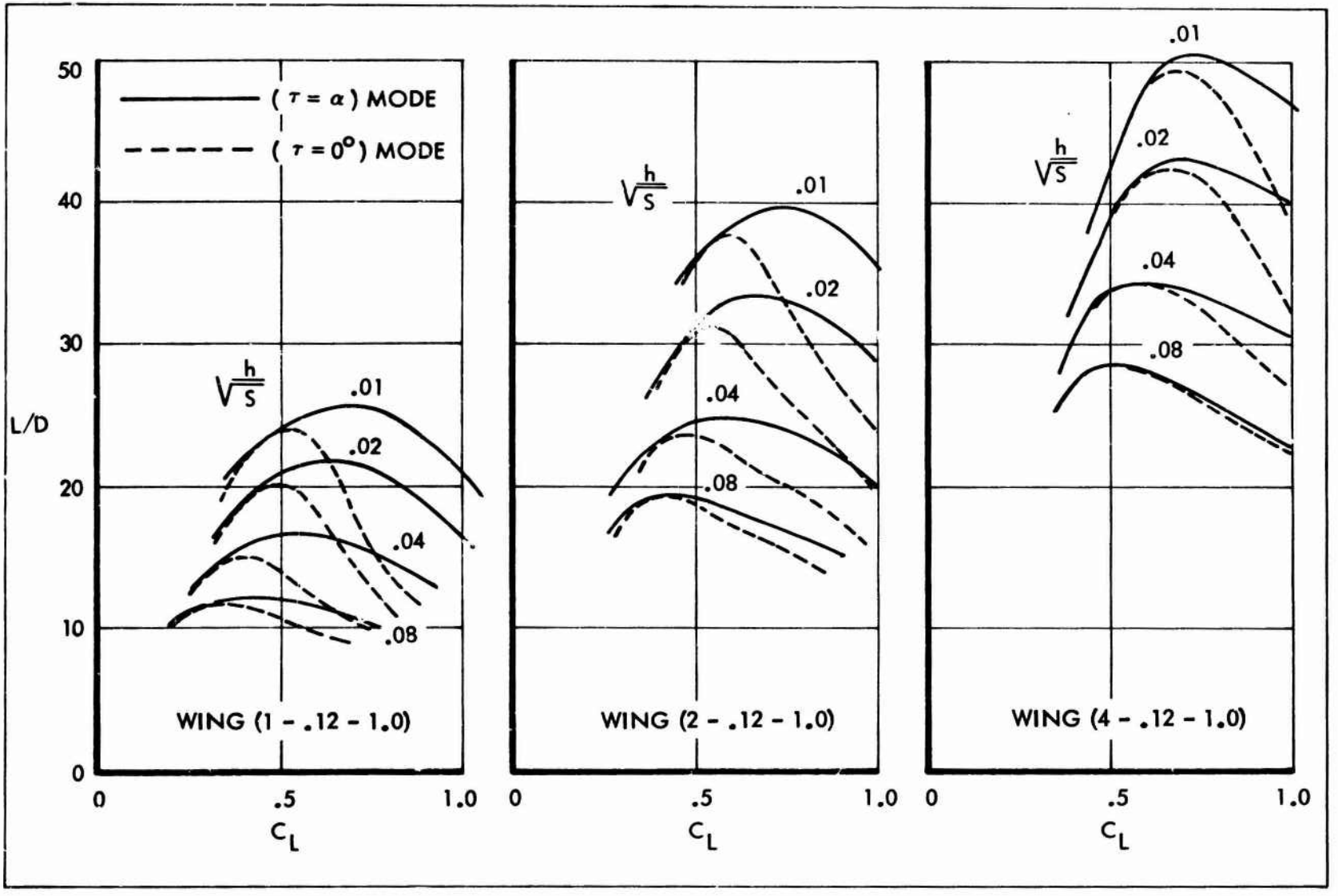

FIGURE 37. L/D VS C_L, ($\tau = \alpha$) AND ($\tau = 0$) MODES, FLAT END PLATES (d/c = .10).

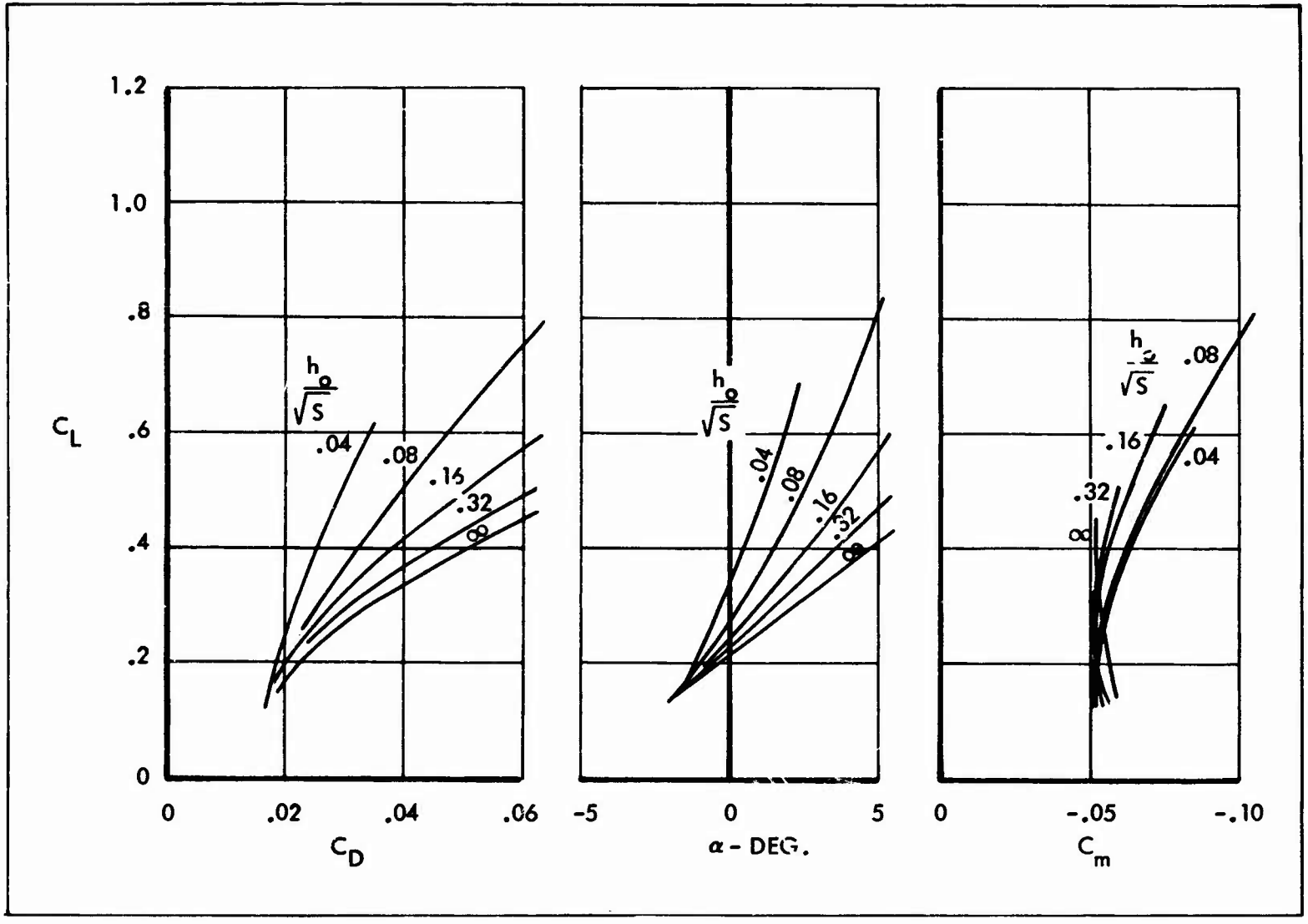

FIGURE 38. WING (1-.12-1.0), FLAT END PLATES (d/c = .10), τ = 0.

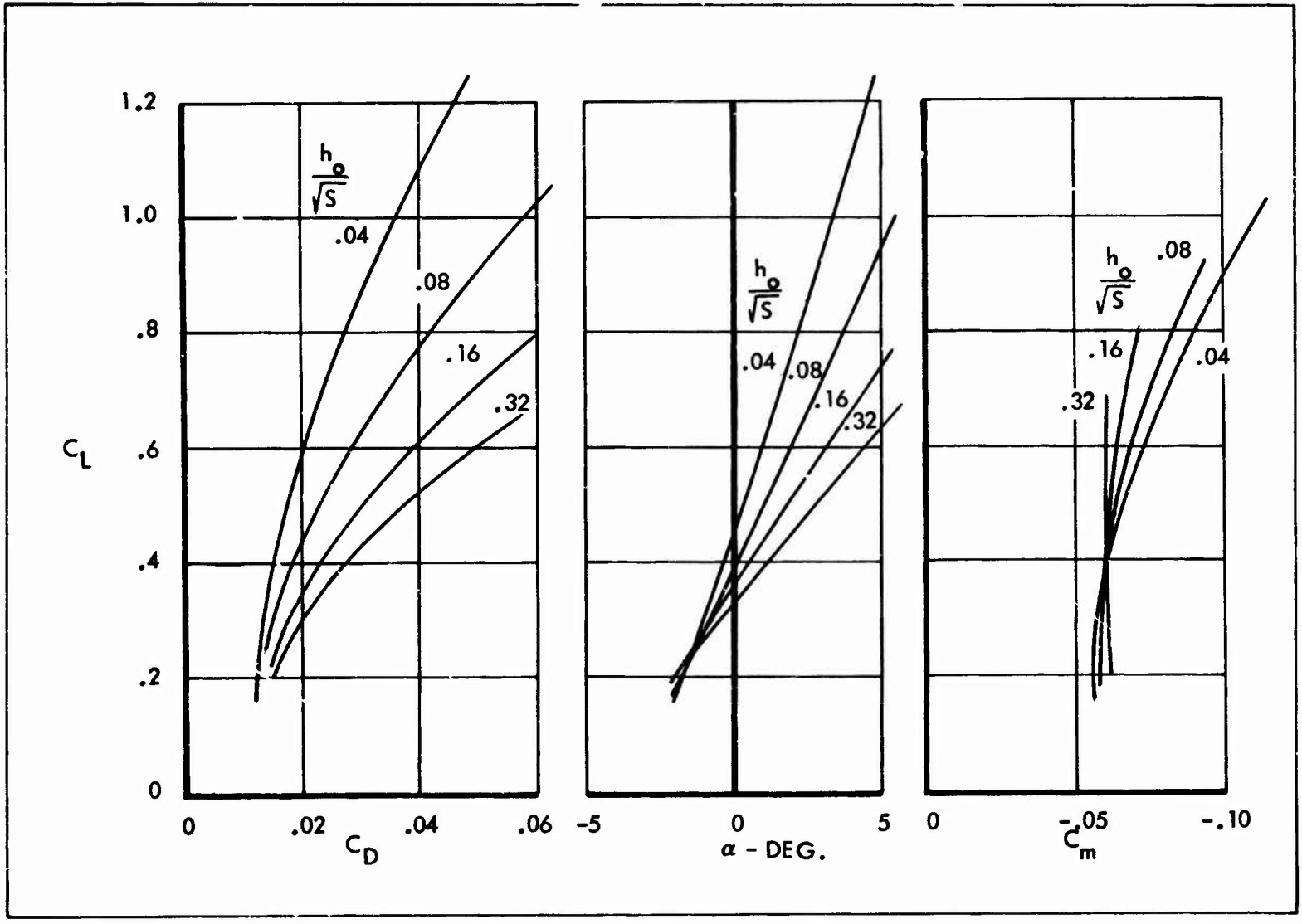

FIGURE 39. WING (2-.12-1.0), FLAT END PLATES (d/c = .05), $\tau = 0$.

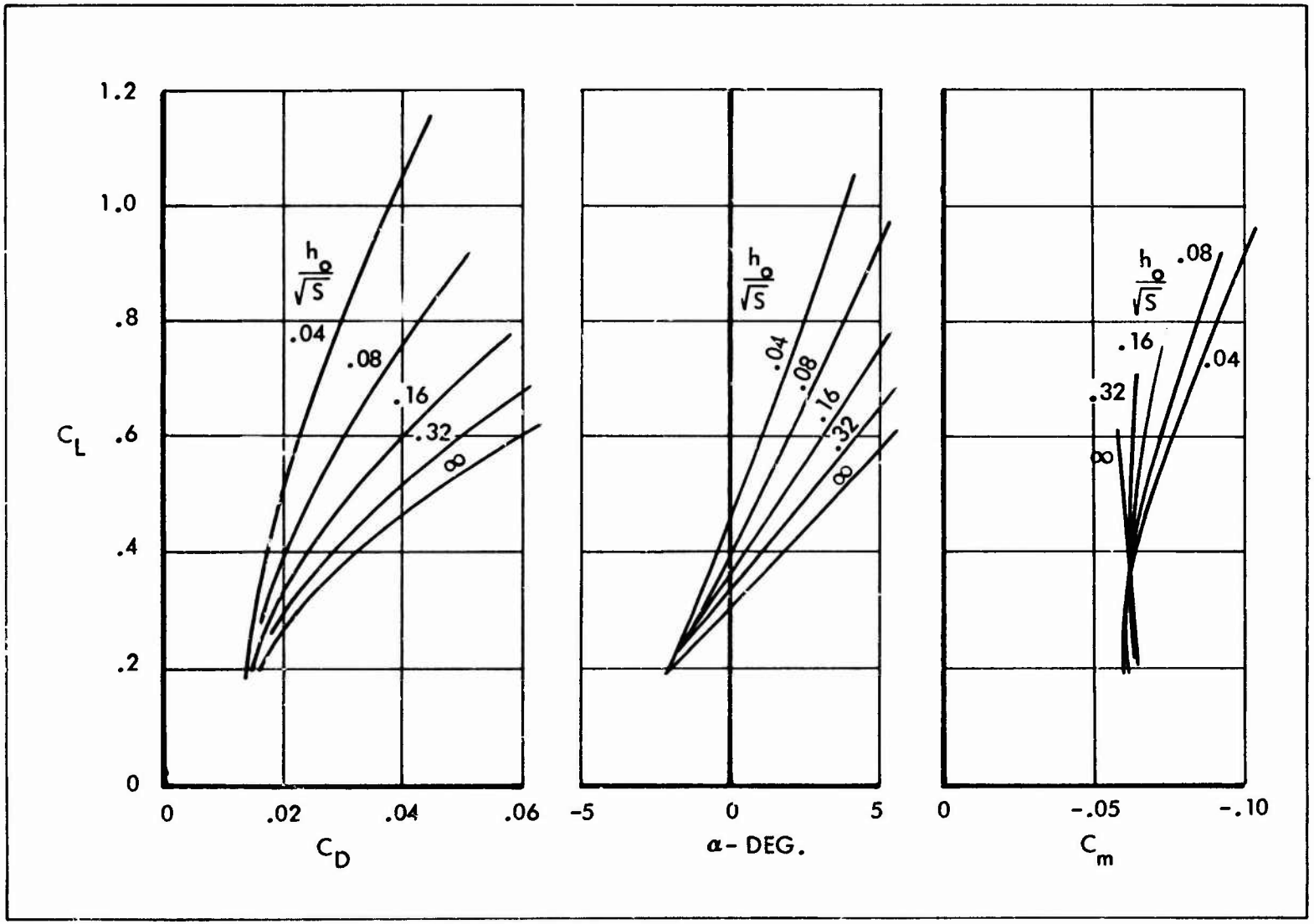

FIGURE 40. WING (2-.12-1.0), FLAT END PLATES (d/c = .10), τ = 0.

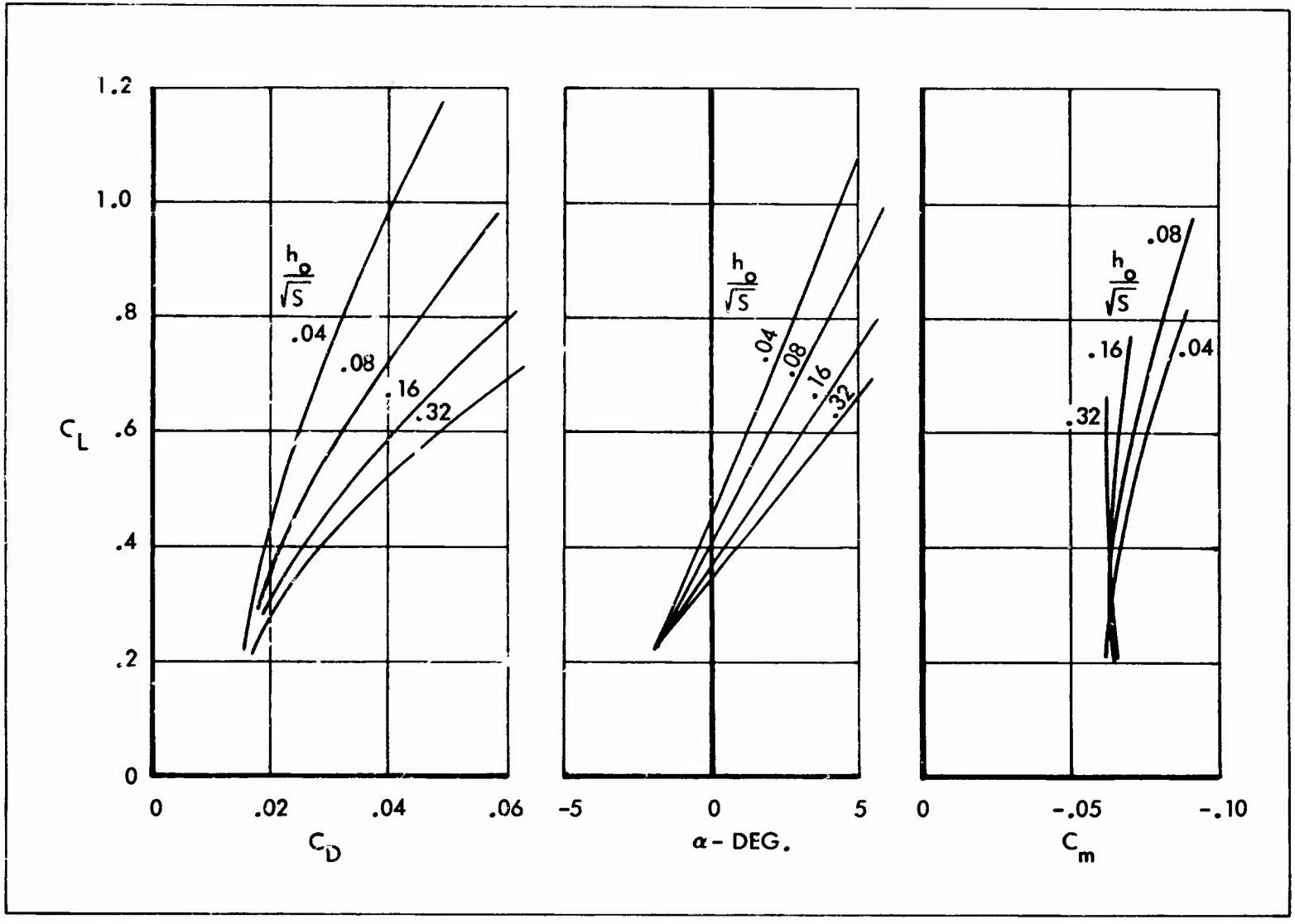

FIGURE 41. WING (2-.12-1.0), FLAT END PLATES (d/c = .15), τ = 0.

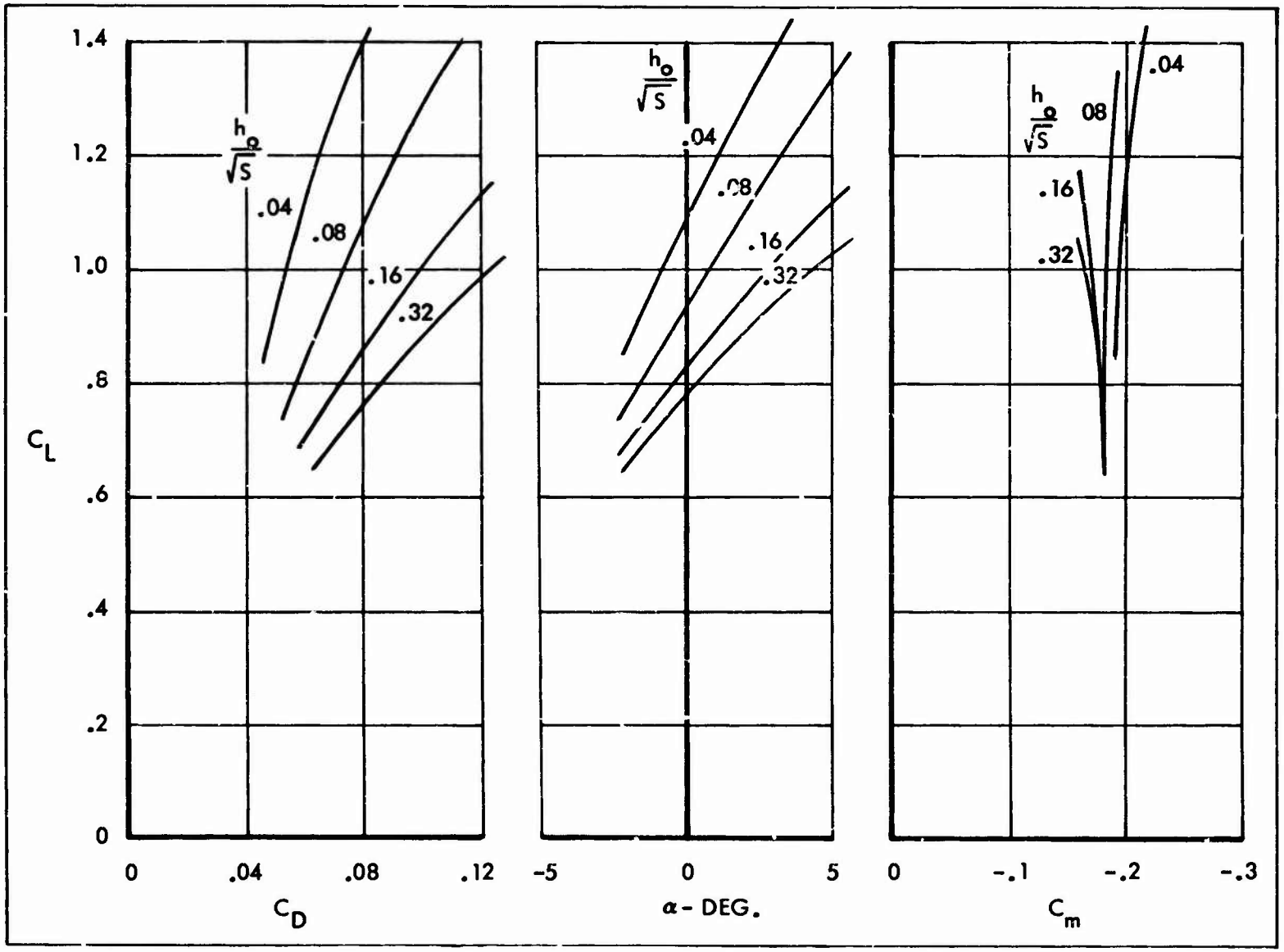

FIGURE 42. WING (2-.12-1.0), FLAT END PLATES, (d/c = .10), τ = 0, 15° FLAP DEFLECTION.

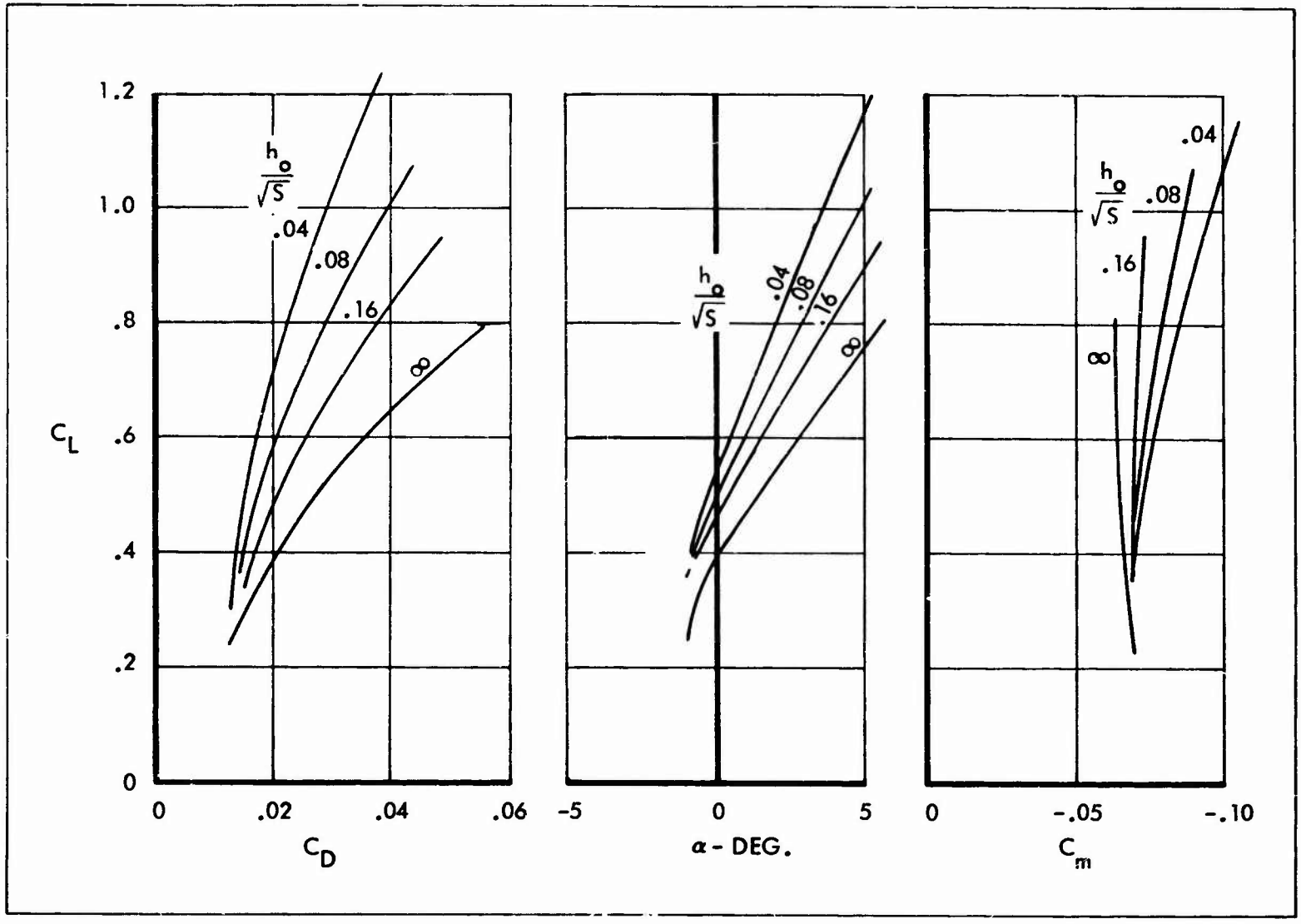

FIGURE 43. WING (4-.12-1.0), FLAT END PLATES (d/c = .10), τ = 0.

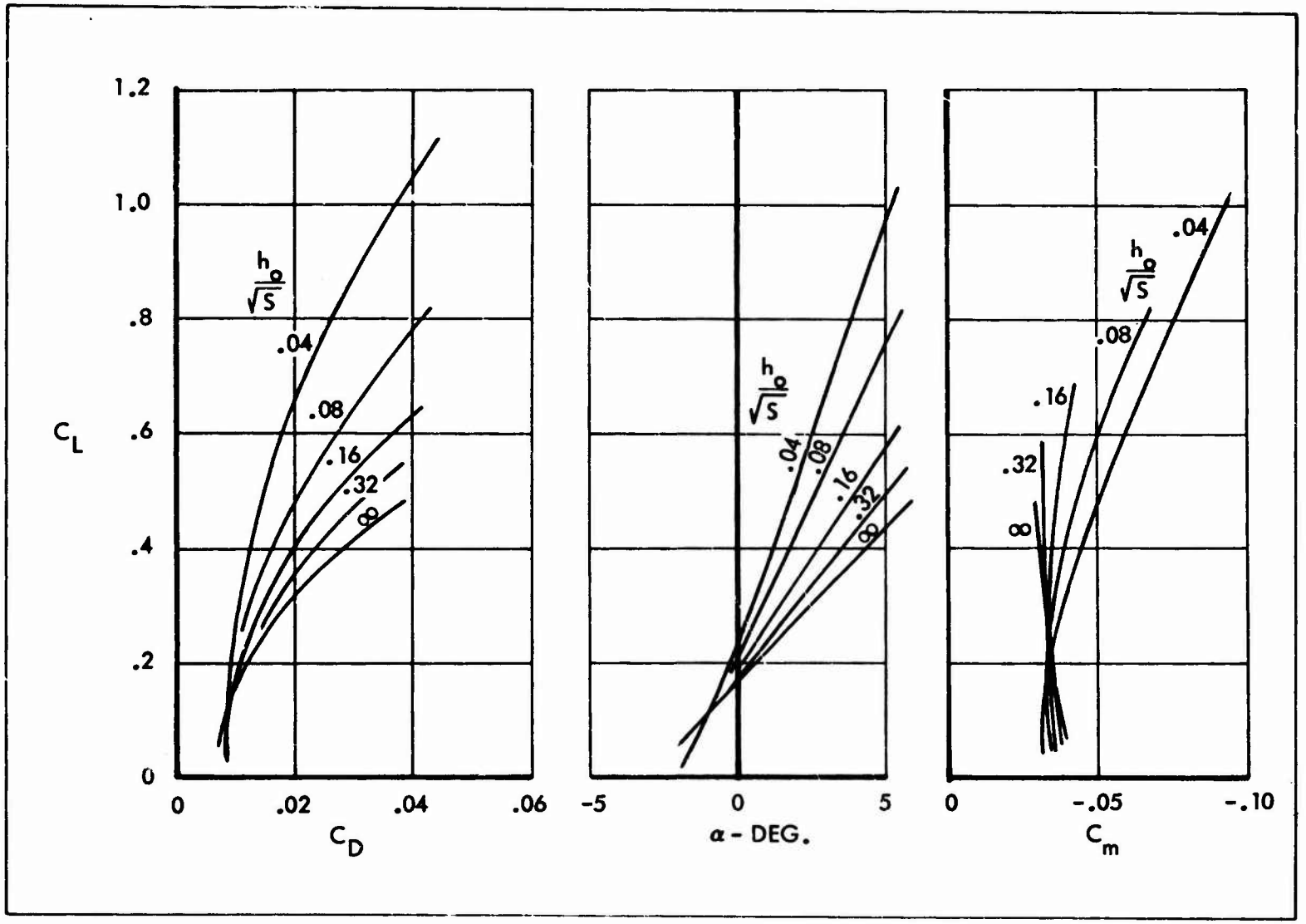

FIGURE 44. WING (2-.06-1.0), FLAT END PLATES (d/c = .10), τ = 0.

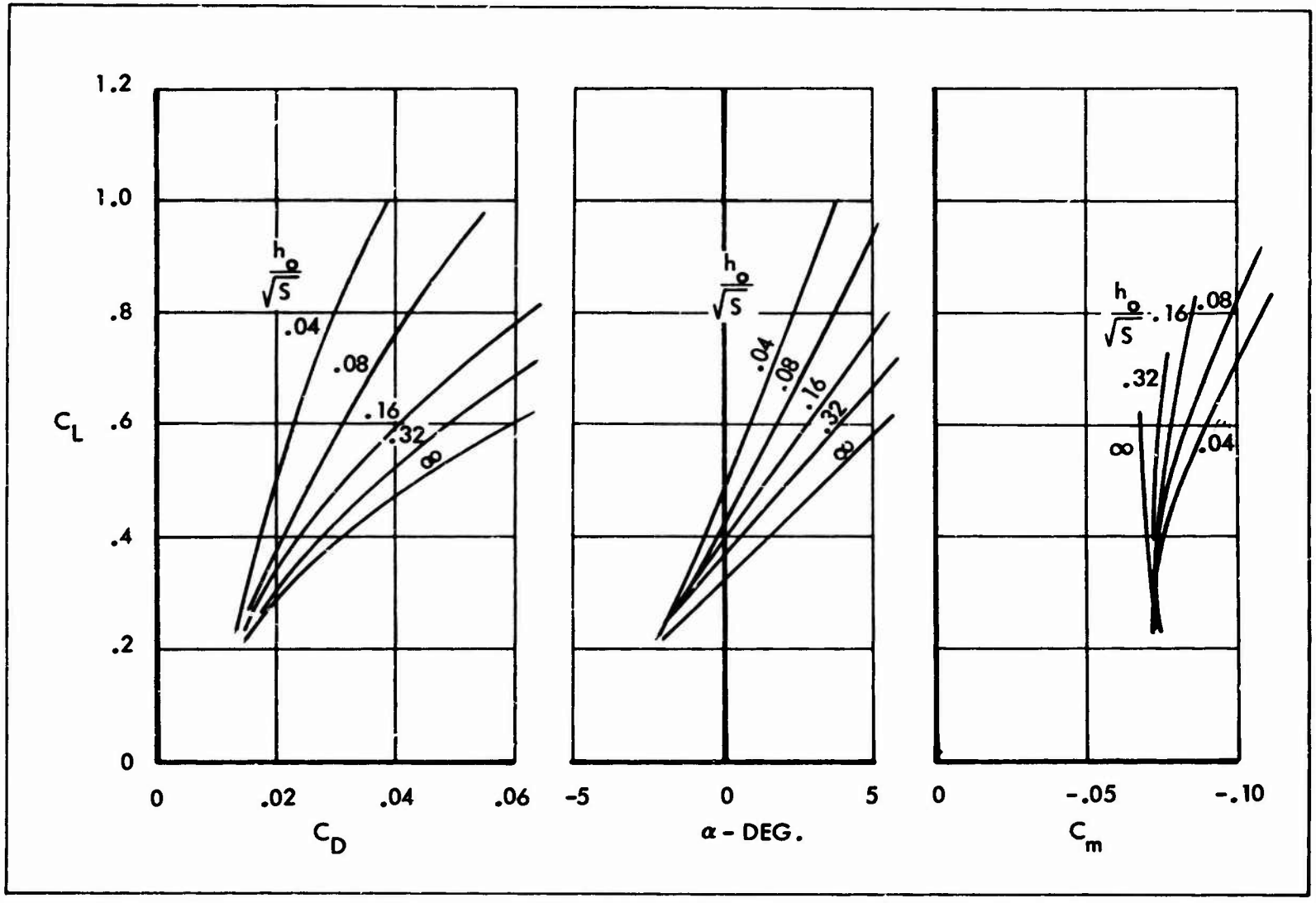

FIGURE 45. WING (2-.12-0.6), FLAT END PLATES (d/c = .10), τ = 0.

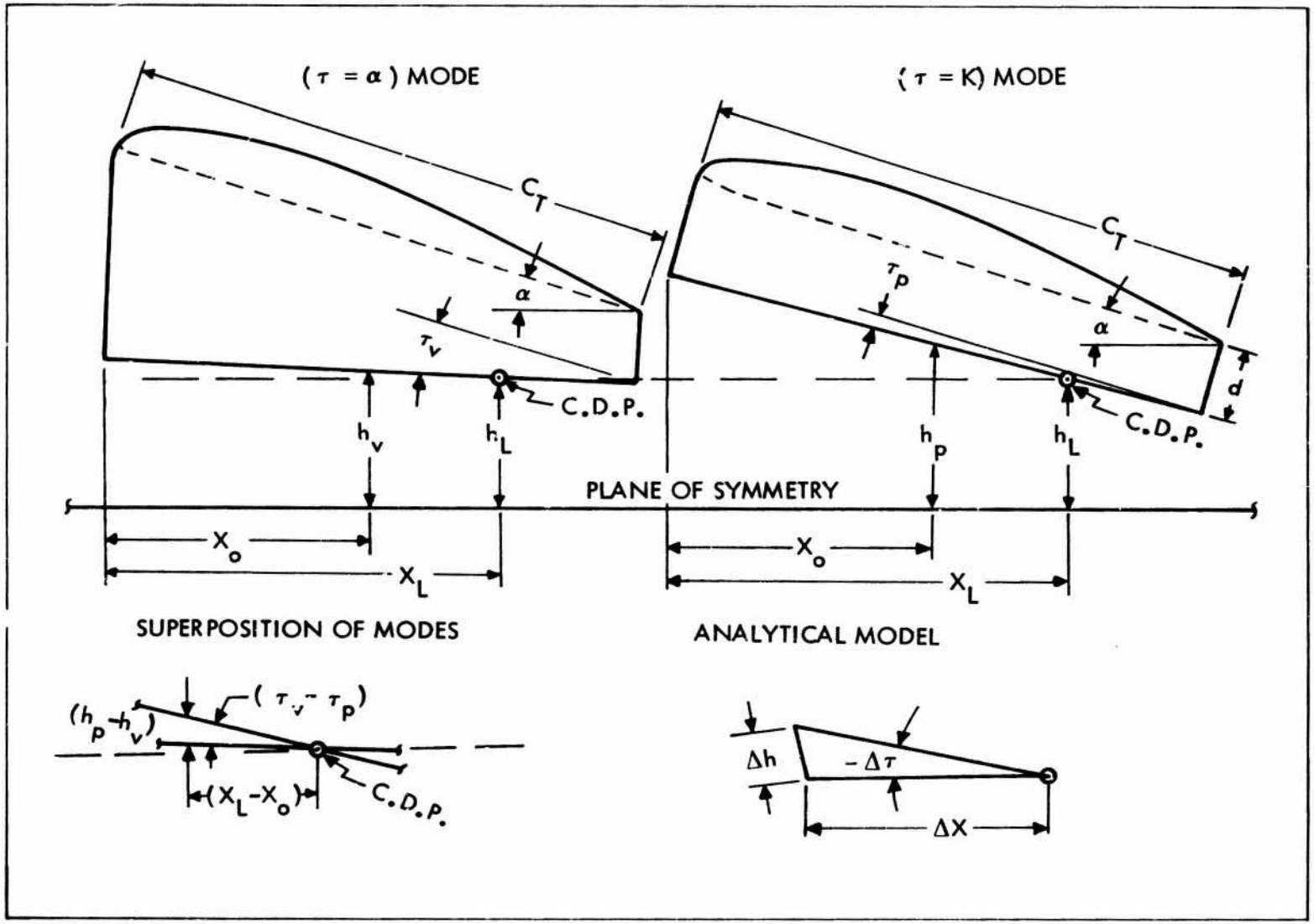

FIGURE 46. GEOMETRIC RELATIONSHIP BETWEEN (τ = α) AND (τ = K) MODES.

NOTE:

WINGS HAVE FLAT END PLATES OF DEPTH d/c = .10

REFERENCE STATION, X_o / c_t - 0.50

COMMON-DATA PIVOT, $X_{L/D} / c_t$ = 0.50

OPEN SYMBOLS AND CURVES ($\tau = 0^\circ$) MODE DATA

SOLID SYMBOLS~ ($\tau = \alpha$) MODE ADJUSTED DATA

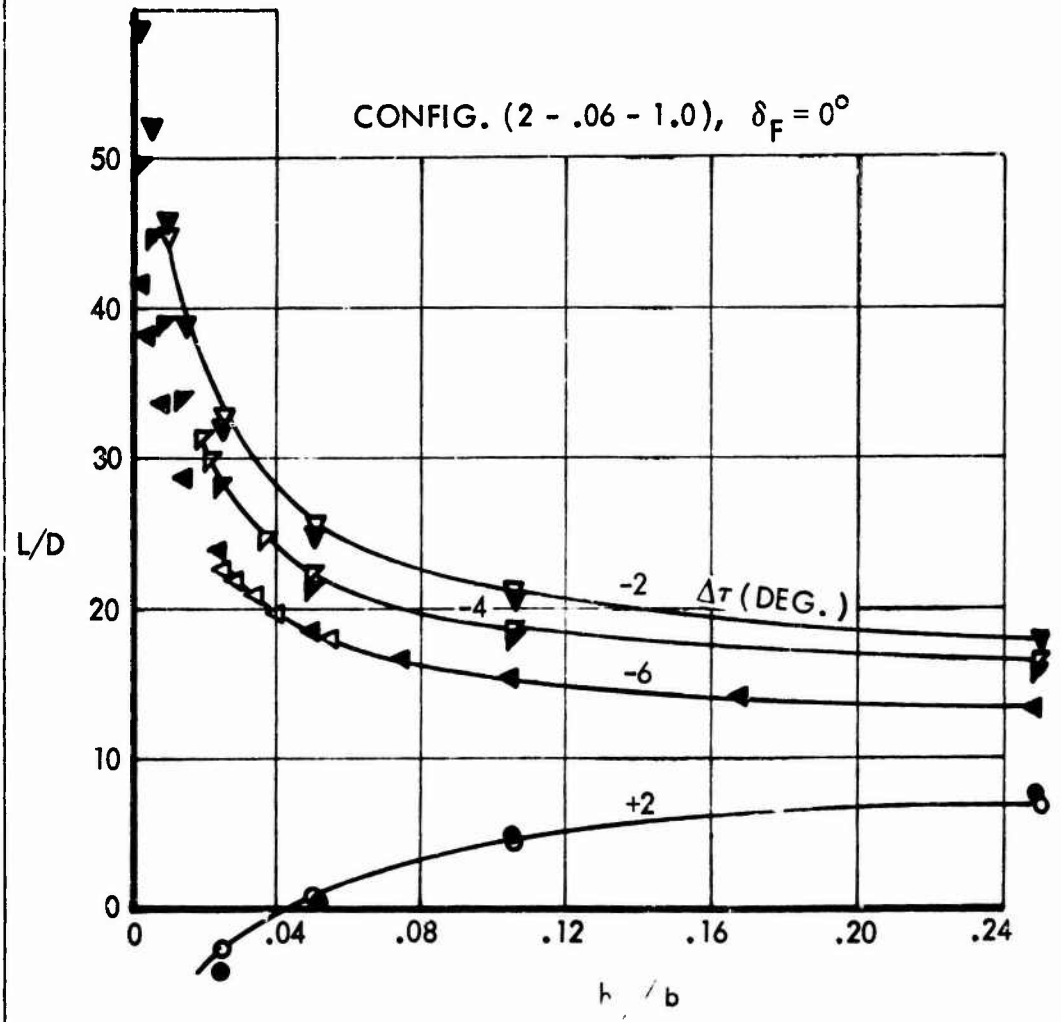

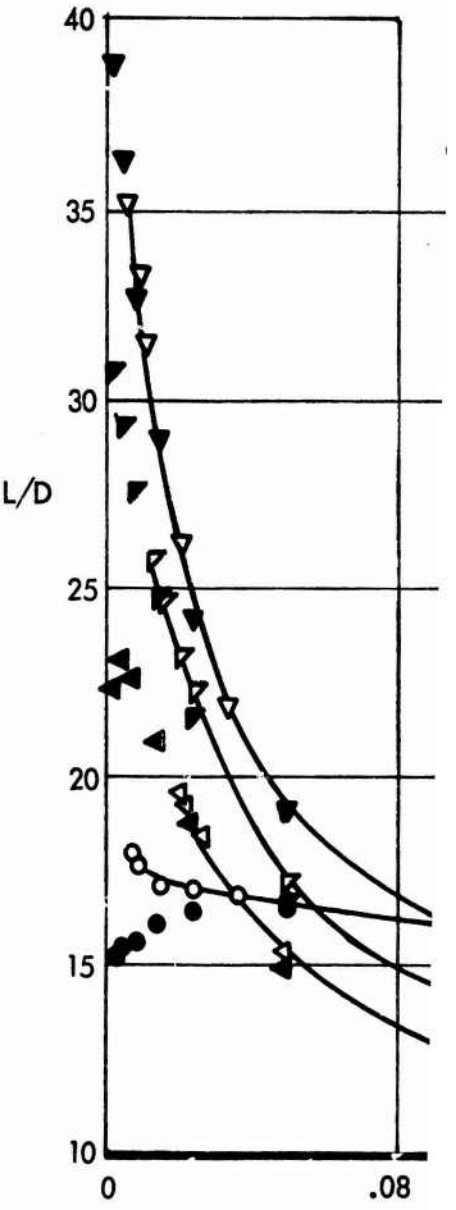

FIGURE 47. COMPARATIVE L/D, ($\tau = \alpha$) AND ($\tau = 0$) MOD

A

ES OF DEPTH d/c = .10

- 0.50

/ c_t = 0.50

($\tau = 0°$) MODE DATA

ODE ADJUSTED DATA

1.0), $\delta_F = 0°$

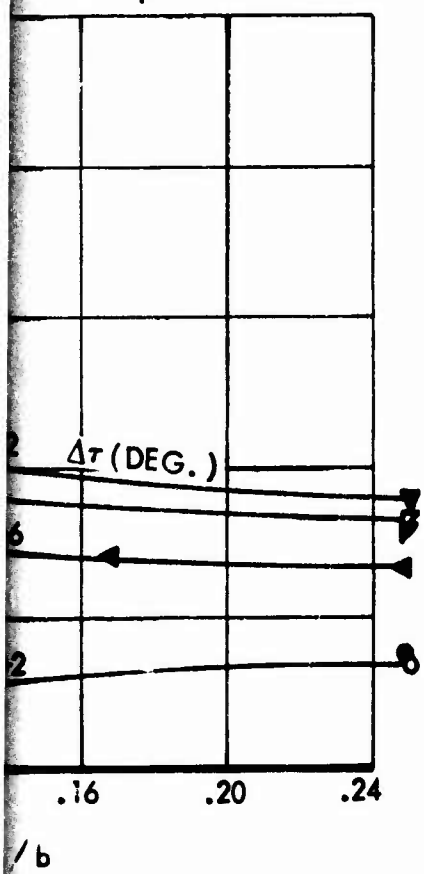

CONFIG. (2 - .12 - 0.6), $\delta_F = 0°$

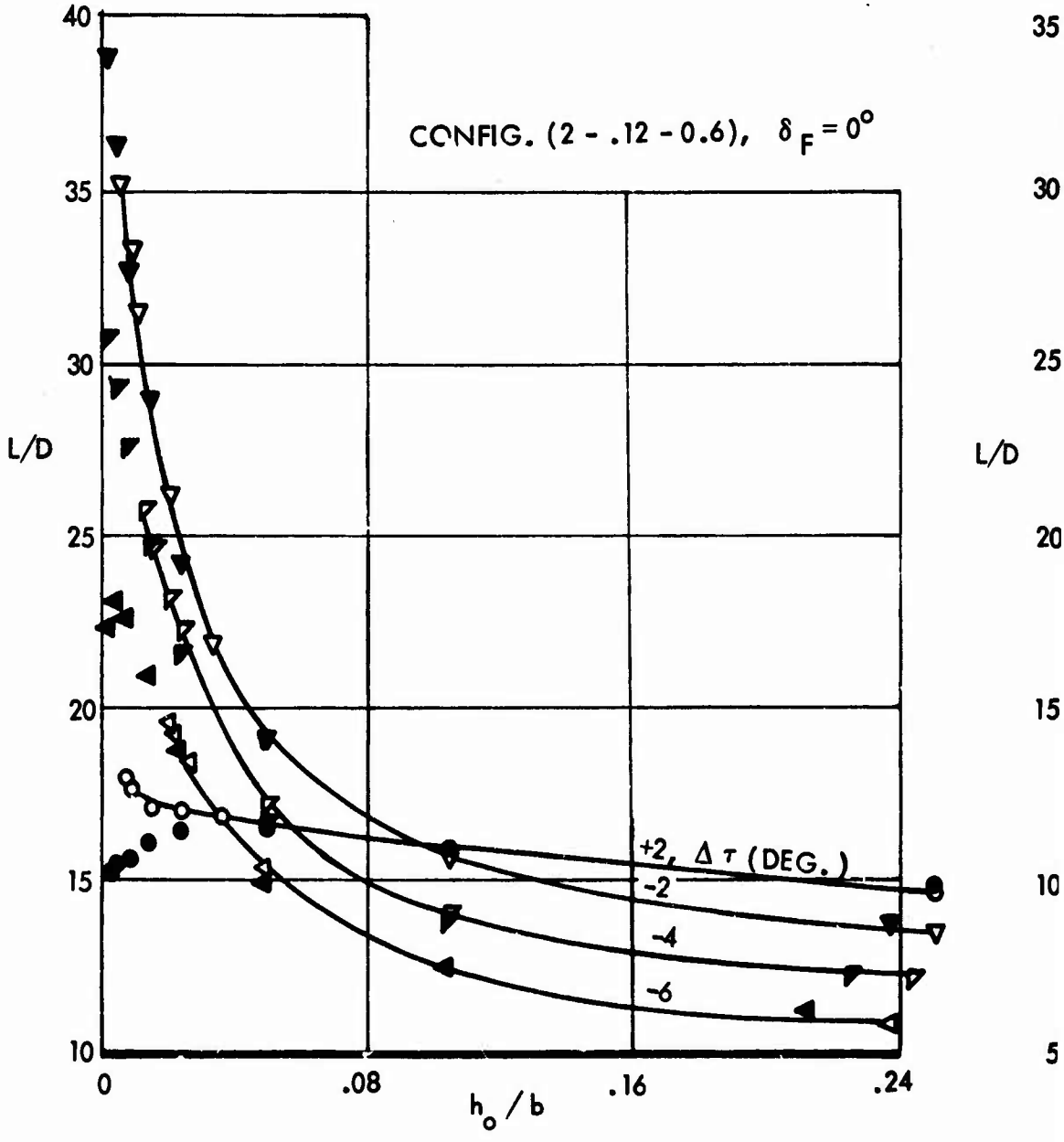

FIGURE 47. COMPARATIVE L/D, ($\tau = \alpha$) AND ($\tau = 0$) MODES, VARIATIONS IN WING THICKNESS, TAPER AND

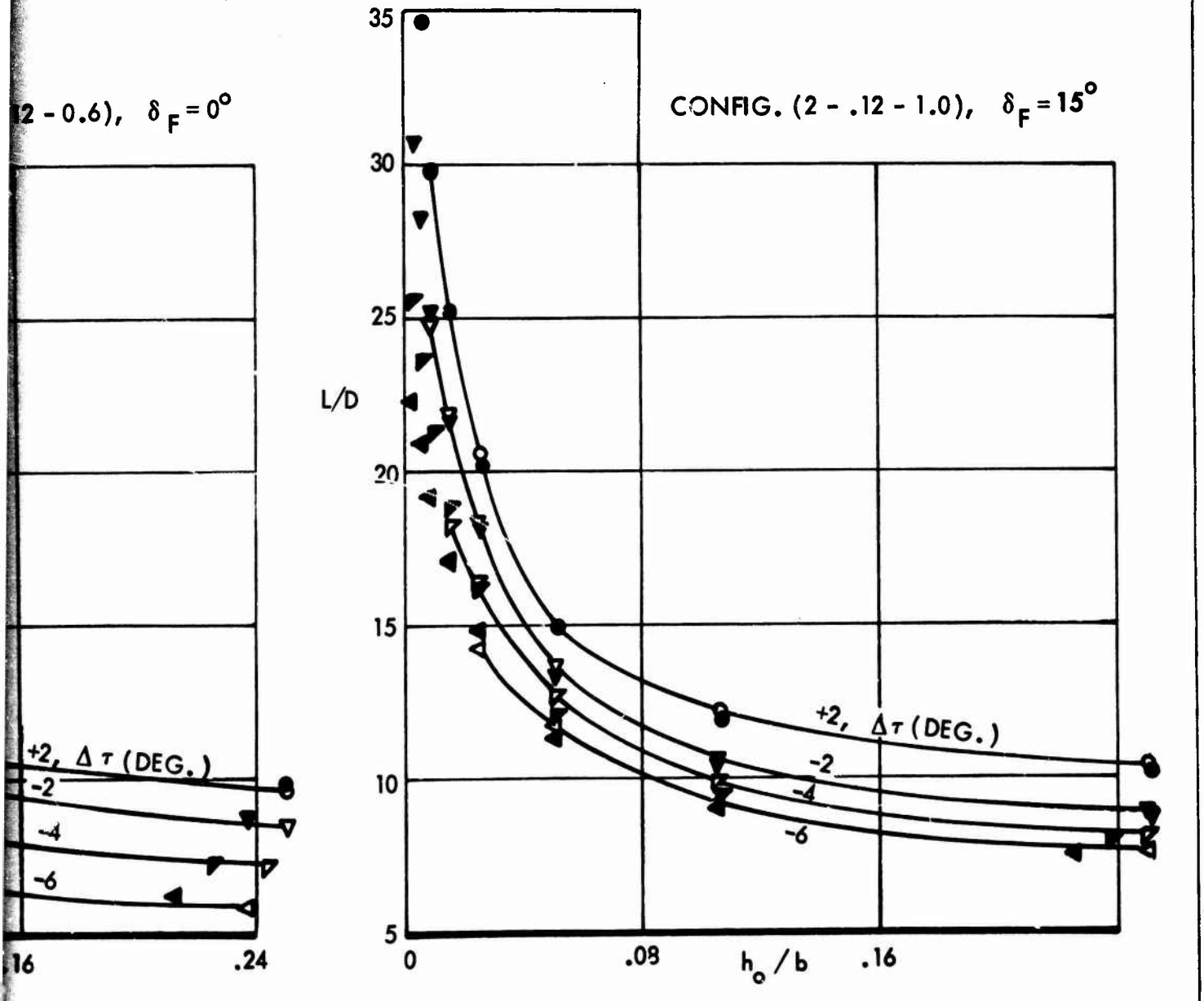

N WING THICKNESS, TAPER AND FLAP DEFLECTION.

C

NOTE:

WINGS HAVE FLAT END PLATES OF DEPTH d/c = .10
REFERENCE STATION, $X_o / c_t = 0.50$
COMMON-DATA PIVOT, $X_{L/D} / c_t = 0.50$

—○— ($\tau = 0$) MODE
● ($\tau = \alpha$) MODE ADJUSTED

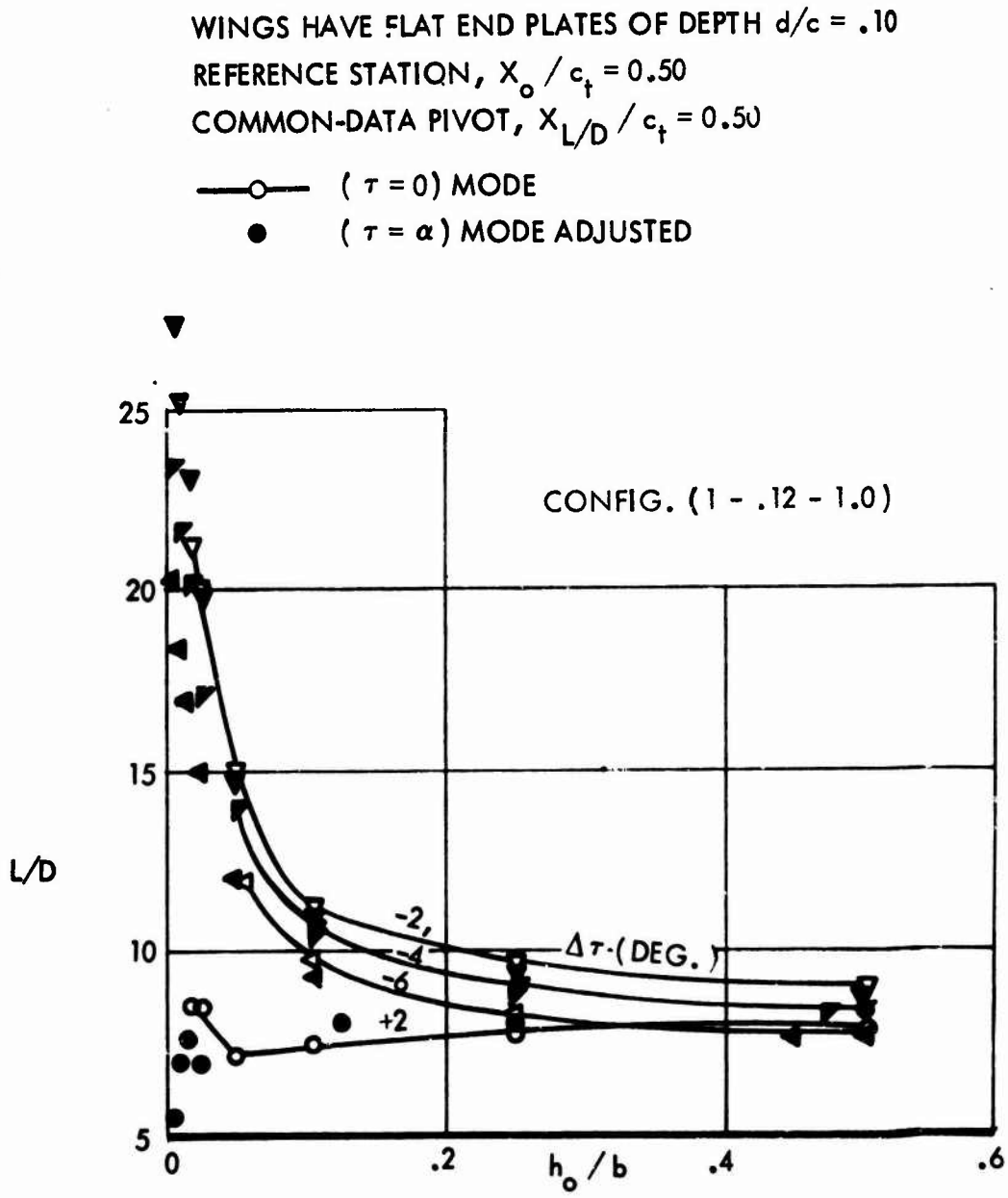

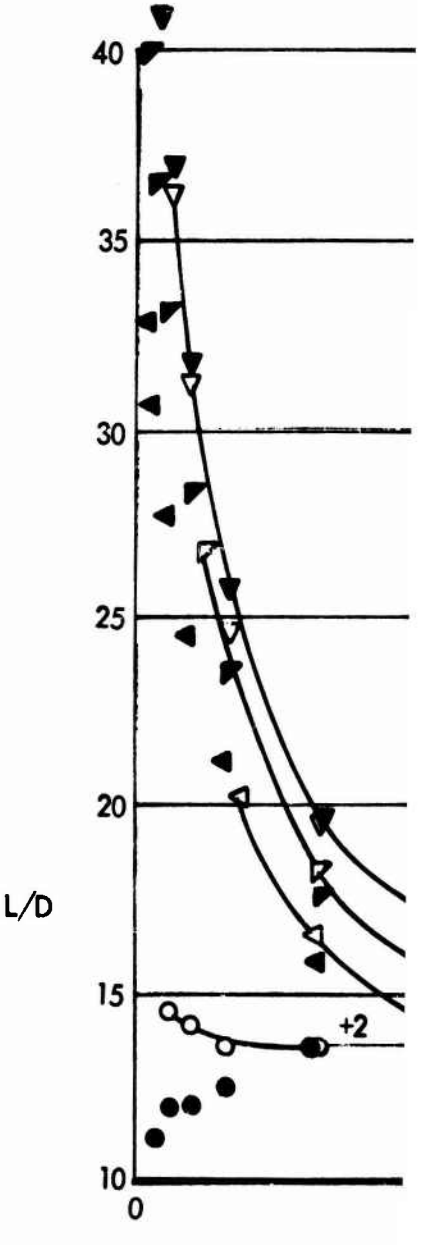

FIGURE 48. COMPARATIVE L/D, ($\tau = \alpha$) AN

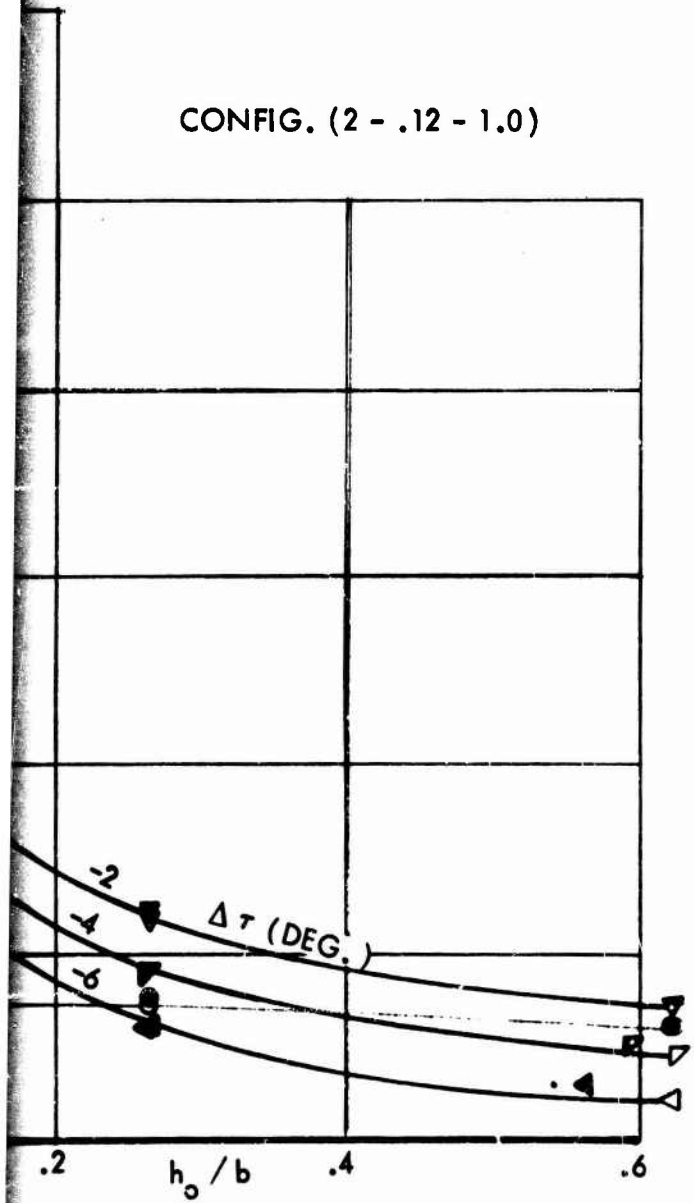

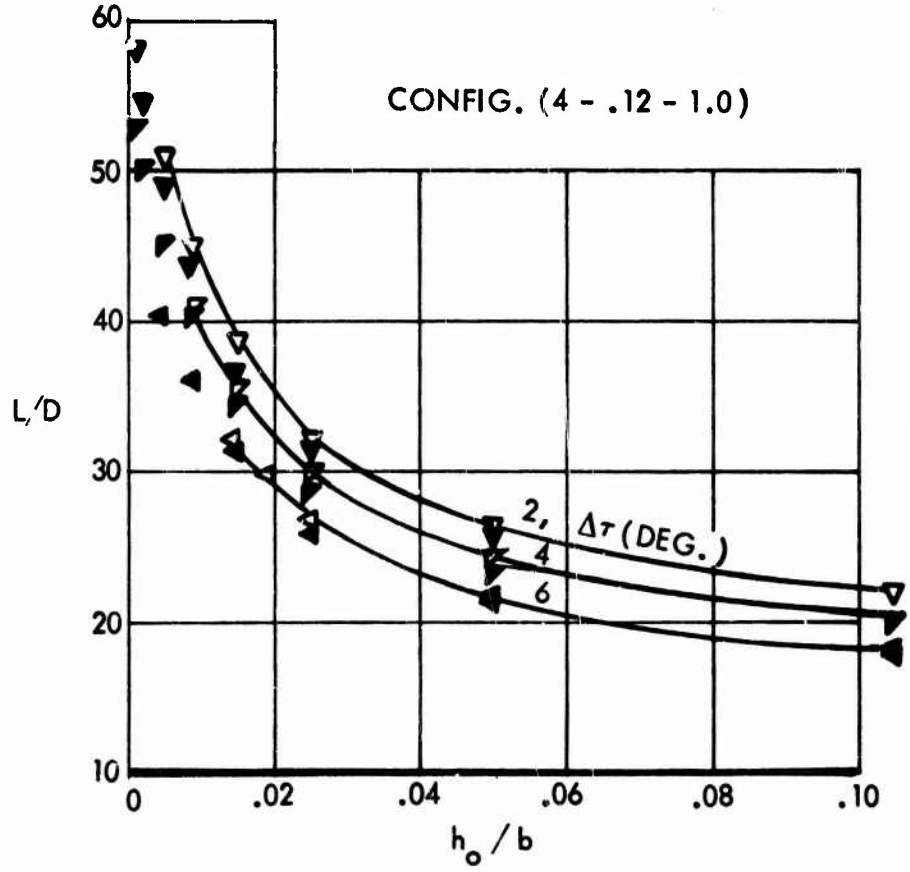

ND ($\tau = 0$) MODES, VARIATIONS IN ASPECT RATIO.

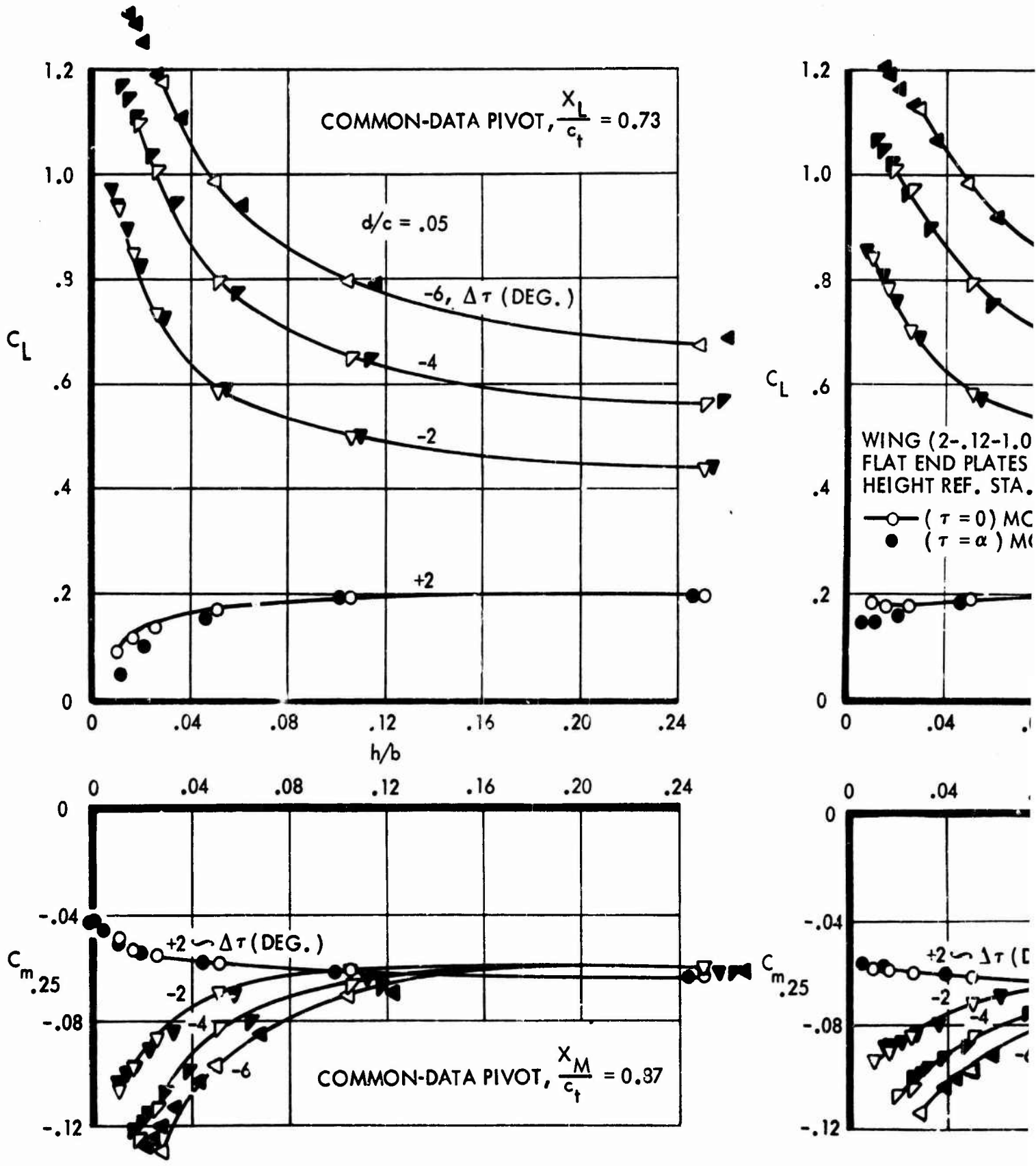

FIGURE 49 - COMPARATIVE C_L AND C_m, (τ =

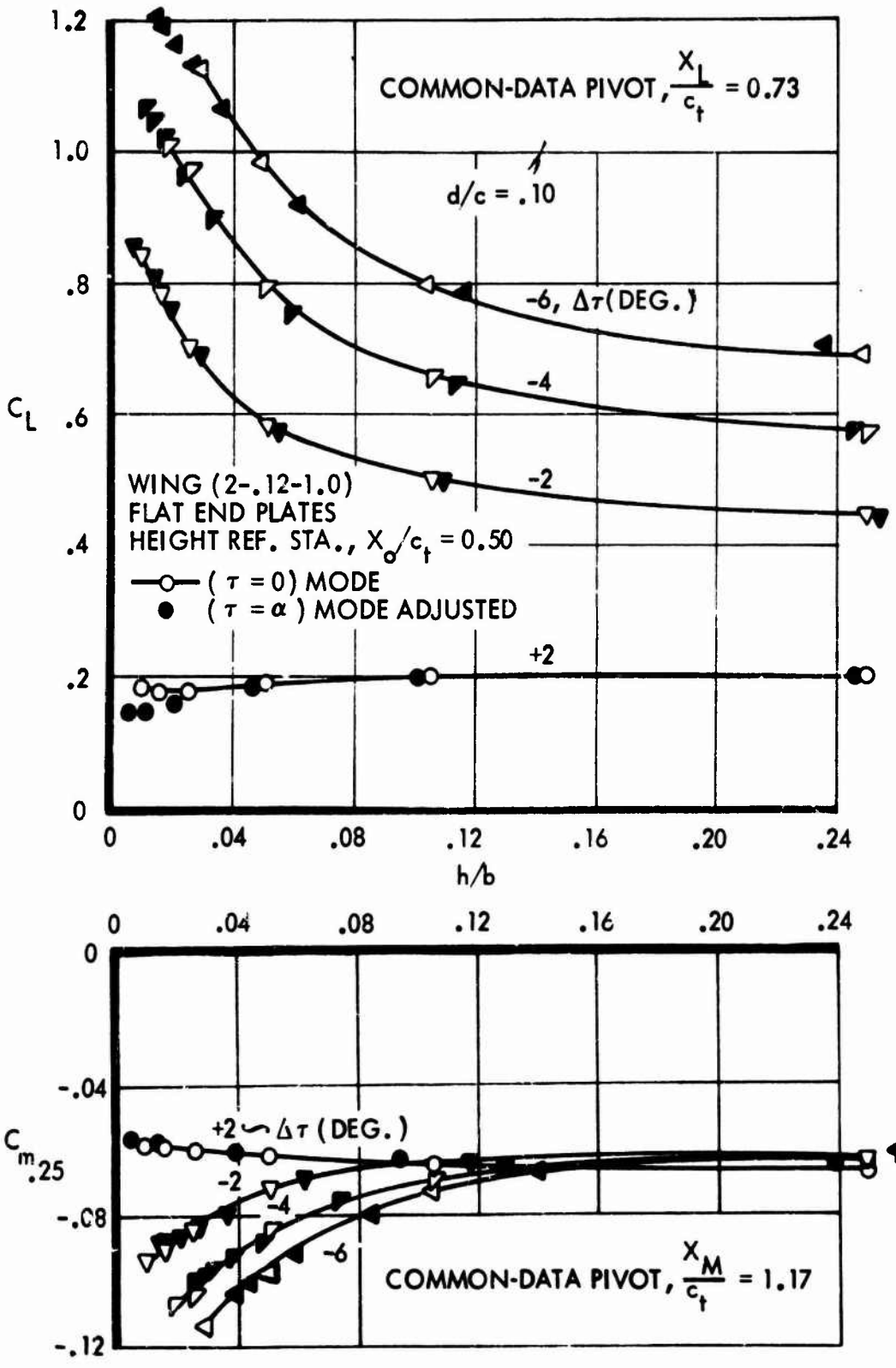

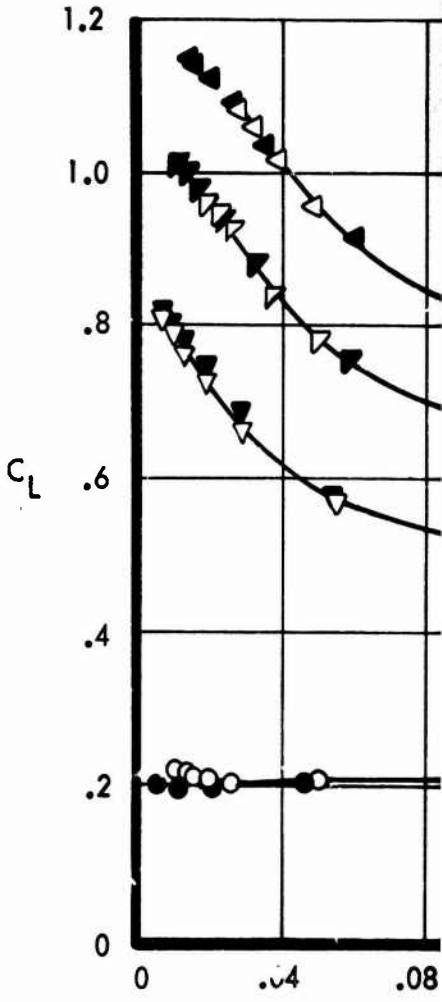

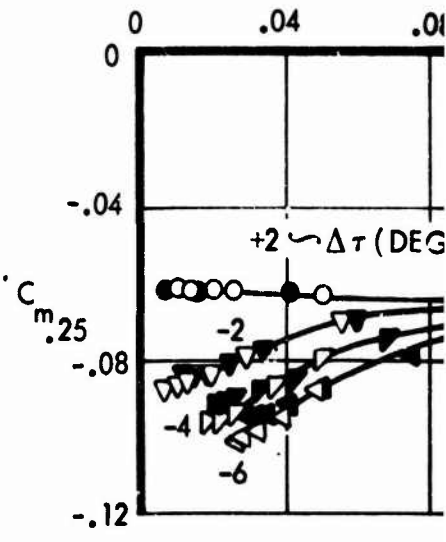

- COMPARATIVE C_L AND $C_{m'}$ ($\tau = \alpha$) AND ($\tau = 0$) MODES, VARIATIONS IN PLATE DEPTH.

Preced

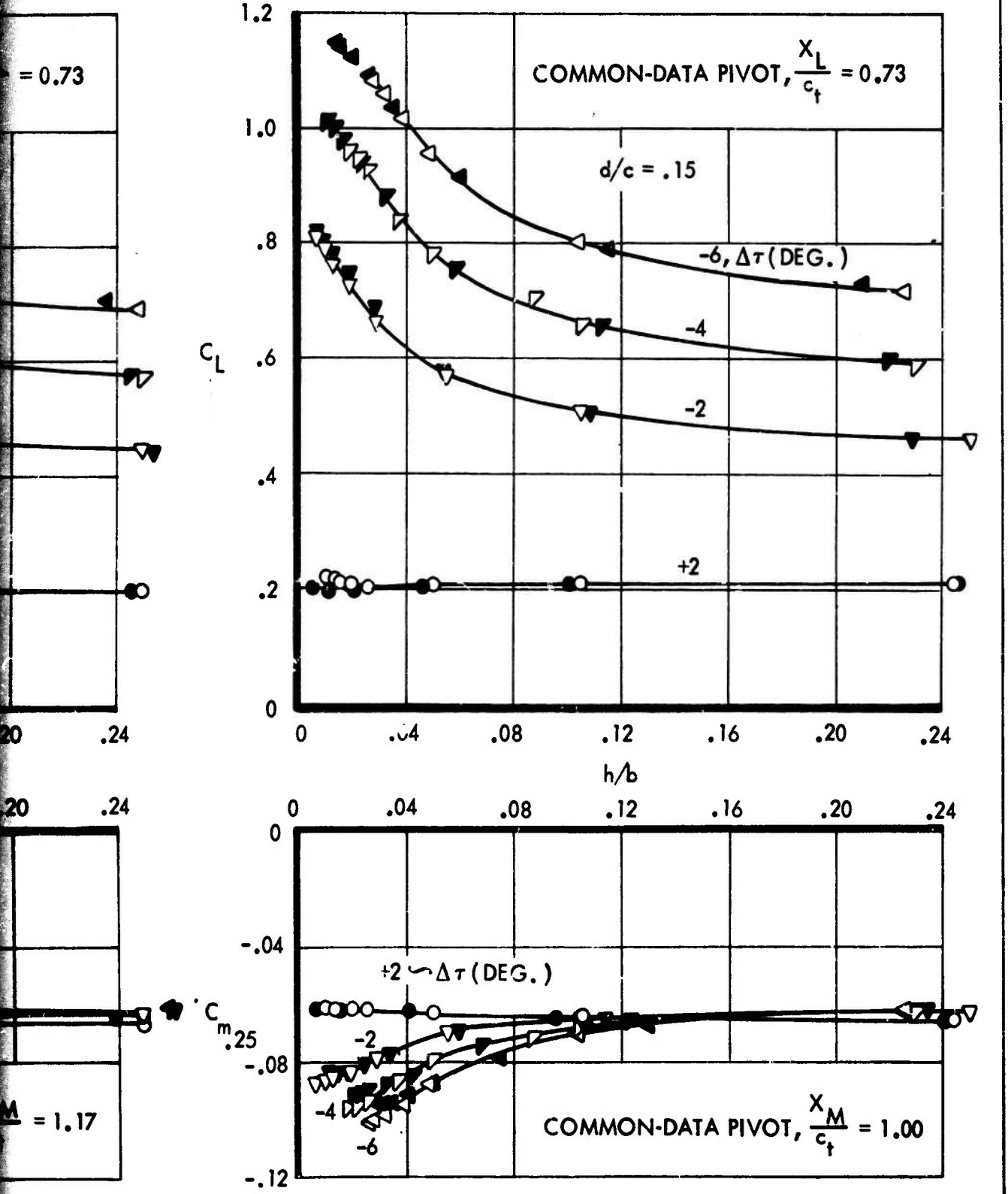

IATIONS IN PLATE DEPTH.

Preceding page blank

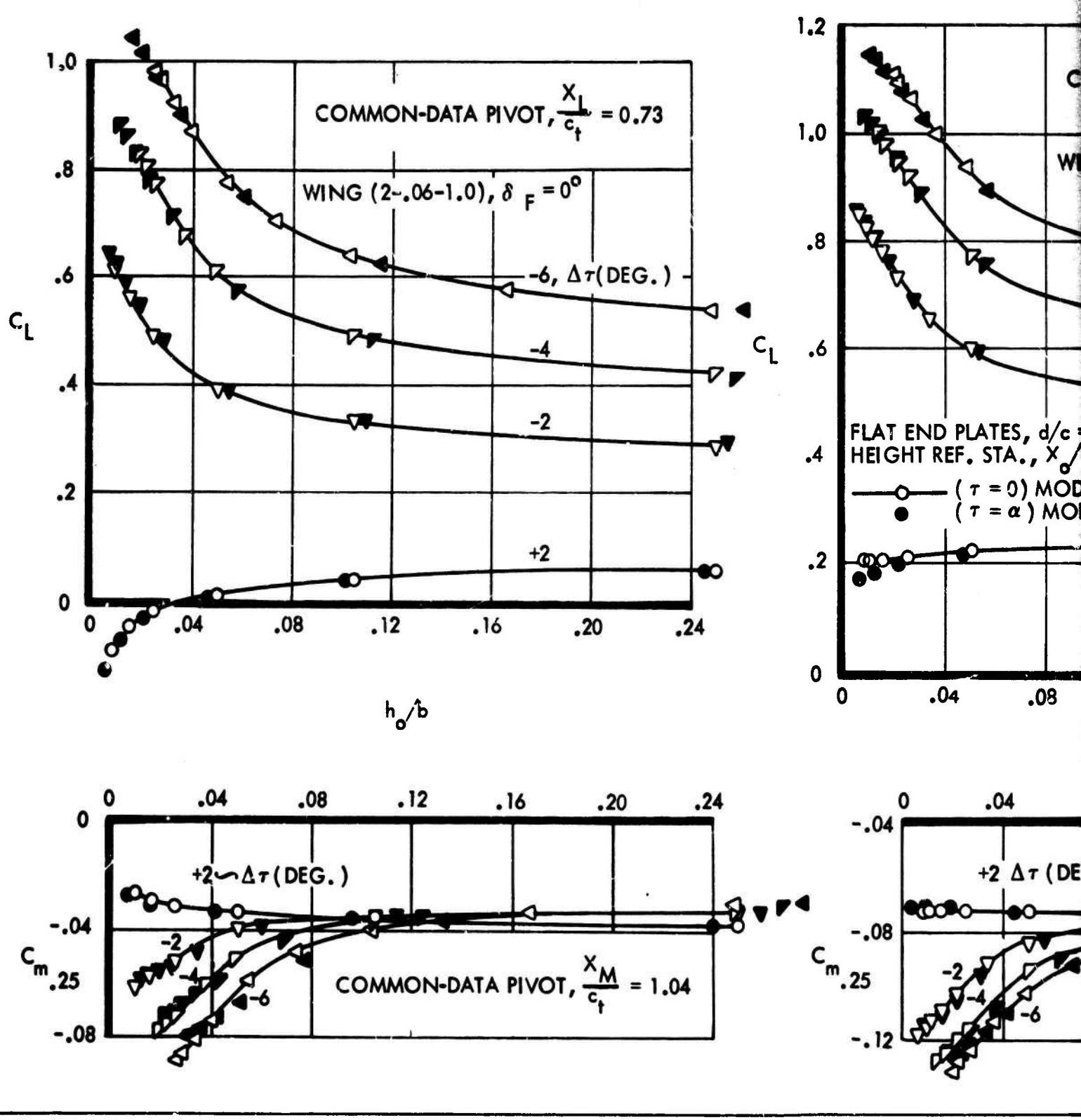

FIGURE 50. COMPARATIVE C_L AND C_m, (τ = α) AND (τ = 0)

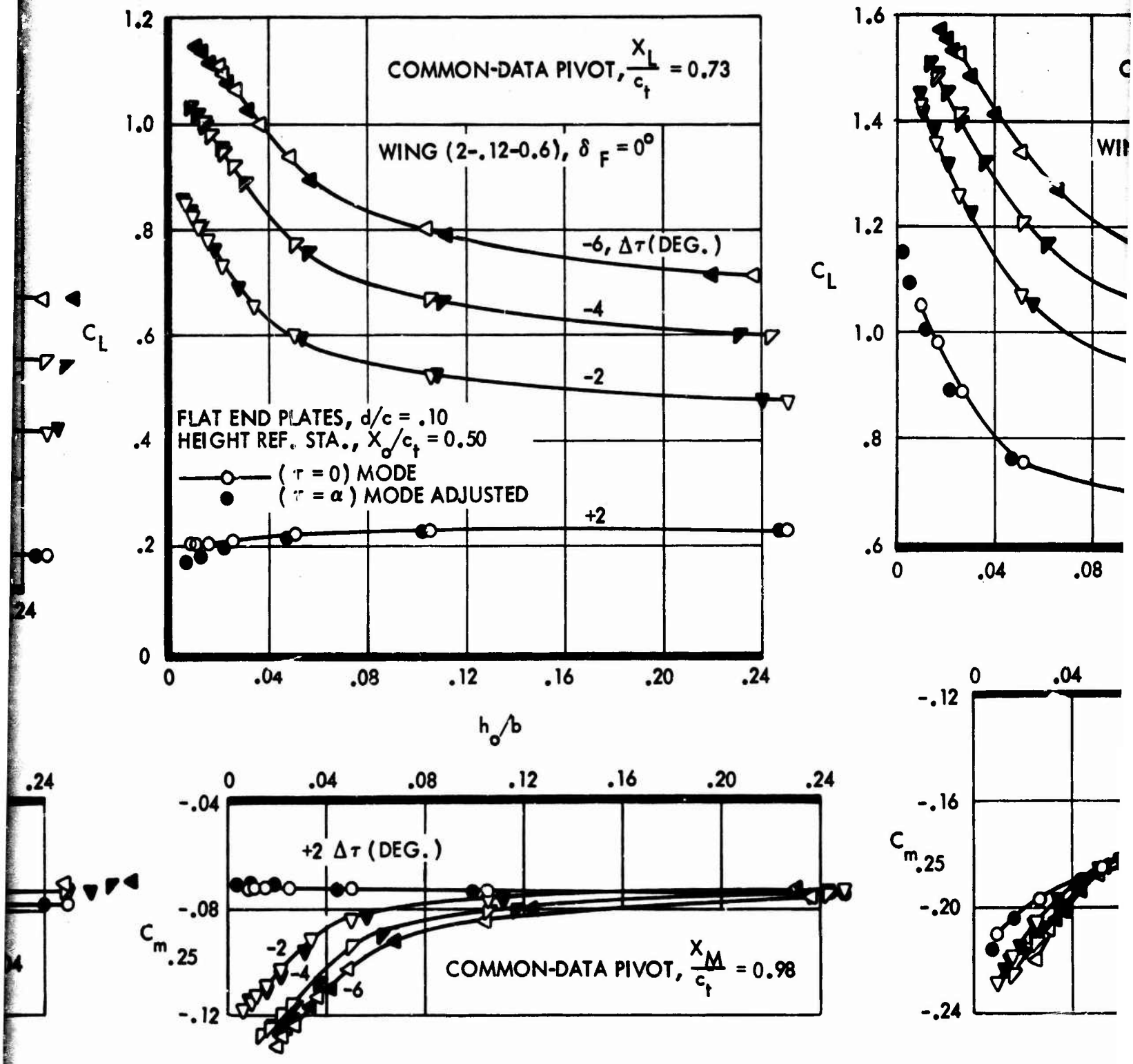

RATIVE C_L AND C_m, (τ = α) AND (τ = 0) MODES, VARIATIONS IN WING THICKNESS, TAPER, AND FLAP DEFLECTIO

B

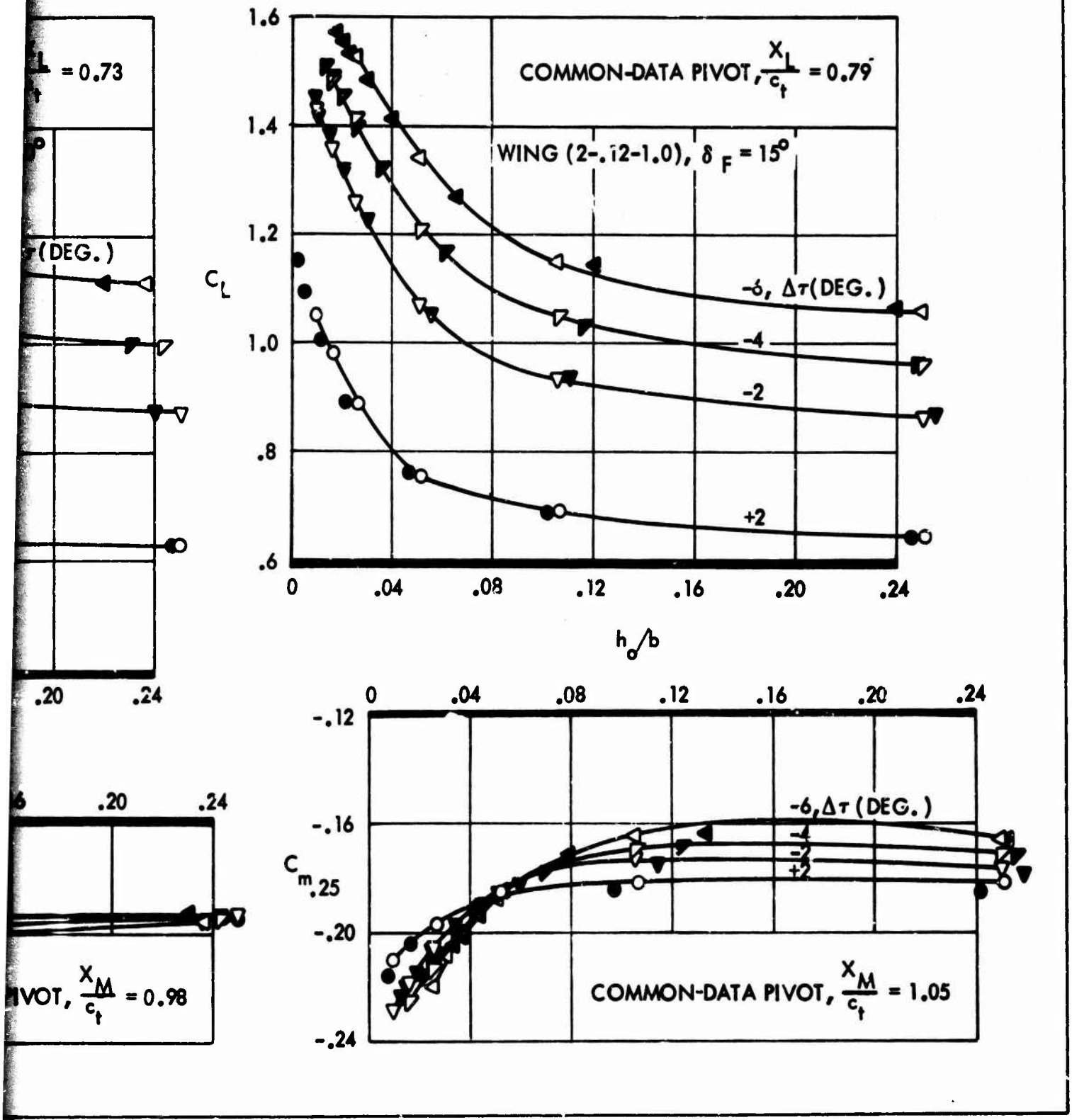

IN WING THICKNESS, TAPER, AND FLAP DEFLECTION.

Preceding page blank

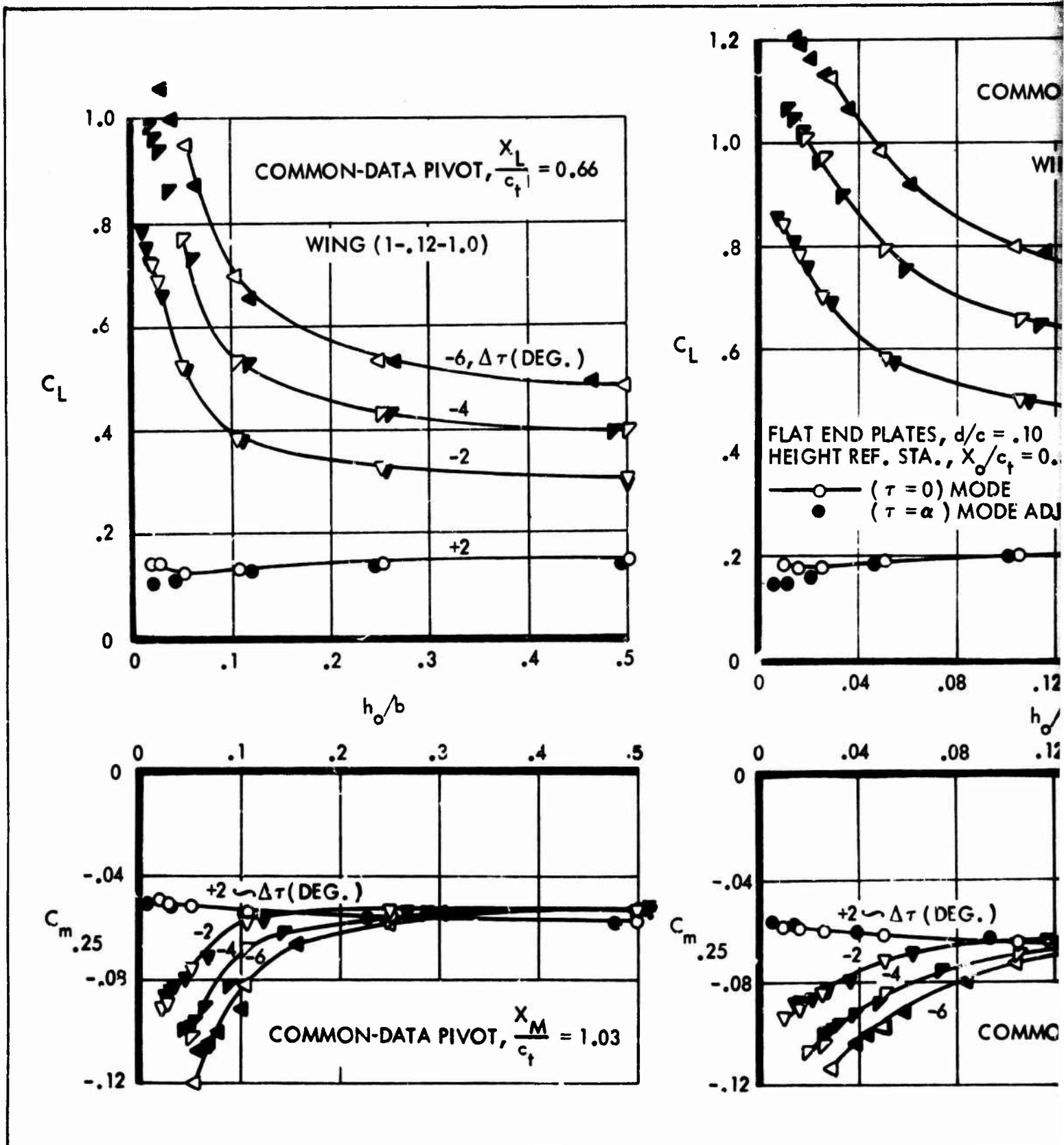

FIGURE 51. COMPARATIVE C_L AND C_m, ($\tau = \alpha$)

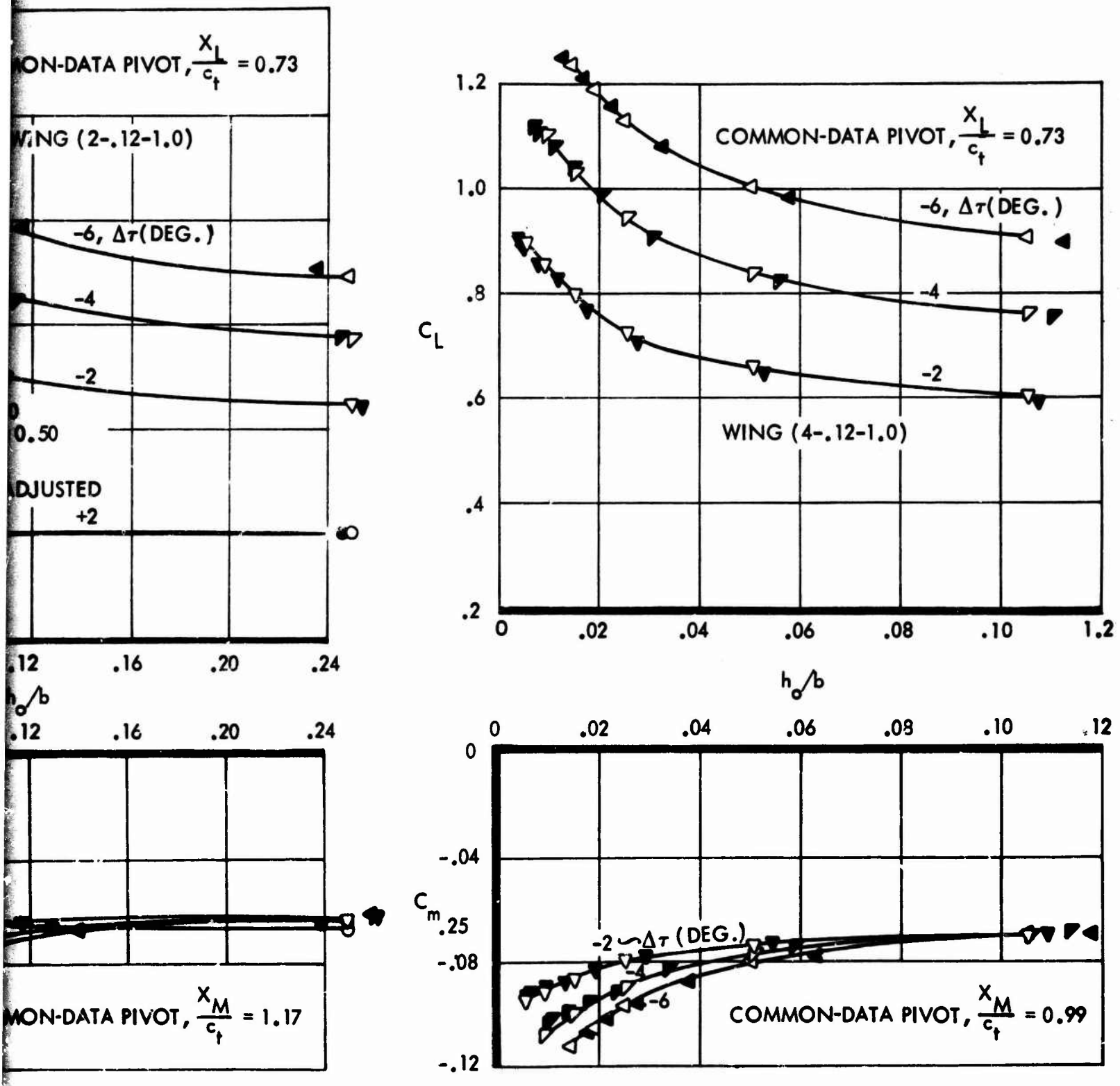

) AND ($\tau = 0$) MODES, VARIATIONS IN ASPECT RATIO.

Preceding page blank

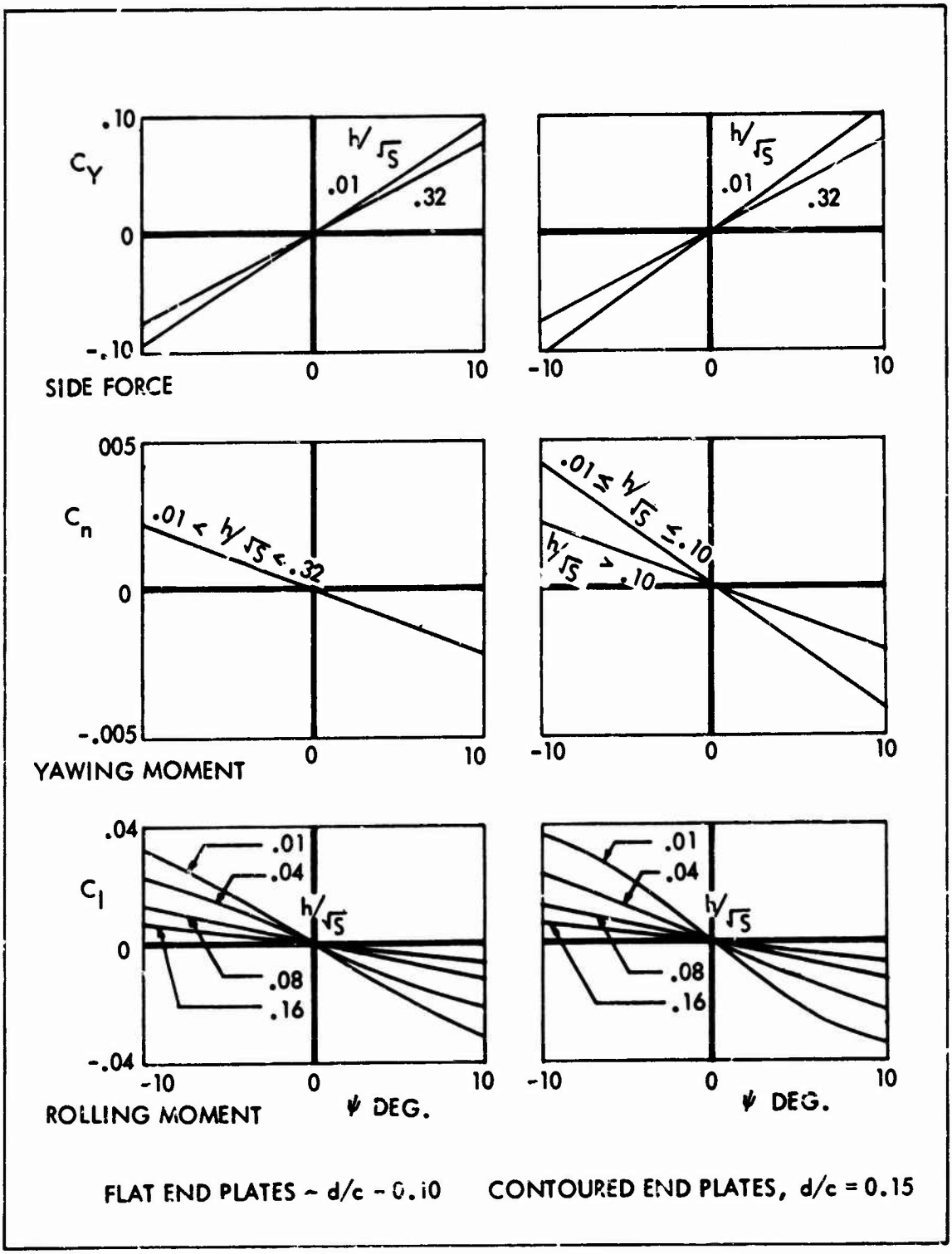

FIGURE 52. WING (2-.12-1.0), YAW AT α = 0, END PLATES.

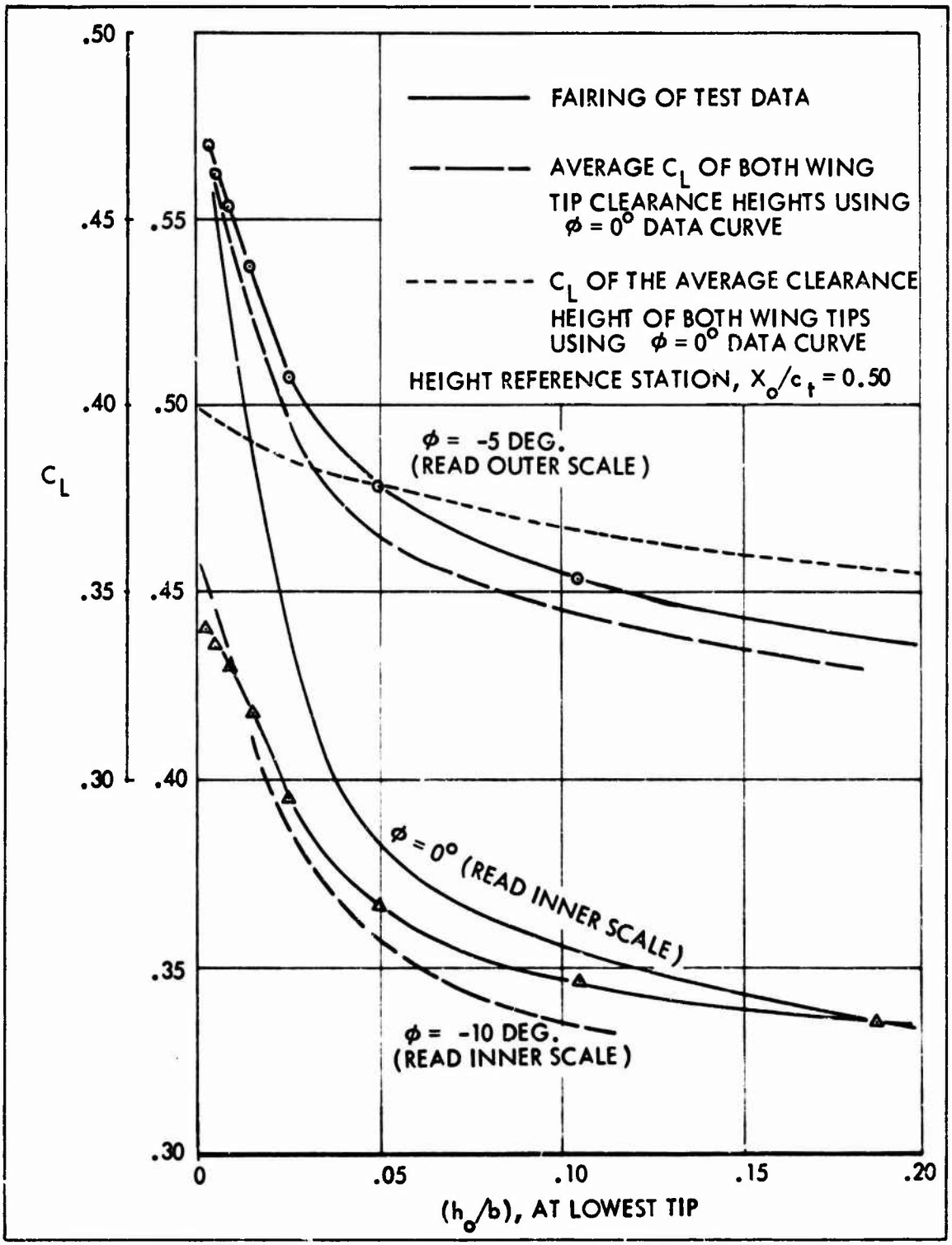

FIGURE 53. WING (2-.12-1.0), EFFECT OF BANK ANGLE ON C_L AT $\alpha = 0$, FLAT END PLATES (d/c = .10).

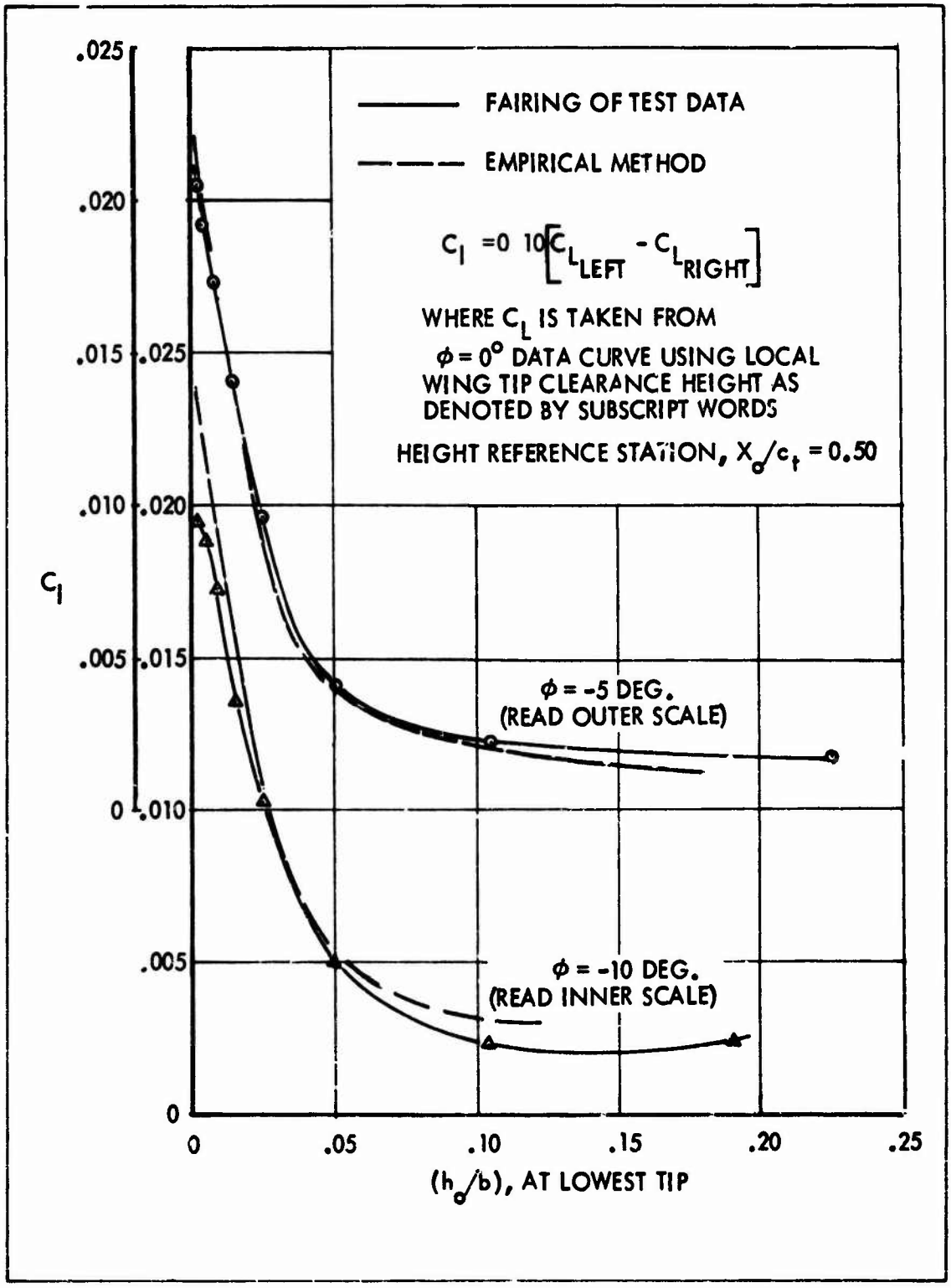

FIGURE 54. WING (2-.12-1.0), EFFECT OF BANK ANGLE ON C_l AT $\alpha = 0$, FLAT END PLATES (d/c = .10).

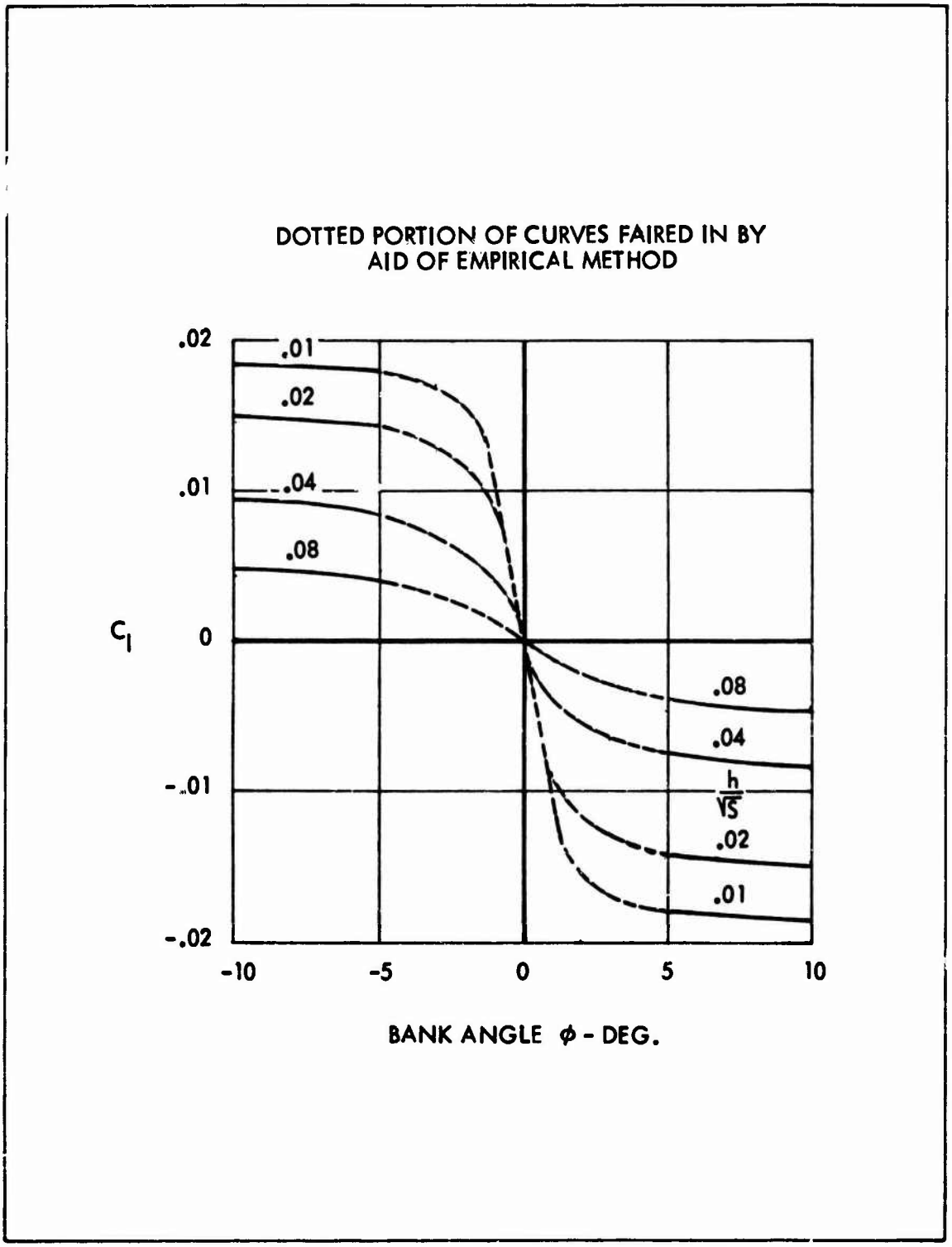

FIGURE 55. WING (2-.12-1.0), ROLL MOMENT VS BANK ANGLE, VARIOUS GROUND CLEARANCES.

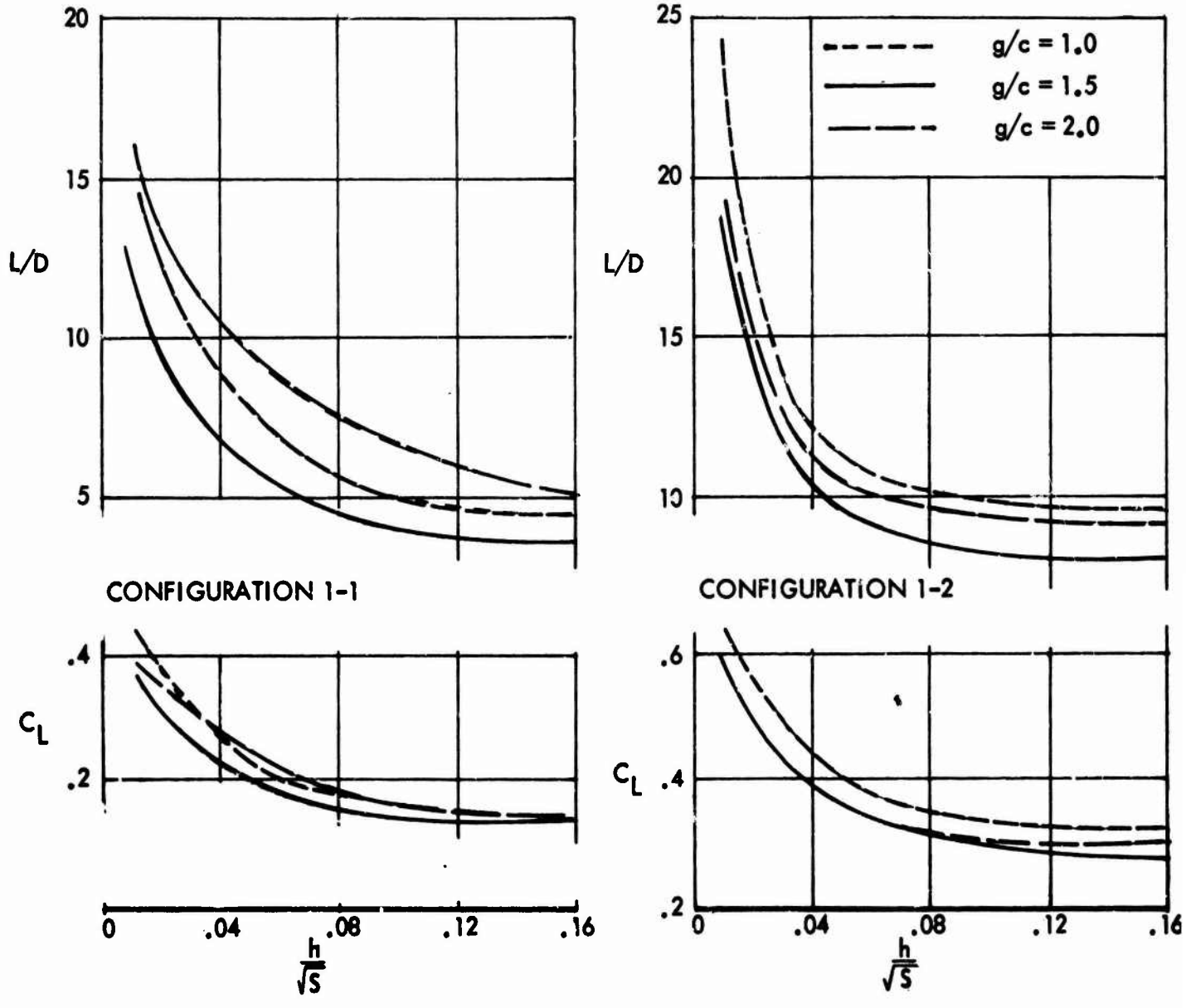
20
15
10
5
L/D
CONFIGURATION 1-1
25
20
15
10
L/D
g/c = 1.0
g/c = 1.5
g/c = 2.0
CONFIGURATION 1-2
.4
.2
C_L
0
.04
.08
.12
.16
$\frac{h}{\sqrt{S}}$
.6
.4
.2
C_L
0
.04
.08
.12
.16
$\frac{h}{\sqrt{S}}$

A

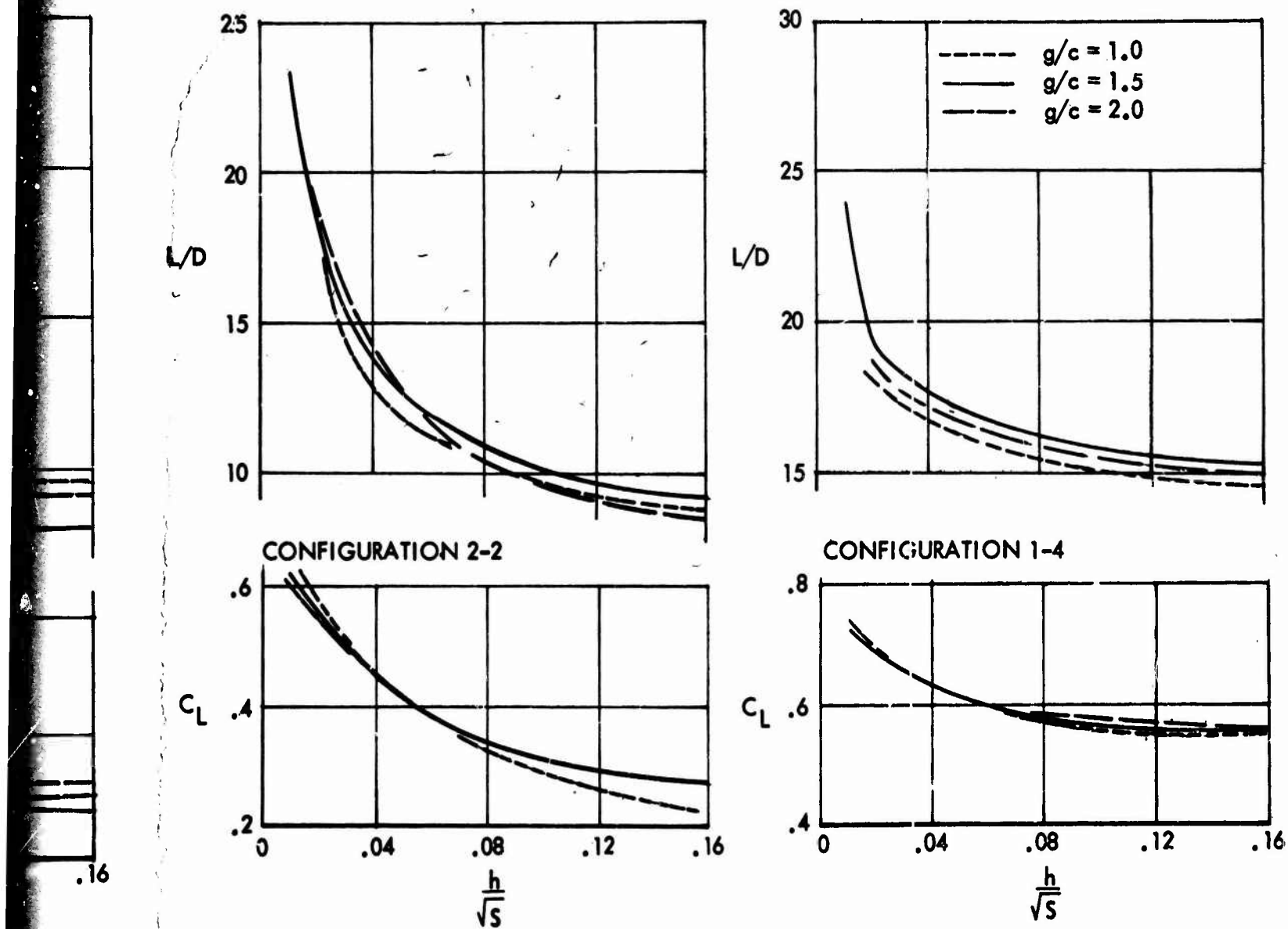

FIGURE 56. EFFECT ON L/D AND C_L, VERTICAL TRANSLATION RUNS, TANDEM WINGS, $\alpha = 0$.

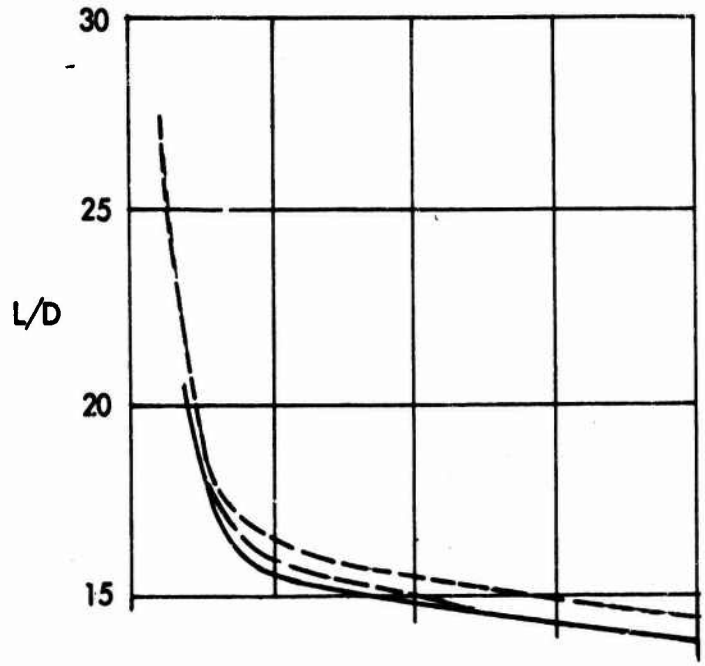

CONFIGURATION 2-4

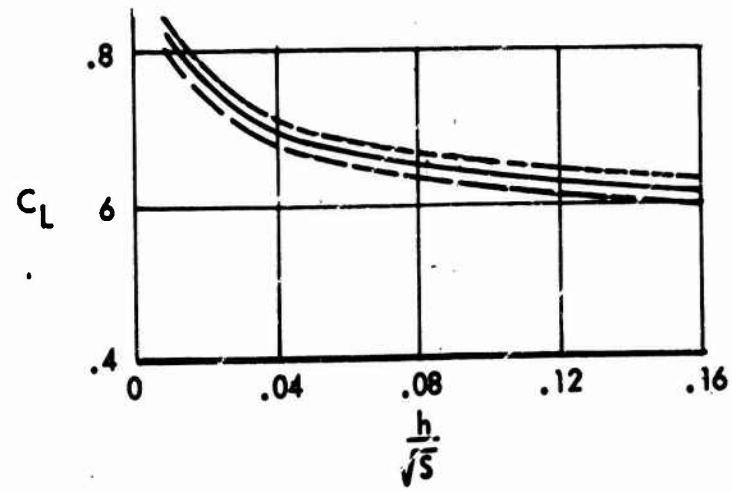

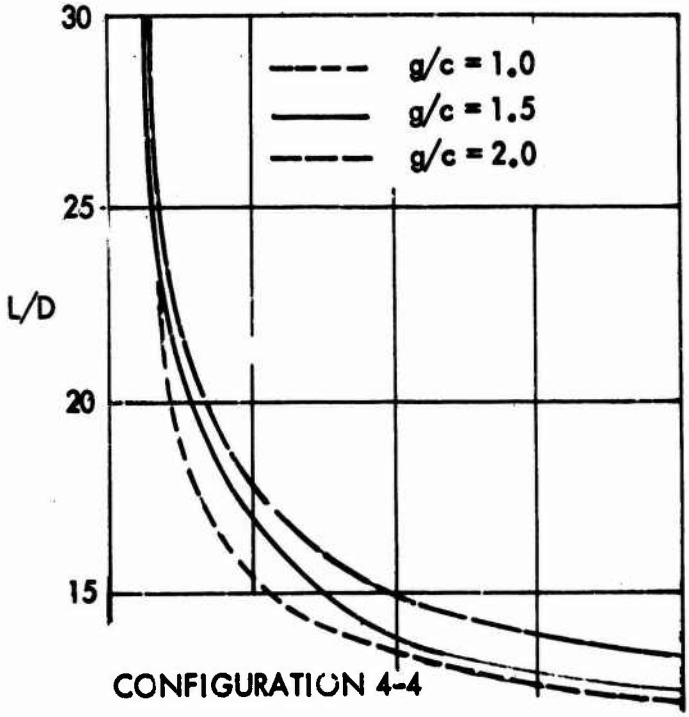

CONFIGURATION 4-4

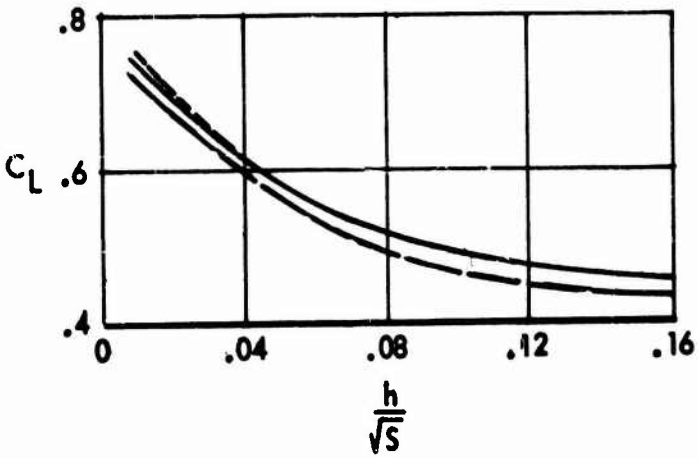

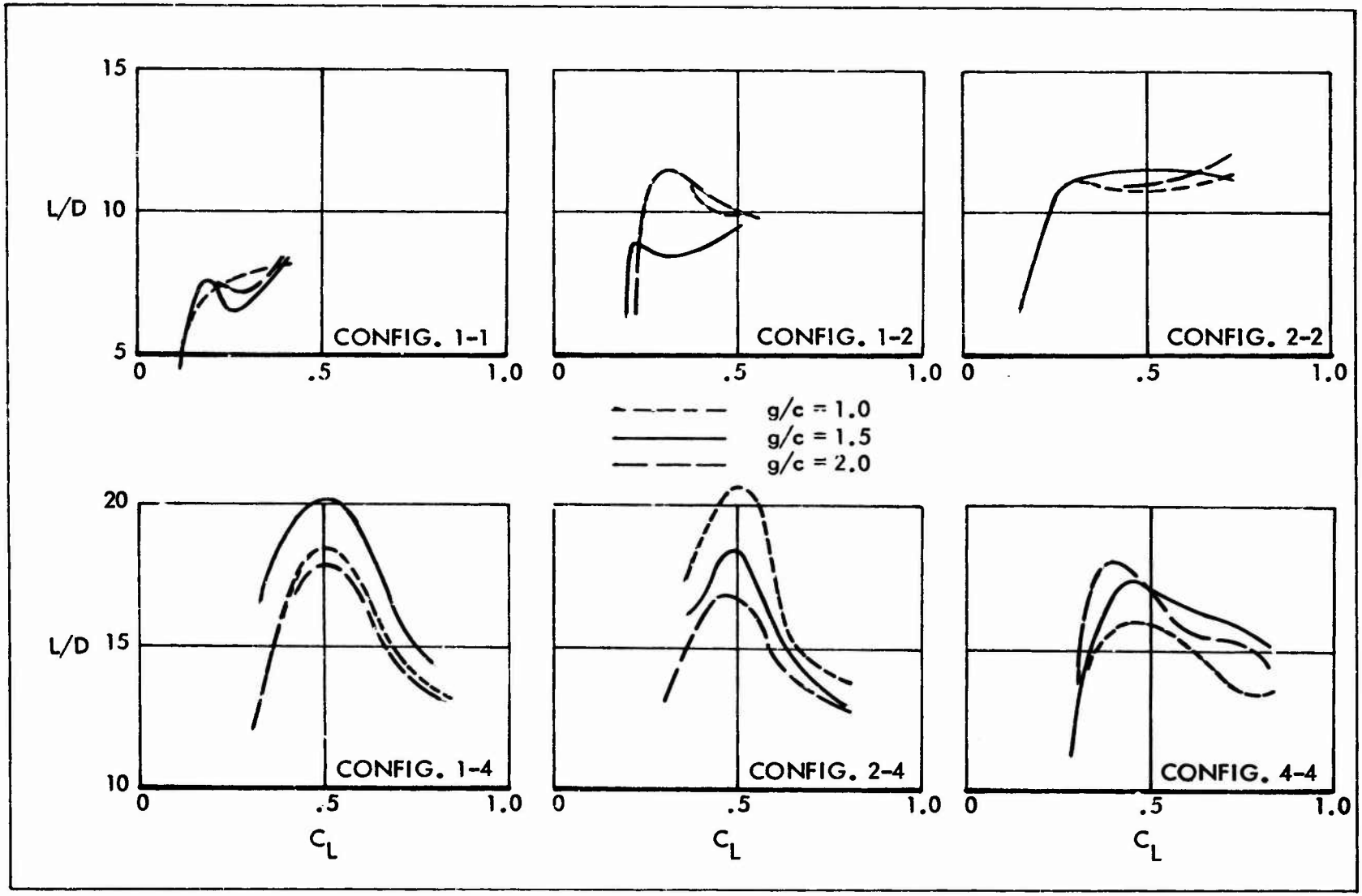

FIGURE 57. EFFECT ON L/D, PITCH RUNS, TANDEM WINGS, $h_o/\sqrt{S} = .06$.

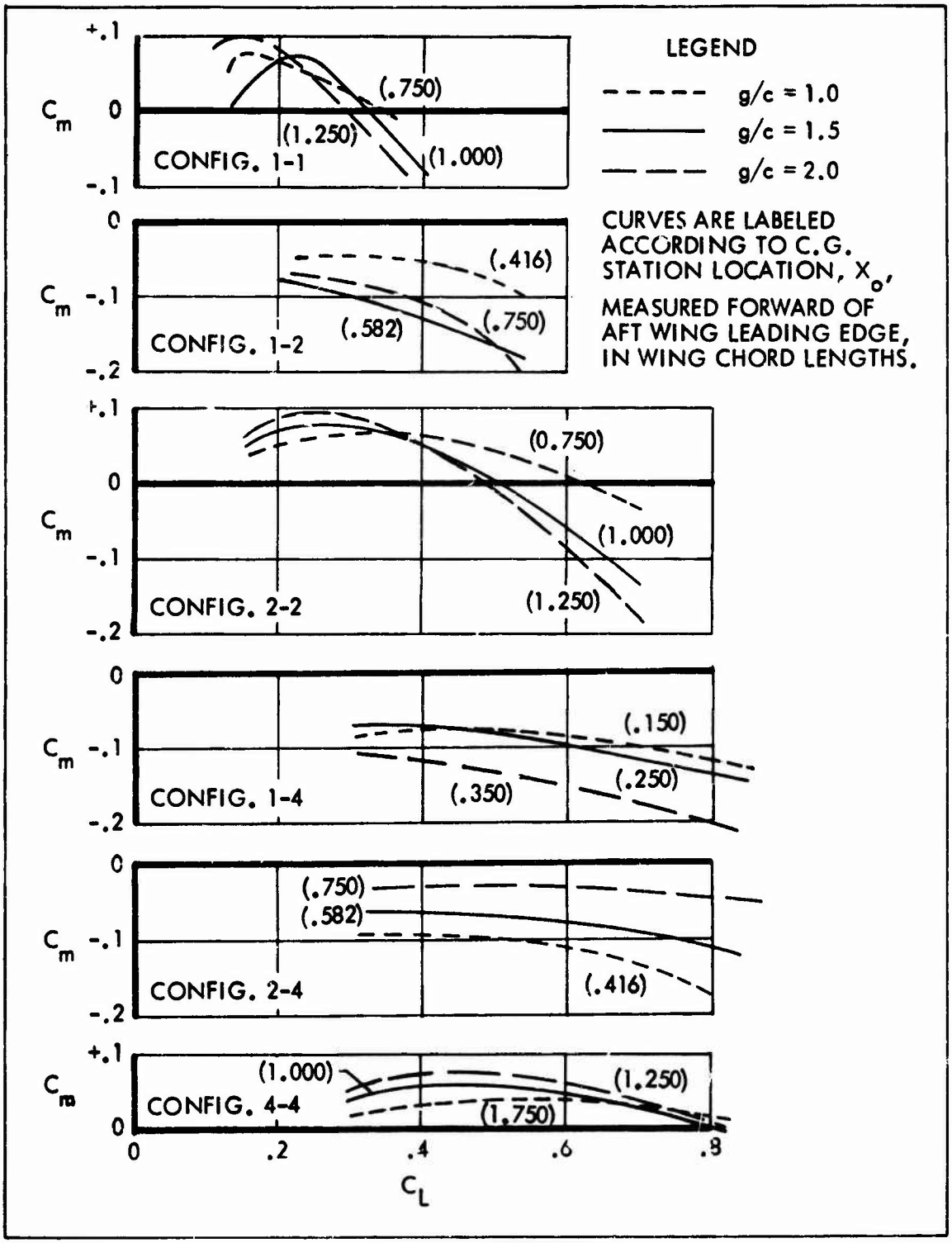

FIGURE 58. EFFECT ON C_m, PITCH RUNS, TANDEM WINGS, $h_o/\sqrt{S} = .06$